EDHEC | Climate Institute

The Global Geography of Long-Term Projected Macroeconomic Damages from Chronic Physical Risk and the Aggregation Problem

An EDHEC Climate Institute Working Paper

March 2026

Table of Contents

Keywords

Climate Econometrics; Climate Damages; Physical Risks; Projections.
JEL N°: Q54, O44, C23.

Declaration of Competing Interest

The author declares that he has no competing interests and, specifically, that he has no financial and personal relationships with other people or organisations that could inappropriately influence (bias) his work, such as, but not limited to, employment, consultancies, stock ownership, honoraria, paid expert testimony, patent applications and registrations, grants or other funding.

Authors and acknowledgments

The author gratefully acknowledges support from the EDHEC Climate Institute (ECI), and particularly Riccardo Rebonato, Lionel Melin and Frederic Ducoulombier for their useful guidance and feedback.

Data and Code

Climate data from GLDAS and NASA-NEX GDDP (CMIP6 GCMs) are available from their corresponding data portals linked in the monograph. Macroeconomic data from DOSE, WDI and PWT are available from their corresponding data portals linked in the monograph. The processed data and associated spatially distributed macroeconomic damages across CMIP6 GCMs and warming scenarios are available in the form of .csv files upon request to the author.

About the Author

Nicolas Schneider, PhD, is a Senior Research Engineer – Macroeconomist at EDHEC Climate Institute. He leads the development of quantitative methodologies to assess long-term physical climate risks and associated projected macroeconomic damages, supporting both the Institute's research activities and its venture initiatives, including Scientific Climate Ratings and Scientific Portfolio. He previously consulted for the New York City Mayor's Office of Climate and served as a fellow in the Coupled Human and Earth Systems Program of the U.S. Department of Energy's Multi-Sector Dynamics Modeling Initiative. He holds a Ph.D. from Boston University, funded by the U.S. Department of Agriculture's National Institute of Food and Agriculture (NIFA), and MSc degrees from the London School of Economics and Paris-Sorbonne University. He has co-authored several peer-reviewed articles and has taught at Harvard University's Department of General Education, in the Quantitative Methods Seminar at the Oxford Smith School, as well as in the joint MSc between EDHEC Business School and Mines Paris-PSL.

Abstract

Does the macro-level relationship between temperature and output comprehensively reflect the patterns observed sub-nationally? This monograph elucidates the heterogeneity of countries' and provinces' productivity growth responses to plausibly exogenous fluctuations in temperature and precipitation, using unbalanced panels over 1970–2018 (166 countries from Penn World Tables 10.01; 1,661 regions from MCC-PIK). We project climate change–driven permanent damages to the level of GDP per capita by compounding physical risk induced-productivity growth deviations over time. These transitory shocks are calculated through combining econometrically estimated response functions with an ensemble of NEX-GDDP CMIP6 simulations from 29 global climate models (GCMs), which we extrapolate to 3,672 provinces covering 95% of global economic production. We find substantial agreement among GCMs of average end-of-century per capita GDP declines of up to 70% attributable to the central component of chronic physical climate risk (i.e., climate change-driven shifts in average temperature), with the largest losses in equatorial and tropical regions under a vigorous SSP5–8.5. First, our study provides a basis for producing spatially disaggregated projections of climate-induced economic damages that consistently encompass most productive regions. Second, we show that accounting for spatially granular climatic exposure and intra-country economic heterogeneity yields aggregated losses that alter the conclusions of previous global GDP models.

1 Introduction

Does the macro-level relationship between temperature and output comprehensively reflect the patterns observed sub-nationally (and ultimately, at the micro-level)? If so, how do these spatially granular effects aggregate to the national and global scales? This monograph contributes to addressing these two important questions. First, we show that country-averaged temperature deviations smooth out critical weather variability relevant for causal inference in climate econometrics. Next, we find that global mid- and end-century damages conceal substantially larger magnitudes when projecting climate change implications on regional economic production.

Global production systems, particularly food and energy, are expected to face increasing pressure from rising demand and a changing climate over the next century (Foley et al, 2005; Bodirsky et al, 2015). A large body of regression-based studies has quantified the environmental determinants of various weather-dependent outputs using micro-data. For instance, crop yields and farmland values have been shown to exhibit a hill-shaped relationship with temperature, with peak outcomes occurring near mean growing-season exposure (Seo et al, 2009; Mendelsohn and Massetti, 2017). These studies have primarily focused on exposure to extreme heat (Blanc and Schlenker, 2017; Massetti and Mendelsohn, 2020; Sue Wing et al, 2021), changes in soil moisture (Ortiz-Bobea et al, 2019), or interactions between the two (Haqiqi et al, 2021).

At the macroeconomic level, empirical analyses have established robust correlations between temperature and aggregate economic output. These relationships have been found using both temporal (panel) (Hsiang, 2010; Dell et al, 2012) and spatial (cross-sectional) variation in econometrics (Nordhaus, 2006; Dell et al, 2009). What remains unclear is whether the macro-level relationship between temperature and output comprehensively reflects the patterns observed sub-nationally (and ultimately, at the micro-level), and, if so, how these spatially granular responses scale up to the national level.

A first intuitive hypothesis is that global assessments tend to underestimate the strong non-linear responses of output to temperature documented in microeconomic studies (Dell et al, 2012)[1]. Why? These estimates rely mainly on data from developed

[1]Mainly due to data availability constraints, studies assessing the weather determinants of agricultural productivity have focused on the U.S. using state- or county-level data. See Schlenker and Roberts (2009);

countries and are difficult to generalize to humid tropical regions, where emerging economies and large populations are concentrated.

This mismatch between micro-level patterns and macro-level conclusions could reveal a potentially bigger *aggregation* problem. Micro-level output declines occur under localized and often extreme thermal conditions. When aggregated across large spatial units, such as countries, and long temporal intervals, such as years, this variability is averaged out. If output losses are concentrated during extreme temperature realizations, aggregation with cooler and more productive periods yields muted responses to changes in mean temperature (Burke et al, 2015). As a result, macro-level analyses may substantially underestimate the true sensitivity of economic output to climate, particularly in countries with high regional climate heterogeneity. Addressing this issue is a core objective of this monograph.

Climate change is shifting the distribution of extreme heat events, making them more intense and frequent over time (Orlowsky and Seneviratne, 2012). Projections based on Shared Socioeconomic Pathways predict continued increases in global mean surface temperature by mid-century (Meinshausen et al, 2020). Recent developments in spatial econometrics and global climate databases have increased spatial resolution, improved temporal persistence, and expanded the density of information that can be ingested into climate econometric models. The implications for regional economic output are substantial but largely unexplored. Recent work by Kotz et al (2024)[2] provides evidence that accounting for regional variability and a broader set of climatic variables

Schlenker and Lobell (2010) and Burke and Emerick (2016). Similar limitations apply in the climate–energy nexus literature (Deschênes and Greenstone, 2011; Auffhammer and Aroonruengsawat, 2011; Auffhammer et al, 2017; Auffhammer, 2022). Temperature–energy demand responses are typically estimated using state-level monthly electricity load (Deschênes and Greenstone, 2011), high-frequency regional data (Franco and Sanstad, 2008; Miller et al, 2008; Allen et al, 2016; Coffey et al, 2015), residential consumption (Auffhammer and Aroonruengsawat, 2011), or city-level utility billing data (Romitti and Sue Wing, 2022), mostly from California and the American South.

[2]Following a recent *Matters Arising* by Bearpark et al (2025), Kotz et al (2024) was retracted by *Nature* on 3 December 2025, attracting non-negligible media attention. The authors are preparing a revised version for peer review. The numerical correction itself, resulting from removing Uzbekistan historical data points, was relatively small: projected 2100 global GDP loss reduces from 19.0% to 17.0%. Although the sign and fundamental conclusion of the paper is unchanged, the retraction was based on the methodological basis that global results are showing *unexpectedly* high sensitivity to a single country where an error had occurred. Additionally, Schötz (2025) highlighted concerns regarding uncontrolled sub-national spatial correlations, which may have led to wider-than-expected uncertainty. This contribution makes an intuitive claim by suggesting that subnational economic regions are not fully independent and that further intra-country trade flows and output reallocation play out in practice.

yields larger and more heterogeneous projected economic impacts than previously reported.

The absence of comprehensive GDP damage projections that account for localized climatic exposure and within-country economic heterogeneity leaves an incomplete picture of macroeconomic adaptation capacity. Existing global GDP response models, constructed from smoothed country-by-year averages, may understate the true economic cost of physical climate risk. This monograph contributes to the literature by investigating interactions between the spatial structure of production systems and the climatic determinants of output sensitivity. Finer-grained damage decompositions may reveal localized disparities masked in aggregate analyses (Burke et al, 2015; Linsenmeier, 2023; Berg et al, 2024; Bilal and Känzig, 2024).

This monograph quantifies weather-driven responses of annual per capita GDP at both the country and administrative province levels for regions accounting for approximately 95% of global economic output. The analysis relies on an unbalanced panel covering 1970–2018, drawing on Penn World Tables version 10.01 and the MCC-PIK Database of Subnational Economic Output (DOSE). Using a panel specification standard in the climate–economics literature, we elucidate heterogenous output' responses to temperature and precipitation, which we attribute to both time-series and cross-sectional variations in plausibly exogenous year-to-year weather fluctuations (i.e., the major propagation channels of climate change, because unanticipated); as well as the identification of long climate normals causing actors' adaptation along the 'extensive margin' (i.e., which manifests itself over time in response to the long stochastic warming process that follows an upward trend). We follow McIntosh and Schlenker (2006) and structure our fixed-effects model with a non-linear polynomial temperature function enabling both within-country and cross-country sources of variation to re-enter our equation, thus implicitly allowing economic units in the dataset to adapt over time. We leverage spatial deviations by considering the exposure of administrative provinces to climate fields, weighted by a time-invariant measure of intra country population density distributions derived from the 2015 Gridded Population of the World dataset (CIESIN, 2004). Meteorological covariates are compiled from historical 3 hourly global surface temperature and precipitation fields on a 0.25 deg. grid from the Global Land Data Assimilation System (GLDAS) (Rodell et al, 2004) and matched to economic data. We

then compare our country-level GDP responses (i.e., *à la* Burke et al (2015)) to our two main propagation channels of climate change impacts (i.e., temperature and precipitation) with those inferred from province-level data (i.e., *à la* Kotz et al (2024)). These response functions are combined with an ensemble of NEX-GDDP CMIP6 Global Climate Model (GCM) simulations to project climate change–driven deviations in productivity growth under moderate (SSP2–RCP4.5) and aggressive (SSP5–RCP8.5) warming scenarios. The resulting transitory deviations are compounded over time to generate permanent changes in GDP per capita. These projections are distributed across administrative regions, future epochs (2030–2099), individual climate models, multi-model medians, and SSP-RCP scenarios. The availability of 29 CMIP6 models provides a unique opportunity to leverage the most temporally and spatially downscaled climate projections for macroeconomic damage assessments.

The remainder of this monograph is organized as follows. Section §2 presents the theoretical framework, data, and econometric approach. Section §3 reports estimated climate–output response functions and damage projections. Section §4 discusses the results and limitations.

2 Methods

2.1 A simple theoretical framework

Where do we stand theoretically? Climate change is inherently a global public good problem, affecting all productive units and locations (Schlenker and Walker, 2016). The absence of a formal *control group* has important implications for impact evaluation, whether historical or projected.

A pioneering formalization of cross-climatic damage aggregation was proposed by Burke et al (2015), which we use as the foundation of our framework. Their model shows how highly non-linear productivity changes at short timescales, across many micro-units, scale up to generate macroeconomic responses over longer periods.

Consider a typical macroeconomy partitioned into industries indexed by i. All individual units within an industry are assumed to respond homogeneously to temperature

shocks.[3] Production occurs across locations ℓ and countries $\mathcal{L}$, where countries are large clusters of locations. Micro-level moments (hours) are indexed by t, and longer periods (years) are indexed by τ. Following Deryugina and Hsiang (2014), capital K_i and labour L_i in each industry have respective productivities A_i^K and A_i^L, which depend on instantaneous temperature $T_{\ell,t}$. The total capital and labour allocated to industry i can vary with temperature. Let p_i denote the output price, and α a constant in this stylized production function. For a sub-unit at location ℓ and time t, production is:

$$Y_{i,\ell,t}(T_{\ell,t}) = p_i \left(A_i^K(T_{\ell,t}) K_{i,\ell,t}(T_{\ell,t})\right)^{\alpha} \left(A_i^L(T_{\ell,t}) L_{i,\ell,t}(T_{\ell,t})\right)^{1-\alpha} \tag{1}$$

Capital and labour reallocation across locations is assumed to be slow. Total labour allocation varies with temperature and is captured through A_i^L, since labour mobility across industries is limited (Graff Zivin and Neidell, 2014). In competitive equilibrium, the capital-to-labour ratio satisfies $\frac{K_{i,\ell,t}}{L_{i,\ell,t}} = \frac{\alpha}{1-\alpha}$, implying constant returns to scale. Define $U_{i,\ell,t} = p_i K_{i,\ell,t}^{\alpha} L_{i,\ell,t}^{1-\alpha}$ as a scalar measure of resources allocated to industry i at location ℓ and time t. Equation (1) can be rewritten as:

$$Y_{i,\ell,t}(T_{\ell,t}) = \underbrace{\left(A_i^K(T_{\ell,t})^{\alpha} A_i^L(T_{\ell,t})^{1-\alpha}\right)}_{f_i(T_{\ell,t})} p_i \, K_{i,\ell,t}^{\alpha} \, L_{i,\ell,t}^{1-\alpha} = f_i(T_{\ell,t}) \, U_{i,\ell,t} \tag{2}$$

The function $f_i(T_{\ell,t})$ captures how productivity in industry i responds to instantaneous temperature. The framework assumes additive separability across sectors and regions. Firms are treated as independent units, although significant climate changes can produce emergent effects through inter-firm spillovers and price dynamics. For example, supply chain disruptions may amplify economic consequences beyond the direct exposure of individual units. If these effects cross borders, country-specific analyses may underestimate the broader economic impacts.

Aggregate output, such as GDP, sums production across industries and integrates over all locations and times:

$$Y_{\mathcal{L},\tau} = \sum_i Y_{i,\mathcal{L},\tau} = \sum \int_{t \in \tau} \int_{\ell \in \mathcal{L}} f_i(T_{\ell,t}) U_{i,\ell,t} \, d\ell \, dt \tag{3}$$

[3] This simplifying assumption ignores heterogeneity in, for example, energy demand responses, which depend on (*i*) individuals' sensitivity to weather; (*ii*) the intensity of climate shifts; and (*iii*) building and indoor adaptation characteristics (Romitti and Sue Wing, 2022).

The spatial and temporal distribution of $U_{i,\ell,t}$ determines the temperatures experienced by individual units. Within country $\mathcal{L}$ and year τ, the marginal distribution of temperature exposure in industry i is denoted by $g_i(\cdot)$. The distribution is centered at zero and can be shifted by the country-average temperature $\overline{T}\mathcal{L}, \tau$. Then $g_i(T - \overline{T}\mathcal{L}, \tau)$ represents the histogram of temperatures experienced by units U_i. When the shape of $g_i(\cdot)$ is stable across countries and years, it has two key properties. First, the total quantity of productive units M_i is the integral over all temperatures:

$$M_i = \int_{-\infty}^{\infty} g_i(T - \overline{T}_{\mathcal{L},\tau})dT = \int_{t\in\tau}\int_{\ell\in\mathcal{L}} U_{i,\ell,t}d\ell dt \tag{4}$$

Second, $g_i(\cdot)$ reflects the spatial and temporal distribution of units:

$$\int_{-\infty}^{x} g_i(T - \overline{T}_{\mathcal{L},\tau})dT = \int_{t\in\tau}\int_{\ell\in\mathcal{L}} U_{i,\ell,t}1[T_{\ell,t} < x]d\ell dt \tag{5}$$

Aggregate production can then be expressed in terms of the average temperature $\overline{T}_{\mathcal{L},\tau}$ and $g_i(\cdot)$:

$$Y(\overline{T}_{\mathcal{L},\tau}) = \sum_i Y_i(\overline{T}_{\mathcal{L},\tau}) = \sum_i \int_{t\in\tau}\int_{\ell\in\mathcal{L}} f_i(T_{\ell,t})U_{i,\ell,t}d\ell dt \tag{6}$$

$$= \sum_i \int_{t\in\tau}\int_{\ell\in\mathcal{L}} f_i(T)g_i(T - \overline{T}_{\mathcal{L},\tau})dT \tag{7}$$

If the shape of $g_i(\cdot)$ is relatively homogeneous across periods, $\overline{T}\mathcal{L}, \tau$ is a sufficient statistic for temperature exposure. Burke et al (2015) show that one can collapse the joint spatial and temporal distributions of temperatures and productive units into $g_i(\cdot)$ and the location parameter $\overline{T}\mathcal{L}, \tau$ — the country's annual average temperature. This parameter serves as the primary regressor in the empirical framework.

Let $f_i(T)$ denote the productive contribution of an individual unit in industry i relative to instantaneous temperature T. For a given country, period, and industry, let m_{i1} be the fraction of unit-hours below a critical threshold and m_{i2} the fraction above it. The distribution of unit-hours across all temperatures is $g_i(T - \overline{T})$, centered at $\overline{T}$. Productivity losses in a single unit-hour are assumed to have limited spillovers, so aggregate production equals the sum over industries and unit-hours:

$$Y(\overline{T}) = \sum_i Y_i(\overline{T}) = \sum_i \int_{-\infty}^{+\infty} f_i(T) \cdot g_i(T - \overline{T}) dT \tag{8}$$

As $\overline{T}$ rises, m_{i2} increases for all productive units that fall inside the warming country. This growing number of hours beyond the temperature threshold imposes gradual but increasing losses on total output $Y(\overline{T})$. Equation (8) predicts that $Y(\overline{T})$ is a smooth concave function. Its derivative is the average of $f_i'(T)$ weighted by the number of unit-hours at each temperature. The peak of $Y(\overline{T})$ occurs below the critical threshold in $f_i(T)$ if the slope above the threshold is steeper than below, consistent with micro-scale evidence (Schlenker and Roberts, 2009). This challenges the assumption that macroeconomic responses directly mirror highly non-linear micro-level responses (Hsiang, 2010; Heal and Park, 2013). Transient productivity shocks may also influence long-term output trajectories by affecting investment in productive assets (Dell et al, 2012; Hsiang and Jina, 2014).

How can we empirically test these derivations? We use panel data on geo-economic production matched to historical meteorological fields from 1970–2018. We extend the Burke et al (2015) country-level econometric model to sub-national regions, following Kotz et al (2024). Ideally, one would compare two identical regions, one exposed to an exogenous temperature increase and the other not, to observe causal impacts. Since such a counterfactual is unobservable, we approximate it by leveraging temporal variability within the same region. Years with anomalously high temperatures serve as the "treatment," while cooler years serve as the "control" (Burke et al, 2015). This within-region, over-time approach avoids the confounding dynamics that undermine the literature on cross-sections (Nordhaus, 2006).

2.2 Data

Our analysis brings together four sets of data:

Historical country-level GDP records. Countries' annual real (inflation-adjusted) per capita GDP series are taken from the Penn World Tables version 10.01[4] (Feenstra et al, 2015), sub-setting 1970-2020 years for 166 economies, from which we compute the first differences of the natural logarithmic transformation. As a robustness, we al-

[4]Available at: https://www.rug.nl/ggdc/productivity/pwt/?lang=en

ternatively process and collect World Development Indicators (WDI) data for identical macroeconomic variables, sample of countries and time periods.

Historical gross regional GDP records. Administrative areas' gross regional product per capita data are taken from the MCC-PIK Database of Subnational Economic Output (DOSE)[5] (Wenz et al, 2023). Its most recent version provides harmonized data on reported economic outputs from 1,661 subnational regions across 83 countries with varying temporal coverage from 1960 to 2019 from which we subset 1970-2018 years. Sub-national units constitute the first administrative division below national. Recent work has used interpolation and downscaling to yield estimates of sub-national economic output at a global scale, but respective data sets based on official, reported values only are lacking. Wenz et al (2023) instead assembled values from numerous statistical agencies and yearbooks prior to apply harmonisation methods free of linear interpolations for both aggregate and sectoral output. Resulting records have been shown to be temporally- and spatially-consistent in regional boundaries, enabling coherent matches with geo-spatial climatic fields. Following the general literature (Gennaioli and La Porta, 2014; Kalkuhl and Wenz, 2020; Kotz et al, 2021, 2022) and most particularly Kotz et al (2024), we focus on real subnational output per capita and convert values from local currencies to US dollars to account for diverging national inflationary tendencies and then account for US inflation using a US deflator. Conversions between currencies are conducted using exchange rates from the FRED database of the Federal Reserve Bank of St. Louis[6] and the national deflators from the World Bank[7].

Historical weather exposures. Countries' and administrative regions' climate exposures are calculated based on 3-hourly 0.25 degree gridded surface temperature and precipitation fields from NASA's Global Land Data Assimilation System[8] (GLDAS—Rodell et al, 2004). GLDAS is a new generation global high-resolution reanalysis data product developed jointly by the National Aeronautics and Space Administration (NASA), Goddard Space Flight Center (GSFC) and National Centers for Environmental Prediction (NCEP) (Ji et al, 2015). GLDAS incorporates satellite and ground-based observations, producing consistent quality-controlled long global gridded time series of

[5]Available at: https://zenodo.org/records/7659600
[6]Available at: https://fred.stlouisfed.org/series/AEXUSEU(2022)
[7]Available at: https://data.worldbank.org/indicator
[8]Available at: https://ldas.gsfc.nasa.gov/gldas

optimal fields of land surface states and fluxes in near real time; while making available other meteorological variables that are not commonly available in other reanalysis data products either as consistent long time series, or at a high-spatial resolution[9]. GLDAS 0.25 degree fields are then collapsed into daily meteorological records over 1970-2018, and matched to the spatial and temporal resolution of our GDP realizations using a two-stage method.

Land-surface reanalyses provide some of the most robust historical climate data, combining model simulations with observations through data assimilation to maximize observational coverage and reduce limitations of purely model-based outputs (Dee et al, 2011). Although their spatial resolution is finite, it remains high for global coverage. Higher-resolution simulations, such as Regional Climate Models (RCMs), are computationally intensive and limited in extent, and very high-resolution models (e.g., convection-permitting simulations below 4 km) require explicit representation of additional processes, introducing further challenges and uncertainties.

First, we spatially aggregate the 0.25 degree grid-cell-level[10] (x) weather exposure estimates to the administrative level (i) of GRP records (i.e., level 1 provinces) and GDP records (i.e., level 0 countries) by day (d), using the population weighting method[11] presented below.

We use our network of NASA's GLDAS 0.25 deg. coordinates to compute time-invariant weights (w) from high-resolution population density estimates ($D_{x,w}$), derived from downscaled, time-invariant 2015 data in the Gridded Population of the World raster dataset[12] (updated version) (CIESIN, 2004). Each country or province (i) is linked to all NASA GLDAS centroids (x) that fall within its boundaries. The population-density-weighted daily (d) average weather for country/region i, for example the temperature component ($T_{i,d}$), is then computed from grid-cell-level daily

[9]Other reanalysis data products available have either (i) a coarser spatial resolution (e.g. ECMWF-ERA40 and JRA-55, both available from the mid-1950s but at 1.125 deg.) or (ii) a shorter time series (e.g. newly released ECMWF-ERA5 at 0.281 deg. from 1979–present day and NCEP-CFSv2 at 0.205 deg. from 2011–present day).

[10]Latitude (Y) and longitude (X) values are concatenated (Y_X) to generate a grid-cell string variable uniquely identifying each 0.25 deg. resolved location of weather records; denoted x hereafter.

[11]We alternatively test the unweighted approach to straightforwardly aggregate NASA's GLDAS grid-cell-level information to the spatial resolution of our GDP records. Estimated responses, available upon request, exhibit slightly weaker statistical power and are less reliable as they do not account for the heterogeneously distributed populations within countries.

[12]Available at: https://sedac.ciesin.columbia.edu/data/collection/gpw-v4

climate values ($T_{x,d}$) matched with location-specific population densities (D_x):

$$T_{i,d} = \frac{\sum_{x \in i} D_x \, T_{x,d}}{\sum_{x \in i} D_x} \tag{9}$$

Second, resulting daily (d) weather records matching each country/region-day are collapsed to the yearly frequency of our GDP observations t. We thus compute annual measures of heat and moisture exposures –i.e., average temperature values ($\overline{T}_{i,t}$ in deg. C) and cumulative precipitation (in mm/year); are matched to each country/region-year output observation. Our raw estimation dataset contains 166 countries $\times$ year (∼9,000 obs.) and 1,661 administrative region $\times$ year (∼82,000 obs.) spanning 1970-2018.

Simulations of climate change driven shifts in average temperature exposure. This corresponds to *the* central component of chronic physical climate risk. We conduct a large-scale processing of high-resolution time- and spatially downscaled climate forecasts from NASA's Earth Exchange Global Daily Downscaled Projections (NEX-GDDP CMIP6). NEX-GDDP CMIP6 is an ensemble of 29 distinct global climate models (GCMs) simulated under the Coupled Model Intercomparison, Phase VI (CMIP6—Eyring et al, 2016) exercise, whose outputs are biased-corrected and downscaled to a 0.25 deg. grid[13]. Temperature projections are truncated to the historical geographic extents of the GDP realizations, and used to calculate variables, as in the estimation dataset, for years in the historical (1980-2010[14]) and future epochs (2021-2040, 2031-2050, ..., 2099) under vigorous and moderate warming scenarios (SSP5-8.5 and SSP2-4.5, respectively).

To account for uncertainty in the temporal realization of scenario-based temperature projections, we first average GCM-specific simulated temperatures over 20-year windows centered on our mid-points of interest. For example, the 2041–2060 average is considered a more robust estimate of expected 2050 conditions than the GCM-simulated value for 2050 alone. We then compute the difference between current and future epoch means to derive the 'Delta' values. These Delta values are used as in-

[13]The raw NetCDF4 files weigh approximately 14TB. Processing and computation stages are performed using a High Performance Computing (HPC) cloud system.

[14]Burke et al (2015)'s baseline growth rate-absent climate change counterfactual assumes climate fixed at its 1980-2010 average. The mid-point (i.e., year 1995) and associated average climate $\overline{T}$ of this counterfactual is approximately equivalent whether we chose 1980-2010 or 1985-2004.

puts to our global GDP model in the projection exercise, which has been previously calibrated using historical responses estimated econometrically in §2.3.

Note that defining climate states using 20-year averaging windows is consistent with current scientific and institutional practice in a non-stationary climate. While 30-year normals remain widely used, major authorities explicitly adopt shorter windows alongside them. NOAA (Arguez et al, 2010) documents both 20- and 30-year climate averages, reflecting the need to balance variability reduction with temporal relevance. The IPCC (2021) AR6 (WG I) standardizes future climate states using 20-year periods (e.g. 2041–2060 and 2081–2100), arguing that such windows are sufficiently long to suppress internal variability while short enough to capture evolving climate trends. Similarly, the WMO (2023)'s *Global Annual to Decadal Climate Update* represents current global warming using a 20-year mean that combines observations and near-term model predictions, explicitly recognizing the limitations of longer windows under non-stationarity. Methodological work further supports this approach: Arguez and Vose (2011) show that traditional 30-year normals can integrate obsolete climate conditions, leading to biased estimates of present or future climates. Together, these points justify the use of 20-year windows as a defensible compromise between statistical stability and responsiveness to climate change.

Burke et al (2015) pointed out that estimates of the economic effects of climate change are GCM-sensitive, and hence, multi-median impacts should be simulated from a wide ensemble of GCMs. Other sources of uncertainty propagation are attributable to downscaling and bias-correction which can potentially alter local climate projections in CMIP6 (Lafferty et al, 2023). A final concern is that a subset of CMIP6 GCMs may be "too hot", with representations of cloud feedbacks in some models associated with higher-than-consensus global surface temperature response to doubled atmospheric CO_2 concentrations—equilibrium climate sensitivity (ECS) and global warming after 70 years of a 1% per annum increase in CO_2—transient climate response (TCR) (Sherwood et al, 2020; Tokarska et al, 2020; Zelinka et al, 2020; Hausfather et al, 2022). To mitigate the threat of bias potentially introduced by this phenomenon, we follow Hausfather et al's (2022) recommended procedure of excluding models with TCR and ECS outside "likely" ranges (1.4-2.2°C, 66% likelihood, and 2.5-4°C, 90%

likelihood, respectively). That leaves us with 15 "likely" GCMs[15] that form the basis of our impact projections.

Maps of 2000-2015 linear trends in temperature and precipitation (i.e., expressed as the ratio of the total trend for the 16-year period [°C per 16 years] normalized by the historical standard deviation σ of year-to-year fluctuations for the period 1985-2015) in each of the 249,000 unique 0.25 × 0.25 grid-cells from NASA's Global Land Data Assimilation System (GLDAS) and covering all land surfaces globally are provided in Fig. 1. Looking forward, one could construct an ensemble of absolute temperature changes (Δ) to characterize the spatial distribution of climatically driven shifts in average temperature under both the SSP2-RCP4.5 and SSP5-RCP8.5 scenarios. This would be obtained by computing inter-epoch differences between the multi-GCM median of 20-year centered mean future epochs—namely 2021–2040 (midpoint 2030), 2031–2050 (midpoint 2040), ..., 2080–2099 (midpoint 2090)—and the local historical baseline over 1985–2004. The calculation would be performed for each 0.25 × 0.25 grid cell in the NEX-GDDP CMIP6 dataset, thereby providing a spatially explicit estimate of projected temperature shifts relative to historical conditions.

[15]The exhaustive list of 15 "likely" models that we subset from the full *ensemble* of 29 GCMs is provided in Table A.1.

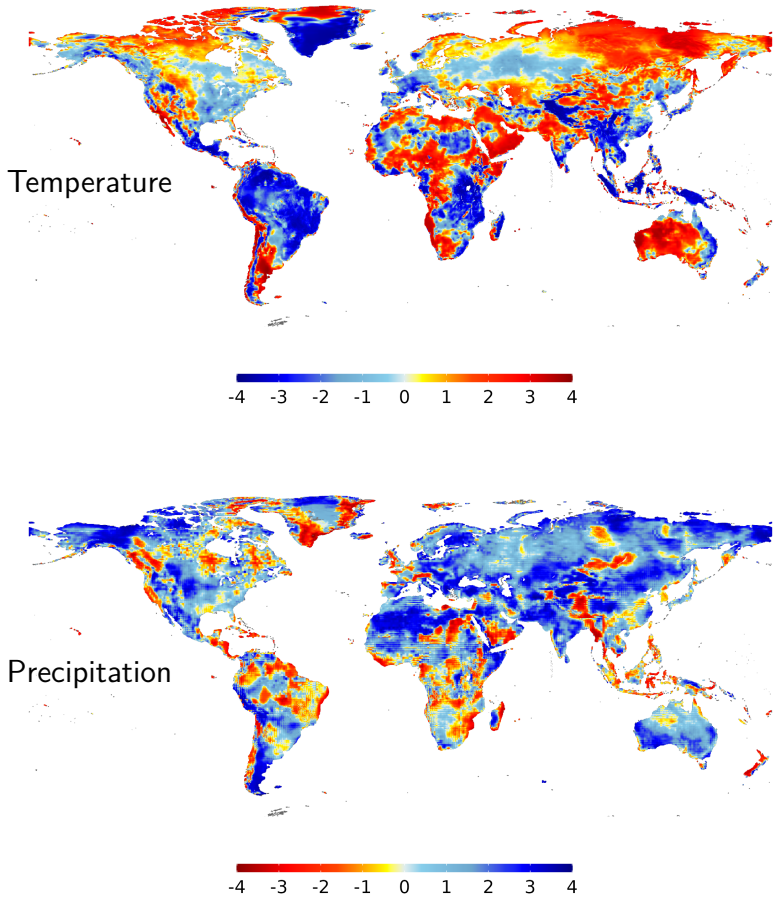

Figure 1: Maps of the 2000-2015 linear trend in average temperature (top-panel) and precipitation (bottom-panel) in each of the 249,000 unique 0.25 × 0.25 grid-cells from NASA's Global Land Data Assimilation System (GLDAS) and covering all land surfaces globally.

For each grid cell, trends are computed as the ratio of the trend effect estimated via a linear model (lm) over a 16-year period (i.e., $\hat{\beta} \times 1$ year $\times 16 = °C$ per 16 years), normalized by the historical standard deviation (σ) of year-to-year average weather-component fluctuations over the period 1985–2015. For instance, a temperature trend of 1.0 indicates that temperatures at the end of the period are $1.0\,\sigma$ higher than at the beginning of the period. This metric locally captures the magnitude of observed historical warming relative to what the cell has *normally* experienced.

2.3 Econometric modeling of historical responses

We first empirically model the responses of per capita GDP to weather (temperature and precipitation) using a 49-year longitudinal sample of 166 countries covering the most recent period. A panel fixed-effects (FEs) OLS model is employed, following specifications commonly used in the climate economics literature (Schlenker and Roberts, 2009; Burke et al, 2015; Kotz et al, 2024).

Indices i and t denote countries and years, respectively. Historical data provide annual observations of the first-differenced natural logarithm of per capita GDP (ΔY), representing per-period growth rates in income. We decompose the factors potentially affecting these changes via a polynomial function of temperature and a quadratic function of cumulative precipitation (P). The benchmark empirical model is:

$$\Delta y_{i,t} = \Delta \ln Y_{i,t} = \mu_i + \nu_t + f[t; \Theta_{z(i)}] + f_T(T_{i,t}) + \lambda_1 P_{i,t} + \lambda_2 P_{i,t}^2 + \epsilon_{i,t}. \tag{10}$$

Country-specific constants μ_i (fixed effects) capture unobserved, idiosyncratic, spatially-varying, time-invariant influences such as history, culture, or topography. Given the long span of the dataset, attributing year-to-year, plausibly exogenous variations in per capita income to weather allows the use of low-frequency controls such as year fixed effects ν_t, which account for abrupt global events (e.g., shocks to energy markets or global recessions) without over-controlling for cyclical temperature fluctuations.

In addition to year dummies, gradual changes in individual countries' growth rates, driven by slowly evolving factors (e.g., demographic shifts, trade liberalization, and political institutions), are captured by flexible time trends (Dell et al, 2012). These trends are formalized as $f[t; \Theta_{z(i)}]$, a zone-specific[16] function of time that captures unobserved, country- or region-specific time-varying dynamics influencing per capita income and correlated with climate. To implement this, we use the Database of Global Administrative Areas (GADM)[17] , intersecting grid-cell coordinates with subnational administrative region identifiers. Output is provided at GID(0), GID(1), and GID(2) levels for countries, provinces, and counties/districts, respectively. Finally, $\epsilon_{i,t}$ denotes

[16] Zones start at unity ($z(i) = 1$ for a country) and may extend to economic, trade, or geographic clusters of countries likely to share common trends.

[17] Available at: https://gadm.org/data.html

a random disturbance term capturing variations in per capita GDP orthogonal to both time and local climate conditions.

Our methodology simultaneously accounts for both persistent (time-invariant) and transient (time-varying) determinants of output, offering a more robust framework than approaches relying solely on observed covariates. Traditional regressions conditioning on explicit controls (e.g., demographic, political, or institutional variables) are vulnerable to mismeasurement and fail to accommodate heterogeneous effects across countries. In contrast, our specification allows these factors to affect each country's GDP level differently over time without requiring explicit modeling of each covariate. For instance, demographic trajectories may evolve non-linearly and vary in magnitude and timing across countries, and their measurement may be imperfect. Our model absorbs such heterogeneity, capturing the net influence of these trends on output even in the presence of measurement error. Moreover, many standard control variables are potentially endogenous to climatic shocks. Including them naively can introduce bias, a phenomenon often referred to as "bad control" (Angrist and Pischke, 2009; Hsiang et al, 2013). By relying on a fixed-effects structure with flexible temporal components, our approach mitigates these risks and produces estimates of climate impacts that are robust to omitted variable bias and confounding from mismeasured or climate-responsive controls.

The parameters of interest are the per capita GDP growth impacts of the potentially non-linear effects of heat, captured by $f_T(T_{i,t})$, and precipitation (λ). Idiosyncratic changes in local annual temperatures have been shown to correlate with variations in precipitation (Auffhammer et al, 2013). We begin by estimating $f_T(T_{i,t})$ using the simple quadratic specification in Eq. (11), and subsequently explore more flexible functional forms (see §2.5).

$$f_T(T_{i,t}) = \beta_1 T_{i,t} + \beta_2 T_{i,t}^2 \tag{11}$$

We then transpose this econometric framework to a spatially-downscaled structure, using the same variable parametrization as in Eq. (10). Indices r and t denote 1,661 subnational administrative regions at level I (GID(1)) and years. The panel FEs specification becomes:

$$\Delta y_{r,t} = \Delta \ln Y_{r,t} = \mu_r + \nu_t + f[t; \Theta_{z(i)}] + f_T(T_{r,t}) + \lambda_1 P_{r,t} + \lambda_2 P_{r,t}^2 + \epsilon_{r,t} \quad (12)$$

The remaining structure of this augmented model is identical to the baseline in Eq. (10). Although the motivating micro evidence focuses on the effect of temperature on output levels, we explicitly model the effect of temperature on output growth (Δ) because measures of GDP within a country exhibit extremely high serial correlation ($\rho = 0.999$). These time series are nearly indistinguishable from a random walk (i.e., they present a unit root), which can lead to spurious estimates and invalid test statistics (Granger and Newbold, 1974; Angrist and Pischke, 2009; Hsiang et al, 2013).

Using first-differenced GDP or GRP values, combined with year fixed effects and country-specific quadratic growth trends, reduces serial correlation in the outcome to a much lower level ($\rho = 0.125$), besides ultimately enabling projections of damages on growth first rather than level. Some residual serial correlation persists even after differencing. To address this, we cluster standard errors at the country level following (Cameron et al, 2011), accounting for spatial correlation and arbitrary autocorrelation patterns within each location.

In this framework, as for countries in Eq. (10), each administrative area is allowed its own level and non-linear growth trend. The effect of temperature on growth is identified from deviations within each region relative to its trend. Controlling for trends and convergence in incomes using location-specific trends has been shown to outperform autoregressive models (Barro, 2003; Hsiang and Jina, 2014).

2.4 Shock persistence and heterogeneous effects

Transitory versus persistent productivity effects. High-frequency temperature realizations are typically interpreted as affecting economic performance through contemporaneous fluctuations in growth rates, as formalized in Eq. (10). However, in settings characterized by persistent growth dynamics (i.e., unit-root properties of output), climatic disturbances can induce long-lasting deviations in income paths. Two non-mutually exclusive mechanisms underpin such persistence. First, temporary growth shocks can alter future capital accumulation trajectories, an effect that may be amplified when

physical climate risk diverts resources toward costly adaptation investments (Pindyck, 2013). Second, temperature changes may directly impact the rate of technological progress—the fundamental engine of long-run growth in canonical models—through, for example, adverse impacts of heat exposure on cognitive performance and innovative capacity (Graff Zivin et al, 2018; Dell et al, 2014).

When climate-induced temperature shocks translate into permanent growth effects, the macroeconomic implications of climate change are substantially magnified, as even modest differences in annual growth rates compound into large divergences in income over long horizons. Distinguishing between level effects and growth effects is therefore central for welfare analysis and optimal policy design (Moore and Diaz, 2015). Following the empirical strategy of Dell et al (2012), we augment Eq. (12) with lagged temperature terms to explicitly test for the temporal persistence of temperature impacts on output. We include lagged temperature effects up to $K = 5$ years, where $k = 0$ corresponds to the contemporaneous effect. For simplicity, all models in the remainder of this subsection are presented at the country level i, although equivalent specifications exist (and are tested) at the subnational level r.

$$\Delta y_{i,t} = \Delta \ln Y_{i,t} = \mu_i + \nu_t + f[t; \Theta_{z(i)}] + \sum_{k=0}^{K} f_T^{(k)}(T_{i,t-k}) + \lambda_1 P_{i,t} + \lambda_2 P_{i,t}^2 + \epsilon_{i,t} \quad (13)$$

A concern is that the base specification in Eq. (10) and Eq. (12) could implicitly assume an absence of adaptation. In fact, under a fixed-effects framework with a linear temperature term, identification exploits only within-country deviations from long-run mean climate, which are inherently difficult for agents to anticipate. When temperature enters the model non-linearly, however, identification draws jointly on within- and between-country variation. As shown by McIntosh and Schlenker (2006), this structure allows countries with different long-run climate conditions to display heterogeneous sensitivities to short-run temperature shocks. Consequently, the model implicitly captures historical adaptation to prevailing climate conditions, while still treating interannual temperature variability as largely unanticipated. In projections, increases in a country's mean temperature are therefore mapped to empirically observed responses of other countries operating at comparable temperature levels. A formalization of of this

assumption is provided in § A.2; see also McIntosh and Schlenker (2006).

The global response function $f_T(\cdot)$. A core assumption of the pooled framework is that a single global temperature–response function $f_T(\cdot)$ governs all observational units. We evaluate this assumption by estimating the model across multiple subsamples. This aims to answer the following questions. Does the non-linear pattern documented in Fig. 2 reflect a genuinely global relationship? Or does it instead arise from compositional differences between hot, low-income economies and cooler, high-income ones? If the former is true, it would suggest the existence of pronounced structural instability in $f_T(\cdot)$. Additionally, one may test an interaction-based specification where temperature enters the model linearly. Its marginal effect is allowed to vary systematically with long-run climatic conditions and income levels,

$$f_T(T_{i,t}) = \left(\beta_1 + \beta_2 \overline{T}_i + \beta_3 \overline{Y}_i\right) T_{i,t} \tag{14}$$

$\overline{T}i$ and $\overline{Y}i$ denote the long-run average temperature and the long-run average (log) GDP per capita of country i, respectively. In the absence of income-related heterogeneity (i.e., $\beta_3 = 0$), a globally concave temperature–response function consistent with Fig. 2 is characterized by $\beta_1 > 0$ and $\beta_2 < 0$, implying that marginal temperature impacts decline as baseline climatic conditions become warmer. By contrast, if the observed non-linearity primarily reflects income-related heterogeneity, where poorer countries are both hotter and more sensitive to temperature, then including income interactions should reduce the temperature–climate effect, yielding $\beta_2 = 0$, $\beta_1 < 0$, and $\beta_3 > 0$. This pattern would imply that temperature damages decrease as income rises.

Responses may be significantly differentiated across income groups. To evaluate this hypothesis, we allow temperature effects to differ between them by estimating group-specific response functions. Temperature and precipitation variables in Eq. (10) are allowed to vary according to whether a country's purchasing-power-parity-adjusted (PPP)[18] per capita income was below the global median in 1990. Let $D_i = 1$ denote countries below this threshold and $D_i = 0$ otherwise. The temperature response function is then written as:

[18]PPP measures adjust incomes for cross-country price differences.

$$f_T(T_{i,t}) = (1 - D_i)\left(\beta_1 T_{i,t} + \beta_2 T_{i,t}^2\right) + D_i\left(\beta_3 T_{i,t} + \beta_4 T_{i,t}^2\right) \tag{15}$$

Under this specification, (β_1, β_2) describe the temperature response for higher-income countries, whereas (β_3, β_4) characterize the response for lower-income countries. Equality of the two response structures corresponds to the joint null hypothesis $(\beta_1, \beta_2) = (\beta_3, \beta_4)$. Rejection of this hypothesis indicates systematic non-homogeneity in output sensitivity to temperature across income groups.

2.5 Empirical uncertainty

We account for empirical uncertainty by varying the functional form (FF) of the (i) temperature component and (ii) and the specification fixed effects.

FF of the temperature-GDP response function. Given the considerable uncertainty surrounding the shape of the temperature–GDP response function, we test multiple specifications to capture its potential impact on output. Both historical and projected economic effects are expected to be largest at temperate extremes. The quadratic functional form in Eq. (11) captures this convexity, allowing the marginal impact of a given temperature change to vary across locations. In addition, we explore more flexible functional forms to better characterize the temperature effect.

Why? This is because linear fixed-effects models estimate consistent marginal parameters under unobserved heterogeneity. The identification is solely driven by deviations from the group mean, equivalent to jointly demeaning the dependent and all independent variables. Introducing a quadratic term modifies the identification, which then draws on both within-unit variation over time and between-unit variation in means (McIntosh and Schlenker, 2006). Because it is unclear whether a standard quadratic fixed-effects model relies solely on within-unit variation, estimating climate impacts on output first requires considering higher-order polynomial functions.

To this end, we test higher polynomial orders in a parametric FE-OLS framework, as described in §2.3. We also estimate restricted cubic splines with 2–7 semi-parametric knots to capture potential N-shaped relationships. Finally, non-parametric smoothed splines are fitted via Generalized Additive Models (GAM) (Wood, 2004), including location and time fixed effects. The system of equations below presents both country-

level (top, extending Eq. 10) and administrative region-level (bottom, extending Eq. 12) specifications.

$$\begin{cases} \mathbb{E}\left[\ln Y_{i,t(i)}\right] = \Psi^T\left[\mathcal{T}_{i,t(i)}; \boldsymbol{\theta}^T\right] + \mu_i + \nu_t + f[t; \Theta_{z(i)}] \\ \mathbb{E}\left[\ln Y_{r,t(r)}\right] = \Psi^T\left[\mathcal{T}_{r,t(r)}; \boldsymbol{\theta}^T\right] + \mu_r + \nu_t + f[t; \Theta_{z(r)}] \end{cases} \tag{5}$$

To clarify the structure underlying Eq. (5), the temperature response function $\Psi^T(\cdot)$ is modeled as a smooth function of temperature that minimizes parametric assumptions. In practice, $\Psi^T(\cdot)$ is represented as a linear combination of spline basis functions:

$$\Psi^T\left(\mathcal{T}_{u,t}; \boldsymbol{\theta}^T\right) = \sum_{k=1}^{K} \theta_k^T \, B_k(\mathcal{T}_{u,t}) \,, \tag{16}$$

$u \in \{i, r\}$ indexes countries or administrative regions, $B_k(\cdot)$ denote spline basis functions (e.g. cubic regression or thin-plate splines), $\boldsymbol{\theta}^T$ is a vector of unknown coefficients, and K is the dimension of the spline basis. Estimation proceeds via penalized least squares. The objective function solved by the Generalized Additive Model (GAM) estimator is:

$$\min_{\boldsymbol{\theta}^T, \mu, \nu} \sum_{u,t} \left(\ln Y_{u,t} - \Psi^T\left(\mathcal{T}_{u,t}; \boldsymbol{\theta}^T\right) - \mu_u - \nu_t - f\left(t; \Theta_{z(u)}\right)\right)^2 + \lambda \, \boldsymbol{\theta}^{T\prime} \mathbf{S} \boldsymbol{\theta}^T, \tag{17}$$

$\mathbf{S}$ is a known penalty matrix governing spline curvature and λ is a smoothing parameter selected by generalized cross-validation (Wood, 2004). The fitted temperature response function is then given by:

$$\widehat{\Psi}^T(\mathcal{T}) = \sum_{k=1}^{K} \widehat{\theta}_k^T \, B_k(\mathcal{T}), \tag{18}$$

The fitted temperature splines, denoted $\widehat{\Psi}^T(\mathcal{T}) = \Psi^T(\mathcal{T}; \widehat{\boldsymbol{\theta}}^T)$, are subsequently combined with historical average temperatures and future scenario-dependent temperature trajectories to generate both retrospective and forward-looking physical risk-induced damage estimates; first on productivity growth, second on the level of GDP per capita (by compounding cumulatively the former over time).

Moreover, we complement our empirical approach with a panel version of Eq. (10)

that links per capita income to a broader range of temperature exposures across the full distribution. Instead of using cumulative degree days (base 0°C) aggregated by year, we construct a vector of dummies counting the number of days in each country-year in which the daily mean temperature falls within the j_T^{th} of twelve 3°C bins (0–3, 3–6°C, etc.): $\sum_{j_T} \Phi^T\left(T_{i,t}^{j_T}\right)$. This quantile-bin approach reduces parametric assumptions while imposing a single functional restriction: the impact of daily mean temperature on annual GDP is constant within each 3°C interval. The choice of twelve bins reflects a balance between flexibility and precision, allowing the data, rather than parametric assumptions, to determine the temperature–income relationship while maintaining empirically robust estimates.

Finally, we evaluate a more parsimonious specification that isolates the contribution of extreme temperatures by focusing exclusively on the lower and upper tails of the daily temperature distribution, denoted $T_{i,t}^0$ and $T_{i,t}^{12}$, respectively. The remainder of the model retains the same structure as the baseline specifications in Eqs. (10) and (12):

$$\ln Y_{i,t} = f_T\left(T_{i,t}^0, T_{i,t}^{12}\right) + f_P\left(P_{i,t}\right) + \mu_i + \nu_t + f\left[t; \Theta_{z(i)}\right], \tag{19}$$

$f_T(\cdot)$ and $f_P(\cdot)$ denote temperature and precipitation response functions, μ_i and ν_t are country and time fixed effects, and $f[t; \Theta_{z(i)}]$ is a flexible country $\times$ trend function. The next step is to calibrate the most relevant functional form of the fixed effects. This is now what we turn to.

Flexible functional form of fixed effects. Omitted variables that influence both temperature trajectories and economic outcomes may bias estimated effects if not properly accounted for. Starting from a simple linear trend in Eq. (20), we test extensions that allow more flexible evolution of growth over time,

$$f[t; \Theta_{z(r)}] = \Theta_{i,1}\, t, \tag{20}$$

First, we increase the order of Chebyshev polynomials from quadratic to octic, capturing potential non-linearities in country-specific time trends

$$f[t;\Theta_{z(i)}] = \sum_{j=1}^{8} \Theta_{z(i),j}\, t^j, \tag{21}$$

Second, we examine variation in the spatial aggregation of these flexible trends by redefining $z(i)$ to correspond to administrative level I regions, individual countries, or multi-country clusters that may share a common temporal trend.

Our preferred trend specification follows Burke et al (2015) and is quadratic country-specific time trends, $f[t;\Theta_{z(i)}] = \Theta_{i,1}\, t + \Theta_{i,2}\, t^2$. This allows both levels and trends in growth to vary by country.

2.6 A simple annual damage projection framework: the *Delta* method

Our fitted regional GDP model in Eq. (12) facilitates projection of long-run GRP per capita changes associated with climate change-driven shifts in the temperature mean factor. We first provide below a simplified formalization of the base projection framework at the region i level: the Delta method.

Using $\mathbf{w} = \{\bar{T}\}$, we denote the physical risk factor considered here. Recall that in §2.2, we have truncated climate change simulations from GCMs to the *sub-national* geographic extents of *all* provinces i available globally, by intersecting NEX-GDDP CMIP6 grid-cell coordinates with the subnational administrative region GADM identifiers in which they fall; and re-calculated the climate variables of the historical estimation dataset for years in the historical (1995-2014) and future epochs (2026-2100) under moderate (SSP2-RCP4.5) and aggressive (SSP5-RCP8.5) warming scenarios.

Next, we calculate inter-epoch difference between future years and the historical 1995-2014 means and obtain sub-national region shifters ($\Delta\mathbf{w}$) covering most productive provinces globally. These offsets are added to the 1995-2014 historical mean, denoted t^0, of our predictors $\bar{\mathbf{w}}$ in the historical estimation dataset constructed in §2.2.

We may now construct projections of future physical risk. Recall from §2.2 that $\mathbf{w}$ are temporally collapsed by future epochs and spatially aggregated by region i (following concatenating and population density weighting approaches defined prior), simulated from global climate model g under SSP-RCP scenario S,

$$\tilde{\mathbf{w}}_{i,t,g,S} = \bar{\mathbf{w}}_{i,t^0,g,S} + \Delta\mathbf{w}_{i,t,g,S} \tag{22}$$

The latter is combined with our fitted global GRP model to project changes to productivity growth induced by these region-specific *shifters* linked to climate and future epochs. For communication purpose, we simplify the ensemble of physical risk factor-level responses to a semi-elasticity $\widehat{\beta}_s^w$ that comes with a linearly aggregated climate vector—instead of its actual ensemble of parameters derived from our non-linear function of average temperature $f_w^{(\rho)}(\mathbf{w}_{i,t}) = \sum_{\ell=0}^{\rho} f_w(\mathbf{w}_{i,t-\ell})$ in Eq. (13). A simple projection framework at any given future epoch t^* is:

$$\Delta\tilde{y}_{i,t^*,g,S} = \widehat{\mu}_i + \widehat{\nu}_{t^*} + f[t^*; \widehat{\Theta}_{z(i)}] + \widehat{\beta}^{\,w}\, \tilde{\mathbf{w}}_{i,t^*,g,S} \tag{23}$$

And our historical benchmark at period t^0:

$$\Delta y^0_{i,t^0,g} = \widehat{\mu}_i + \widehat{\nu}_{t^0} + f[t^0; \widehat{\Theta}_{z(i)}] + \widehat{\beta}^{\,w}\, \bar{\mathbf{w}}_{i,t^0,g} \tag{24}$$

Facilitating the computation of our primary impact metric: the projected fractional change (%) in GRP per capita growth as the inter-epoch difference $\left(\Delta\tilde{y}_{i,t^*,g,S} - \Delta y^0_{i,t^0,g}\right)$ in outputs; such that the sub-national region × future epoch × GCM × climate scenario combination of climate shift-induced % change in GRP per capita growth can be computed as:

$$\Psi_{i,t^*,g,S} = \widehat{\beta}^{\,w} \left(\tilde{\mathbf{w}}_{i,t^*,g,S} - \bar{\mathbf{w}}_{i,t^0,g}\right) \tag{25}$$

Where $\tilde{\mathbf{w}}_{i,t^*,g,S} = \overline{\mathbf{w}}_{i,t^0,g} + \Delta\mathbf{w}_{i,t^*,g,S}$; and $\overline{\mathbf{w}}_{i,t^0,g}$ denotes the average climate in region i between 1995-2014 (i.e., the historical or base period). This leaves us with a wide *ensemble* of i region-specific projected damages, denoted $\Psi_{i,t^*,g,S}$, available globally. These are distributed across future epochs $t = t^* > t^0$ (2026–2100), GCMs $g \in \mathcal{G}$ (15 "likely" subset from the raw ensemble of 29 GCMs), and the two SSP-RCP scenarios $S \in \{\text{SSP2-RCP4.5}, \text{SSP5-RCP8.5}\}$.

Region-damages are projected globally over most productive provinces. The simultaneous combination of multi-dimensional granularity—across regions, and years—and comprehensive geographic coverage is a competitive advantage of this paper. This is

also made possible by the burgeoning availability of SSP-RCP-aligned GCM simulations from CMIP6. These offer a unique opportunity to integrate the most achieved time- and spatially downscaled climate change projections into our damage modeling.

Note that unlike Burke et al (2015), our approach does not rely on the constraining assumption of endpoint temperature anchoring combined with deterministic linear interpolation. In their implementation under RCP8.5, Burke et al (2015) extracted CMIP5 GCM projections, computed population-weighted country-level temperatures by averaging across grid cells, and implicitly assumed a linear temperature path between the end of the historical baseline (2010) and the projected country-level temperature in 2100. Formally, for country i, temperatures evolved according to $T_{i,t} = \overline{T}_{i,2010} + \frac{t-2010}{90}\left(\overline{T}_{i,2100} - \overline{T}_{i,2010}\right)$. For example, the implied 2030 temperature became $T_{i,2030} = \overline{T}_{i,2010} + \frac{19}{90} \times 4.8°\text{C}$, where $4.8°\text{C} = \overline{T}_{i,2100} - \overline{T}_{i,2010}$ denotes the population-weighted country-level warming projected for 2100 under RCP8.5. This approach effectively interpolated more than 75 annual observations from only two endpoints (2010 and 2100), thereby imposing a deterministic and linear warming trajectory that abstracts from transient dynamics and model-specific non-linearities embedded in the original GCM outputs. By contrast, our projections of climate change-driven shifts in physical risk factors, because derived from raw daily CMIP6 simulations aggregated by year (see §2.2), (i) do not mechanically interpolate intermediate years; (ii) preserve the temporal structure of climate dynamics; (iii) maintain plausible inter-annual climate variabilities.

2.7 Extrapolative properties

How to predicting damages *where* GRP data are unreported? §2.6 introduces heterogeneity for each sub-national region, leading to equally heterogeneous macroeconomic impacts. Production units within each geography are assumed homogeneously exposed to climate, consistent with the framework described in § 2.1–2.3.

It should be noted that the historical economic dataset alone does not provide a complete geographic coverage globally. But which dataset does? This is an obstacle that the macroeconomic damage literature (Burke et al, 2015; Kotz et al, 2024) has systematically faced. For instance, the global DOSE dataset of reported sub-national

economic output used by Kotz et al (2024) exhibits both temporal and spatial inconsistencies, with coverage restricted to 83 countries. A key characteristic of DOSE is its strict reliance on officially reported macroeconomic data from diverse national statistical offices and yearbooks, as Wenz et al (2023) deliberately excluded interpolation methods to address data gaps. While this approach ensures fidelity to observed values, it also results in discontinuous time series, particularly in under-reported provinces as in some African and Middle-Eastern countries. Moreover, challenges related to administrative boundary consistency persist due to historical changes, which can lead to spatial mismatches when integrating with geospatial climate data.

The solution lies in the extrapolative properties of the damage projection framework presented in §2.6. It allows estimated relationships to be extended beyond the historically observed geographic coverage. Conceptually, Section 2.3 relies on a representative panel of countries (spanning income groups, trade specializations, and climate zones) to estimate a global vector of *semi-elasticities* associated with temperature and precipitation. Following Burke et al (2015), Kalkuhl and Wenz (2020) and Kotz et al (2024), we assume that this transfer function represents a stable manifold describing the global climate–GRP relationship. This transfer function, deemed theoretically appropriate to capture both the sign and the functional form of the global relationship, can be combined with the spatially disaggregated NEX-GDDP CMIP6 climate simulations described in Section 2.2, whose geographic coverage is global.

This approach enables the reconstruction of consistent global coverage across more than 3,672 sub-national regions in 200 countries, while retaining the empirically valid structure of the damage estimates.

2.8 Geometric compounding of annual damages

We have used our historical climate-GRP response-functions to generate annual projected future changes in GRP per capita growth under various SSP-RCP warming scenarios, relative to baseline growth rate-absent climate change (i.e., a no-climate-change counterfactual in which climate and its underlying factors, remain fixed at their 1995-2014 historical means).

In §2.4, we discussed the distinction between transitory and persistent productiv-

ity shocks. The reasons for modelling annual climate damages as having potentially permanent macroeconomic effects (and thus justifying a compounding transformation from physical risk-induced growth deviations) can be outlined in three synthetic points. First, even temporary climate shocks can generate long-lasting deviations in GRP due to the inherently non-stationary[19] nature of output growth. Second, temporary shocks can alter future capital accumulation, particularly when resources are diverted to costly adaptation. Moreover, temperature changes may affect the pace of technological progress because the adaptation of productive systems is endogenous to the climate itself (Pindyck, 2013; Graff Zivin et al, 2018; Dell et al, 2014). Third, because growth effects accumulate over time, even modest reductions in annual growth rates can compound into substantially amplified divergences in income over long horizons. Taken together, these mechanisms motivate the construction of compounded damages.

The parameter $\Psi_{r,t^*,g,S}$ is the predicted annual physical risk-induced deviation in gross regional product per capita growth (i.e., regional productivity growth) in year t^*[20], region i, according to the GCM g simulated under the warming scenario S. We compute the geometric compounding of these annual productivity growth-rate deviations over time, yielding cumulative deviations in the level of GRP per capita (% change), relative to a no-climate-change counterfactual in which climate variables remain fixed at their 1995-2014 historical means (i.e., a baseline-absent climate change). For communication purpose, $\Psi_{i,t^*,g,S}$ can be simplified as $\Psi_{i,t}$ hereafter. The evolution of GRP per capita in region i in year t is given by the recursive form:

$$y_{i,t} = y_{i,t-1} \times \left(1 + \eta_{i,t} + \Psi_{i,t}\right) \tag{26}$$

The GRP growth rate absent climate change is given by $\eta_{i,t}$. This is usually labelled as the 'base', 'baseline' or 'counterfactual' output growth scenario in the literature; and is either taken from the SSPs[21] or preferably calculated as the average growth rate over

[19] Output series, whether country- or regional, often exhibit unit-root properties, implying that shocks—whether climate-related or not—may have permanent effects on levels rather than solely transient deviations from a trend. It has long been recognized that such behaviour entails non-stationarity, high autocorrelation, and low mean-reversion (Phillips and Perron, 1988; Perron, 1989).

[20] The equivalent interpretation is that the parameter $\Psi_{i,t^*,g,S}$ is the predicted *additional effect* of warming on GRP per capita growth in year t^*.

[21] This is combined with population projections from the UN World Population Prospects that we transform to compute per capita-weighted proxies. Country-level projected growth rates are available every five years by SSP; one may linearly interpolate to obtain annual values. Of the three SSP research groups, it is

1995-2014.

Iterating over years, Eq. (26) is mathematically equivalent to a cumulative product form that compounds baseline growth and additional effects year by year, starting from the initial value $y_{i,0}$ at base year $t = 0$,

$$y_{i,t} = y_{i,0} \prod_{k=1}^{t} \left(1 + \eta_{i,k} + \Psi_{i,k}\right) \tag{27}$$

This closed-form geometric compounding produces results whose realism is sensitive to (i) the initial magnitude of annual deviations and (ii) the length of the projection horizon. Regions with initially high zonal annual growth damages and/or projections compounded over a long time horizon may yield implausibly large losses as we approach the end of the century.

Damage estimates presented in the rest of the paper result from this geometric compounding of these annual productivity growth-rate deviations over time, yielding cumulative deviations in the level of GRP per capita (% change), relative to a no-climate-change counterfactual in which climate variables remain fixed at their 1995-2014 historical means (i.e., a baseline-absent climate change).

3 Results

3.1 Empirical results

The panel model results showing the log[GDP per capita] responses to country-level annual average temperature exposure [deg.°C] are presented in Fig. 2.

Parametric FE-OLS results in panel **a** of Fig. 2 indicate that country-level economic output is smooth, non-linear, and concave in temperature. The maximum occurs at 13 °C, below the thresholds reported in micro-level analyses (Schlenker and Roberts, 2009) and consistent with predictions from Eq. (8). Cold-country productivity rises with annual temperature until the optimum. Beyond this point, productivity declines gradually, with the rate of decline accelerating as temperatures increase. Our results closely match Burke et al (2015)'s response function (shown in *blue*) despite differences in macroeconomic data sources and the spatial and temporal resolution of

recommended to use the OECD projections: the only ones available at the country level.

climate fields prior to aggregation. This study uses 3-hourly, 0.25° gridded surface temperature and precipitation fields from NASA's GLDAS (GLDAS— Rodell et al, 2004), collapsed to daily records over 1970–2018 and matched to the period of our macro-output data (§2.2). In contrast, Burke et al (2015) used University of Delaware reconstructions with 0.5° monthly averages over 1960–2010. Both studies account for heterogeneous intra-country population distribution, aggregating grid-cell weather exposure using population-weighted methods based on 2015 Gridded Population of the World data (CIESIN, 2004).

The non-linear temperature-GDP pattern is globally representative and not driven by outliers. It remains robust to heterogeneous response functions across income groups and more flexible functional forms than parametric FE-OLS. Following Burke et al (2015), we use country-by-year fixed effects with quadratic country-specific time trends ($\mu_i + \nu_t + \Theta_{i,1}t + \Theta_{i,2}t^2$). This specification allows non-linear growth paths for each country. Because the dependent variable is the derivative of income, each country has its own level and non-linear trend, and the impact of exogenous temperature and precipitation changes is identified from deviations within countries (McIntosh and Schlenker, 2006). Panel **b** of Fig. 2 shows a non-parametric unrestricted spline of average temperature estimated with a Generalized Additive Model (GAM) (Wood, 2004), confirming the inverted-U shape of the response. This method reduces parametric assumptions while allowing flexible smooth functions. Panel **c** presents a semi-parametric restricted cubic spline with 3–8 knots estimated globally. Knots define points along the predictor range where the shape of the smooth function can change, with each section adjusted to minimize error. Panel **d** extends the quadratic temperature transformation with 3^{rd}–7^{th} polynomial orders while holding the parametric setting constant. All macro-econometric models yield similar non-linear global per capita GDP–temperature response functions. Finally, panel **e** shows that global non-linearity is driven by differences in average temperature, not GDP. Orange dots and lines display the marginal effects of temperature on GDP per capita growth evaluated at each country's mean temperature ($\delta y/\delta T_{i,t} = \hat{\beta}_a + \hat{\beta}_b \cdot \overline{T}_i$) and interactions with average GDP ($\delta y/\delta T_{i,t} = \hat{\beta}_a + \hat{\beta}_b \cdot \overline{T}_i + \hat{\beta}_c \cdot \overline{y}_i$). Estimates are similar, indicating that the non-linear response is not due to hot countries being poorer on average. Panel **f** includes lagged temperature variables ($h(T_{i,t-p})$ with $p = [1, 3]$), showing slightly

varying cumulative marginal effects and suggesting that lagged impacts may influence overall macroeconomic damages. This motivates distinguishing short-term (contemporaneous regressors) and long-term (up to five lags) models. Spatial heterogeneity in temperature-GDP relationships gives additional weight to local climate variability, which matters for understanding the heterogeneous spatial distribution of climate shocks (Mahlstein et al, 2013).

This is now what we turn to. The panel model results showing the log[GDP per capita] responses to administrative province-annual average temperature exposure per year [deg.°C] are presented in Fig. 3.

Parametric FE-OLS findings in panel **a** Fig. 3 suggest that sub-national administrative province-level economic production is smooth, non-linear, and concave in temperature, with a maximum at 13 °C, again below the threshold values recovered in micro-level analyses Schlenker and Roberts (2009) and consistent with predictions from equation (8). Cold-province productivity increases as annual temperature increases, until the optimum. Productivity declines gradually with further warming, and this decline accelerates as average temperature rises.

The most central finding of this section is that panel **a** Fig. 3 exhibits a steeper global response curve than panel **a** Fig. 2. We attribute this difference to the smaller-scale variations in localized climate exposure and intra-country economic heterogeneity captured by our regional model, which are not reflected in country-level estimates. The choice of response curve, whether estimated from country-level or province-level data, has important implications for the projection of losses. This is presented in §3.2.

The remainder of Fig. 3 presents a series of robustness checks validating our regional model. We adapt Burke et al (2015)'s preferred fixed-effects specification to the spatial structure of our econometric model: province-by-year constants plus quadratic province-specific time trends ($\mu_r + \nu_t + \Theta_{r,1}t + \Theta_{r,2}t^2$), serving the same purpose as in Eq. (10). Since the dependent variable is the derivative of income, each province is allowed its own level and non-linear trend in growth. The non-linear pattern in panel **a** of Fig. 3, while not driven by outliers, exhibits an additional turning point (N-shaped) under more flexible functional forms. Panel **b** shows a non-parametric unrestricted spline of average temperature estimated globally using a Generalized Additive Model (GAM) (Wood, 2004), confirming the N-shaped response. Panel **c** presents a semi-

parametric restricted cubic spline, which is U-shaped with 3–4 knots and N-shaped with 5–8 knots. Panel **d** confirms these patterns using polynomial orders 2–3 (U-shaped) and 4–6 (N-shaped) in the FE-OLS parametric specification. All province-level climate econometric models, including more flexible functional forms, yield non-linear global per capita GDP–temperature response functions. We further validate this pattern zonally by estimating locally stratified response functions over typical climate zones (Asia [temperate continental], Brazil [tropical savanna], India [tropical monsoon], Sweden [temperate to subarctic]; Fig. A.5). Finally, estimates are robust to variations in fixed-effects specifications[22] and dependent variable transformations (first-differenced log, natural log), as shown in Tables A.2–A.13 and Figs. A.2 (parametric FE-OLS), A.3 (non-parametric GAM), and A.4 (semi-parametric restricted cubic splines).

[22]Separately for PWT, WDI, and DOSE datasets and across parametric FE-OLS, non-parametric, and semi-parametric frameworks, we test the following fixed-effects setups: province-by-year FE with quadratic time trends; province FE with quadratic time trends; province-by-year FE with linear time trends; province-by-year FE excluding province-level time trends.

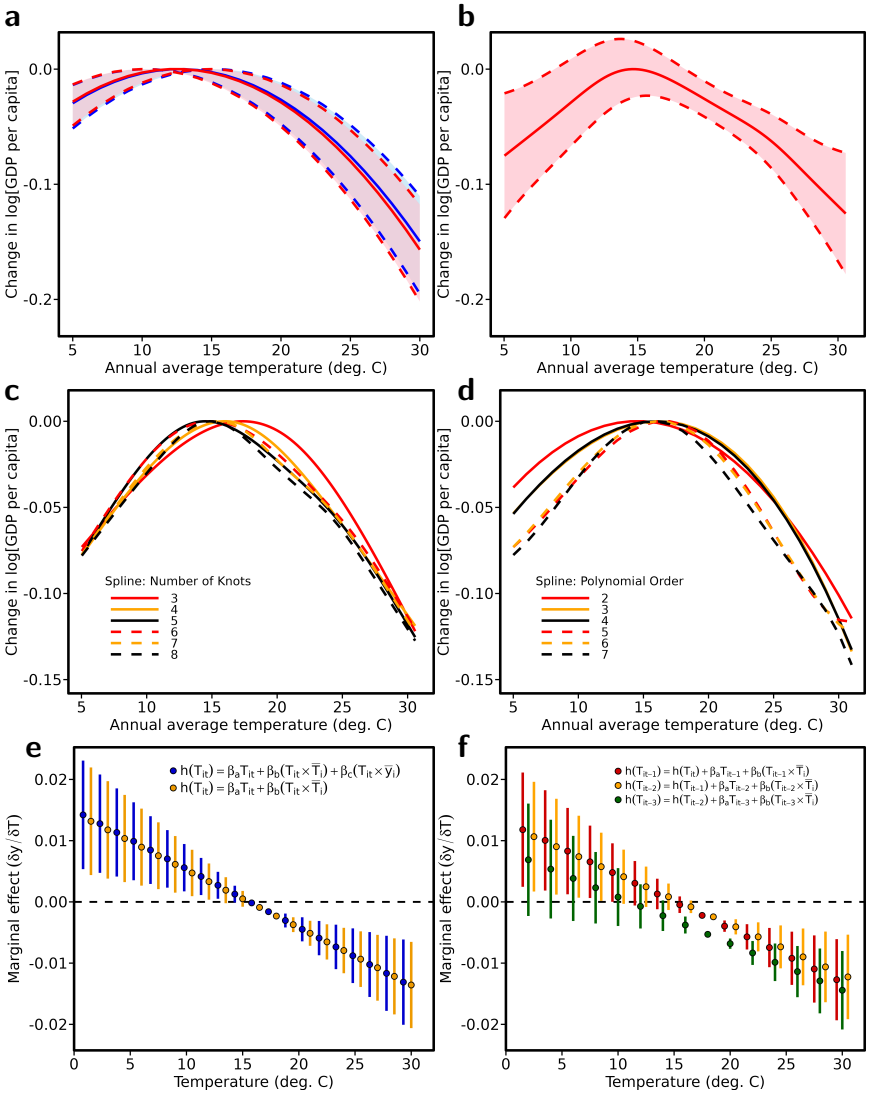

Figure 2: Global non-linear log[GDP per capita] responses to country-annual average temperature exposure per year [deg.°C].

a Parametric FE-OLS results from this study (N=6,697) versus Burke et al (2015) (N=6,584) are shown in solid red and blue lines (respectively) and normalised to the optimums. 95% confidence intervals shown in shaded red (this study) and blue (Burke et al, 2015) are derived from standard errors clustered at the country-level to account for spatial correlation and dependence across units. Regarding climate variables, this study calculates countries' climatic exposures based on 3-hourly 0.25 degree gridded surface temperature and precipitation fields from NASA's Global Land Data Assimilation System (GLDAS— Rodell et al, 2004) collapsed into daily climatic records over 1970-2018, and matched to the period of our macro-output realizations (see *Methods*, §2). Burke et al (2015) used reconstruction data from the University of Delaware containing 0.5 degree gridded monthly average metrological fields over 1960-2010. Both studies account for heterogenous intra-country population allocation and spatially aggregate grid-cell-level weather exposure by country via a weighted collapsing method incorporating time-invariant sub-national population density statistics from the Gridded Population of the World dataset (2015 Version) (CIESIN, 2004).

b-c More flexible functional forms validate the non-linear shape of the global GDP-temperature relationship estimated from parametric FE-OLS in **a**. **b** Non-parametric unrestricted spline of average temperature estimated globally from a Generalized Additive Model (GAM). This has the advantage of reducing the number of parametric assumptions constraining the shape of complex predictor's responses via unrestricted smooth functions. **c** Semi-parametric restricted cubic splines with up to 3-8 Knots estimated globally. Knots are locations along a predictor variable's range where pieces of the smooth function join; and thus where the shape of the smooth function can change. Splines fit the data in sections divided by these Knots, with each section's shape adjusted to minimize error. **d** Parametric FE-OLS splines with up to 2-7 polynomial order in the calibration of the average temperature functional form. All regressions in **a-b-c-d**, whether parametric (**a, d**), non-parametric (**b**) or semi-parametric (**c**); include country-specific quadratic time trends in years of sample, country-by-year fixed effects and precipitation controls. All macro-econometric models (including the more flexible functional forms) yield similar non-linear global per capita GDP-temperature response functions to our main estimates. This suggests that the inverted-U shaped response function in our main specification is not an artifact of the parsimonious 2nd order polynomial.

e Global non-linearity is driven by differences in countries' average temperature, not GDP. Orange dots and lines show the point estimate and 95% CI for the marginal effects of temperature on GDP per capita growth evaluated at different temperature baselines estimated from a model that interacts each country's year-to-year temperature fluctuation with its own average calculated across the sample period (i.e., $\delta y/\delta T_{i,t} = \hat{\beta}a + \hat{\beta}_b \cdot \overline{T}_i$). Orange dots and lines show equivalent estimates from a model that includes an interaction between annual temperature and average GDP per capita (i.e., $\delta y/\delta T_{i,t} = \hat{\beta}a + \hat{\beta}_b \cdot \overline{T}_i + \hat{\beta}_c \cdot \overline{y}_i$). Point estimates are similar across the two models, indicating that the non-linear response is not due to hot countries being poorer on average. **f** Cumulative marginal effect of temperature on per capita GDP as additional lag-transformed temperature variables ($h(T_{i,t-p})$ with $p = [1, 3]$) are included. Solid points and lines indicate the sum of the contemporaneous and lagged marginal effects and its 95% CI at each temperature baseline. For all marginal effect models, standard errors are estimated from 1000 block-Bootstrap resampling iterations.

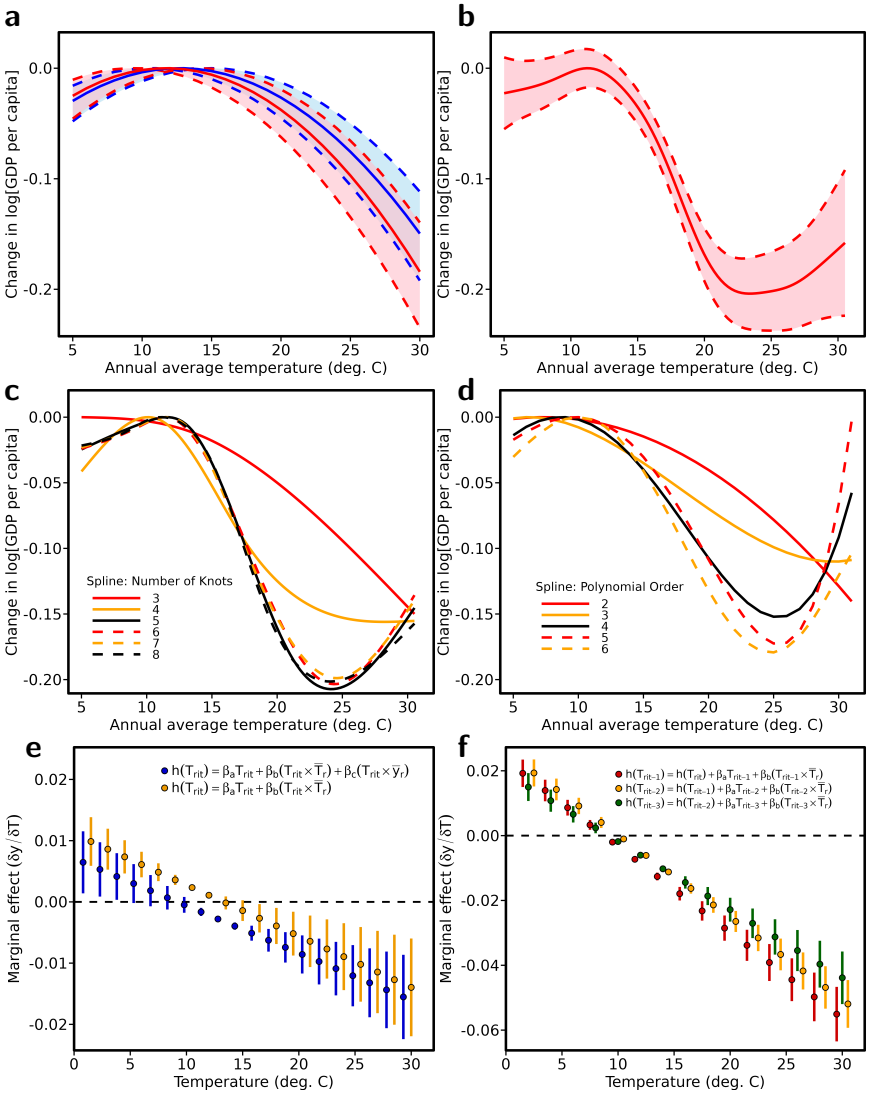

Figure 3: Global non-linear log[GDP per capita] responses to administrative province-annual average temperature exposure per year [deg.°C].

a Parametric FE-OLS results from this analysis on sub-national gross regional product per capita (N=36,583) versus Burke et al (2015)' study performed at the country-level (N=6,584) are shown in solid red and blue lines (respectively) and normalised to the optimums. 95% confidence intervals shown in shaded red (this study) and blue (Burke et al, 2015) are derived from standard errors clustered at the levels of sub-national regions (i.e., administrative provinces) and countries (respectively) to account for spatial correlation and dependence across units. Regarding climate variables, this study calculates sub-national provinces' climatic exposures based on 3-hourly 0.25 degree gridded surface temperature and precipitation fields from NASA's Global Land Data Assimilation System (GLDAS— Rodell et al, 2004) collapsed into daily climatic records over 1970-2018, and matched to the period of our gross regional output realizations (see *Methods*, §2). Burke et al (2015) used reconstruction data from the University of Delaware containing 0.5 degree gridded monthly average metrological fields over 1960-2010. Both studies account for heterogenous intra-country population allocation and spatially aggregate grid-cell-level weather exposure by province/country via a weighted collapsing method incorporating time-invariant sub-national population density statistics from the Gridded Population of the World dataset (2015 Version) (CIESIN, 2004).

b-c More flexible functional forms validate the non-linear shape of the global GDP-temperature relationship estimated from parametric FE-OLS in **a**. **b** Non-parametric unrestricted spline of average temperature estimated globally from a Generalized Additive Model (GAM). This has the advantage of reducing the number of parametric assumptions constraining the shape of complex predictor's responses via unrestricted smooth functions. **c** Semi-parametric restricted cubic splines with up to 3-8 Knots estimated globally. Knots are locations along a predictor variable's range where pieces of the smooth function join; and thus where the shape of the smooth function can change. Splines fit the data in sections divided by these Knots, with each section's shape adjusted to minimize error. **d** Parametric FE-OLS splines with up to 2-7 polynomial order in the calibration of the average temperature functional form. All regressions in **a-b-c-d**, whether parametric (**a, d**), non-parametric (**b**) or semi-parametric (**c**); include province-specific quadratic time trends in years of sample, province-by-year fixed effects and precipitation controls. All macro-econometric models (including the more flexible functional forms) yield similar non-linear global per capita GDP-temperature response functions to our main estimates. This suggests that the inverted-U shaped response function in our main specification is not an artifact of the parsimonious 2nd order polynomial.

e Global non-linearity is driven by differences in sub-national provinces' average temperature, not GDP. Orange dots and lines show the point estimate and 95% CI for the marginal effects of temperature on GDP per capita growth evaluated at different temperature baselines estimated from a model that interacts each province's year-to-year temperature fluctuation with its own average calculated across the sample period (i.e., $\delta y/\delta T_{r,i,t} = \hat{\beta}a + \hat{\beta}_b \cdot \overline{T}_r$). Orange dots and lines show equivalent estimates from a model that includes an interaction between annual temperature and average GDP per capita (i.e., $\delta y/\delta T_{r,i,t} = \hat{\beta}a + \hat{\beta}_b \cdot \overline{T}_r + \hat{\beta}_c \cdot \overline{y}_r$). Point estimates are similar across the two models, indicating that the non-linear response is not due to hot provinces being poorer on average. **f** Cumulative marginal effect of temperature on per capita GDP as additional lag-transformed temperature variables ($h(T_{r,i,t-p})$ with $p = [1, 3]$) are included. Solid points and lines indicate the sum of the contemporaneous and lagged marginal effects and its 95% CI at each temperature baseline. For all marginal effect models, standard errors are estimated from 1000 block-Bootstrap resampling iterations.

3.2 Projected permanent macroeconomic damages

This section presents and decomposes the projection results on economic production ultimately derived from §2.8.

Response functions from Eqs. (10) and (12) are combined with an ensemble of NEX-GDDP CMIP6 Global Climate Model (GCM) simulations to project climate change–driven deviations in productivity growth under moderate (SSP2–RCP4.5) and aggressive (SSP5–RCP8.5) warming scenarios. The resulting transitory deviations are compounded over time to generate permanent changes on the level of GDP per capita. These projections are distributed across administrative regions, future epochs (2030–2099), individual climate models, multi-model medians, and SSP-RCP scenarios. While they differ in terms of economic trajectories and climate stringency forecasts, both set of climate models predict vigorous warming to cause substantially more extreme high temperature circa-2050. Explained in §2.2, a subset of 15 "likely" GCMs is selected for the main analysis to account for the 'hot model' problem (Hausfather et al, 2022). An exhaustive model classification of the full *ensemble* of 29 GCMs is provided in Table A.1.

Fig. 4 shows projected damages derived from SSP5-8.5 vigorous warming GCM simulation scenario. Note that in Panels **a-b**, estimates are econometrically structured from country-level climatic data matched with year-to-year per capita GDP realisations (*à la Burke et al (2015)*). Panel **a** Fig. 4 shows the spatial distribution of the multi-model median impacts from our ensemble of 15 "likely" SSP5-8.5 realizations globally. From changes in temperature alone, end-century median per capita GDP declines are recorded for the most countries with striking heterogenous magnitudes identified in the 5%-55% range, interspersed with isolated regions of negligible losses (0-5%), whereas the largest damages are concentrated in areas overlapping the tropics or near the equator (particularly central Africa, America and Asia). For most countries, strong agreement on net negative climate-shift effect on per capita GDP increasing as the absolute latitude of the country's centroids declines. This geographic pattern empirically confirms previous findings on the heterogenous distribution of climate change effects on crop yields across agro-climatic zones (Sue Wing et al, 2021). Some countries experience slightly net positive per capita GDP increases, which we link to the mini-

mal average temperature baseline at which they are exposed to (i.e., the left-side of the inverted U-shape curve in panel **a** Fig. 2), and the comparatively lower temperature 'delta' (Δ) predicted by CMIP6 in these northern areas. Note that this conclusions holds even under the most vigorous (SSP5-8.5) warming scenario realization.

Panel **b** Fig. 4 graphically summarizes model response $\times$ temporal effect combinations of aggregate percentage per capita GDP impacts. With considerable magnitude, results reveal wide macroeconomic damages ranging at 17%, 25%, 50%, 70% by end-century, depending on the choice of differentiated/short-run, pooled/short-run, differentiated/long-run, pooled/long-run (respectively). Pooled versus differentiated implies that each income group is then allowed its own temperature-GDP response function. We empirically confirm that additionally accounting (long-run model) for lagged temperature regressors up to 5 years leaves larger cumulative per capita GDP changes. This indicates that long-persisting dynamic effects in the initial calibration of the temperature-output response function, in agreement with Kotz et al (2024)'s most recent conclusion. This is the section of this analysis that we now turn to.

The 2^{nd}-to-3^{rd} array of Fig. 4 looks more holistically at the spatial, temporal, climate model distribution of per capita GDP projected damages. Panels **c-g** show estimates econometrically structured from sub-national administrative region-level climatic data matched with year-to-year gross regional per capita product realisations (*à la Kotz et al (2024)*).

Panel **c** Fig. 4 shows the spatial distribution of the multi-model median impacts from our ensemble of 15 "likely" SSP5-8.5 realizations globally. From changes in temperature alone, province-level end-century median per capita GDP declines show further heterogeneity (compared to country-level in panel **a**) ranging from 5%-to-85%.

The central finding of this section is that we empirical confirm the regional patterns identified in the first array of panel Fig. 4, although per capita GDP losses are more severe once we account for intra-country local climatic variability. This is a direct consequence of the steeper response curves unveiled from regional data in panel **a** Fig. 3 in §3, which yield larger projected damages. This is what may fundamentally alter the conclusions of previous country-based GDP models.

General patterns of particularly high zonal impacts include southern Europe, the southwestern United States, western Mali, northern Nigeria, and tropical Asia. The

analysis also identifies specific administrative provinces that are projected to face higher risks in the future (Mahlstein et al, 2013).

In the reminder of the Fig. 4, Panel **d** shows projected per capita GDP damages (%) globally averaged across provinces leaving point-level estimates from each of the 29 CMIP6 GCMs at epoch 2099. We find that SSP5-8.5 (red) vigorous GCMs exhibit structural differences in temperature simulations, thus enabling us to empirically confirm Hausfather et al (2022)'s observation of the 'hot model problem' from their most recent analysis of CMIP6 exercise outputs (see §2.2. SSP2-4.5 (orange) moderate GCMs exhibit similar but more concentrated patterns of model-specific heterogeneity in the prediction of output damages. Panel **e** Fig. 4 displays province-level mean trajectories of multi-model median projected damages (%) from 15 'likely' GCMs distributed across epochs' mid-points. Most sub-national administrative are strongly concentrated around the global mean (captured by the solid black line), prior to diverge with time (i.e., which correlates with increases in both temperature anomalies - level, and their distribution - space), as shown by the relatively wide inter-region × decade range of impacts in the latter epochs. Panel **f** Fig. 4 looks more holistically at the global region-averaged multi-model median projected changes in per capita GDP from 15 'likely' GCMs. Despite heterogenous province-level trajectories of damages shown earlier (Panel **a**, which we link to the persisting weight of local temperature shifts relative to country's average), continent-averages suggest net output losses increasing with time for all global regions. Damages are particularly striking for Africa, South and North America, while more moderated but still significant in Europe and Australia. Finally, panel **g** Fig. 4 compares projected impacts across FE-OLS model specifications (as in panel **b**: pooled/differentiated; short/long run; see *Methods*, §2), where shading represents the 34% and 10% confidence intervals reflecting the 'likely' and 'very likely' ranges of the GCMs (respectively) following Hausfather et al (2022)'s recommended procedure (see §2.2. In panel **b**, we empirically showed that when projected impacts are econometrically structured with lagged temperature regressors (up to 5 years), larger cumulative damages are observed. Panel **g** extends this finding by showing that not only does the model matters (i.e., response' stratification and temporal persistence of the temperature regressor's effect); but also the spatial resolution of the global GDP models (i.e., country×year (panels **a-b**) *à la Burke et al (2015)* versus province×year

(panels **c-g**) *à la Kotz et al (2024)*) used to structure the projections. Our findings therefore concur with those of Kotz et al (2024) suggesting that computing climate damages from the local-provincial level, rather than aggregating by country, yields significantly higher estimates of economic losses, thus leaving large place for patterns of spatial differences. This stems from greater accuracy in capturing localized climate and economic heterogeneity, as our approach better accounts for small-scale variations in exposure to extreme climate impacts and gross regional economic vulnerability, particularly in densely populated regions with higher exposure of infrastructures and sectors to climate risks and lower adaptive capacity. Aggregated, country-level estimates of climate damages may understate the true economic cost of future climate shocks.

In a SSP2-4.5 future, we will have smaller changes in climate change-driven average temperature shifts. Figs. 6 and 5 show projected damages derived from an intermediate mid-point scenario between SSP5-8.5 vigorous & SSP2-4.5 moderate warmings as well as SSP2-4.5 moderate warming GCM realizations (respectively). Compared to Fig. 4, consistent patterns of projected per capita GDP damages are found but in a lower intensity extent and showing early signs of decreasing marginal damages (rather concave shapes after 2060).

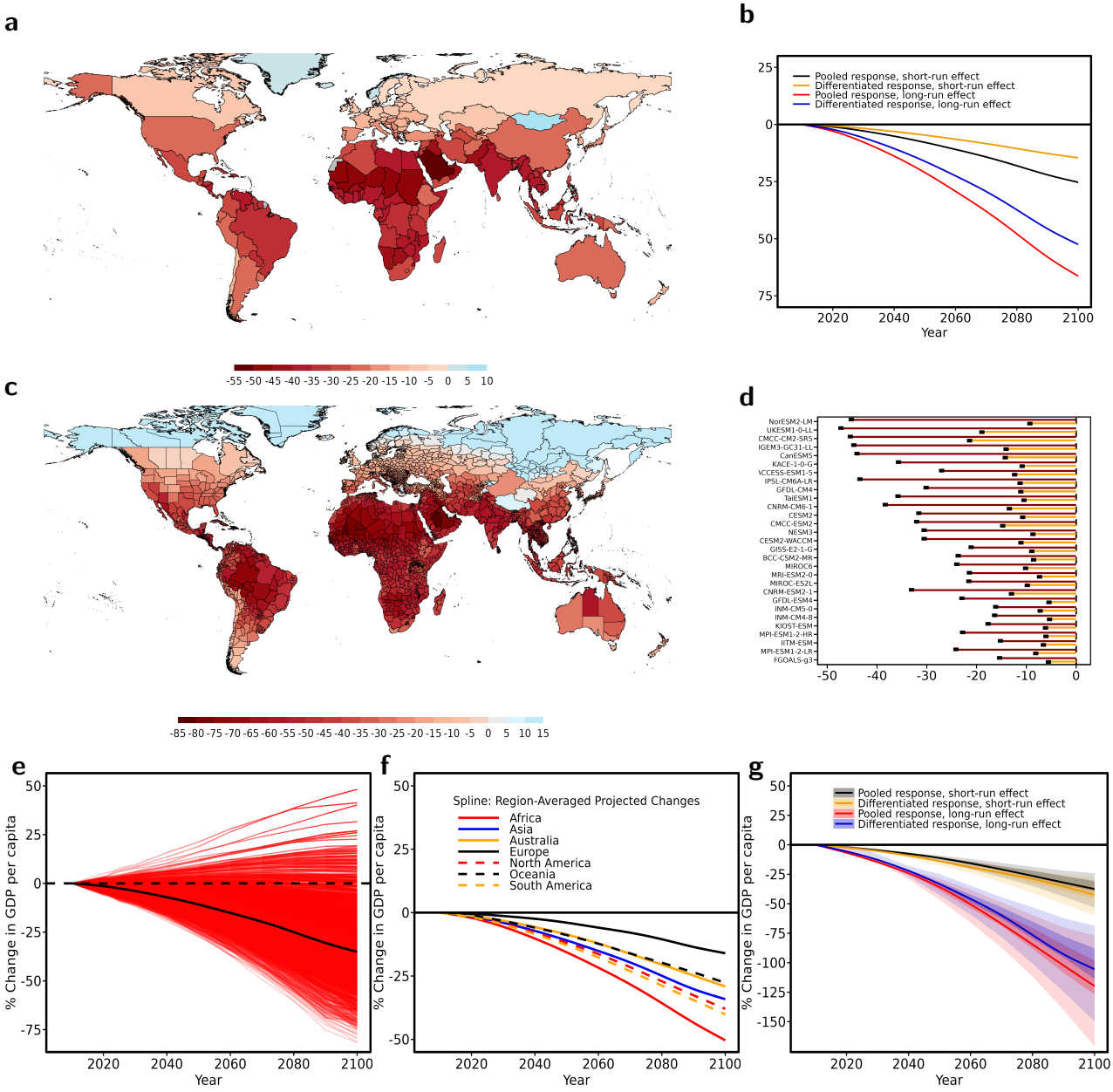

Figure 4: Projected climate-shift impacts (%) on per capita GDP, future epochs relative to constant historical 1980-2010 temperature means, SSP5-8.5 vigorous warming scenario, 15 'likely' CMIP6 global climate models (GCMs).

a Spatially distributed country-level multi-model medians of 15 'likely' CMIP6 Global Climate Models (GCMs) simulated impacts, epoch 2099, econometrically structured from country-level climatic data matched with year-to-year per capita GDP realisations (*à la Burke et al (2015)*). Chosen equation specification to calibrate the projections is pooled FE-OLS accounting for short-run temperature effects only. **b** Comparing projected damages across FE-OLS model specifications using the same econometric approach as in **a**: pooled versus differentiated (each income group is then allowed its own temperature-GDP response function); short run versus long run (the equation additionally accounts for lagged temperature regressors up to 5 years). See *Methods*, §2. **c** Spatially distributed province-level multi-model medians of 15 'likely' CMIP6 GCMs simulated estimates, epoch 2099, econometrically structured from sub-national administrative region-level climatic data matched with year-to-year gross regional per capita product realisations (*à la Kotz et al (2024)*, idem for **d-g**). Chosen equation specification to calibrate the projections is pooled FE-OLS accounting for short-run temperature effects only (idem for **d-f**). **d** Cross-region globally averaged projected damages (%), point-level estimates from each of the full set of 29 CMIP6 GCMs (including those falling inside and outside the 'likely' and 'very likely' ranges) at epoch 2099, SSP5-8.5 vigorous (red) versus SSP2-4.5 moderate (orange) warming scenarios. **e** Province-level mean trajectories of projected damages (%), multi-model medians of 15 'likely' CMIP6 GCMs. Black lines denote the global average. Impacts, in red, are normalised to 0 at epoch 2010. **f** Regionally averaged projected damages, multi-model medians of 15 'likely' CMIP6 GCMs. **g** Comparing projected damages across FE-OLS model specifications: pooled versus differentiated (each income group is allowed its own temperature-GDP response function); short run versus long run (the equation additionally specifies for lagged temperature regressors up to 5 years); see *Methods*, §2. Shading represents our exercise of intra-GCM subset stratification, where the 34% and 10% confidence intervals reflect the 'likely' and 'very likely' ranges (respectively) across the 15 GCMs that formed of the basis of our projections following Hausfather et al (2022)'s recommended procedure (see §2.2.)

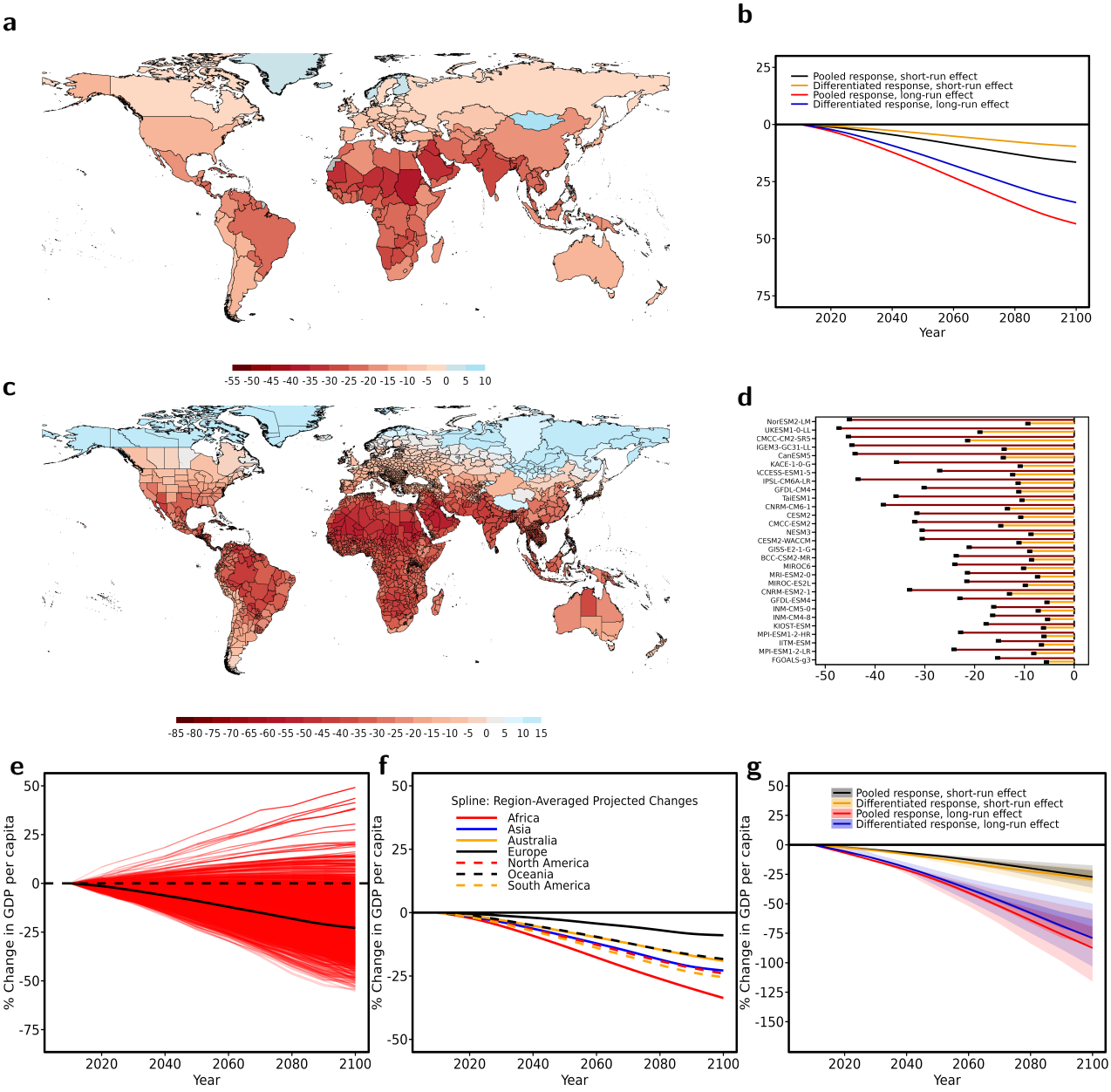

Figure 5: Projected climate-shift impacts (%) on per capita GDP, future epochs relative to constant historical 1980-2010 temperature means, intermediate mid-point scenario between SSP5-8.5 vigorous & SSP2-4.5 moderate warmings, 15 'likely' CMIP6 global climate models (GCMs).

a Spatially distributed country-level multi-model medians of 15 'likely' CMIP6 Global Climate Models (GCMs) simulated impacts, epoch 2099, econometrically structured from country-level climatic data matched with year-to-year per capita GDP realisations (*à la Burke et al (2015)*). Chosen equation specification to calibrate the projections is pooled FE-OLS accounting for short-run temperature effects only. **b** Comparing projected damages across FE-OLS model specifications using the same econometric approach as in **a**: pooled versus differentiated (each income group is then allowed its own temperature-GDP response function); short run versus long run (the equation additionally accounts for lagged temperature regressors up to 5 years). See *Methods*, §2. **c** Spatially distributed province-level multi-model medians of 15 'likely' CMIP6 GCMs simulated estimates, epoch 2099, econometrically structured from sub-national administrative region-level climatic data matched with year-to-year gross regional per capita product realisations (*à la Kotz et al (2024)*, idem for **d-g**). Chosen equation specification to calibrate the projections is pooled FE-OLS accounting for short-run temperature effects only (idem for **d-f**). **d** Cross-region globally averaged projected damages (%), point-level estimates from each of the full set of 29 CMIP6 GCMs (including those falling inside and outside the 'likely' and 'very likely' ranges) at epoch 2099, SSP5-8.5 vigorous (red) versus SSP2-4.5 moderate (orange) warming scenarios. **e** Province-level mean trajectories of projected damages (%), multi-model medians of 15 'likely' CMIP6 GCMs. Black lines denote the global average. Impacts, in red, are normalised to 0 at epoch 2010. **f** Regionally averaged projected damages, multi-model medians of 15 'likely' CMIP6 GCMs. **g** Comparing projected damages across FE-OLS model specifications: pooled versus differentiated (each income group is allowed its own temperature-GDP response function); short run versus long run (the equation additionally specifies for lagged temperature regressors up to 5 years); see *Methods*, §2. Shading represents our exercise of intra-GCM subset stratification, where the 34% and 10% confidence intervals reflect the 'likely' and 'very likely' ranges (respectively) across the 15 GCMs that formed of the basis of our projections following Hausfather et al (2022)'s recommended procedure (see §2.2.)

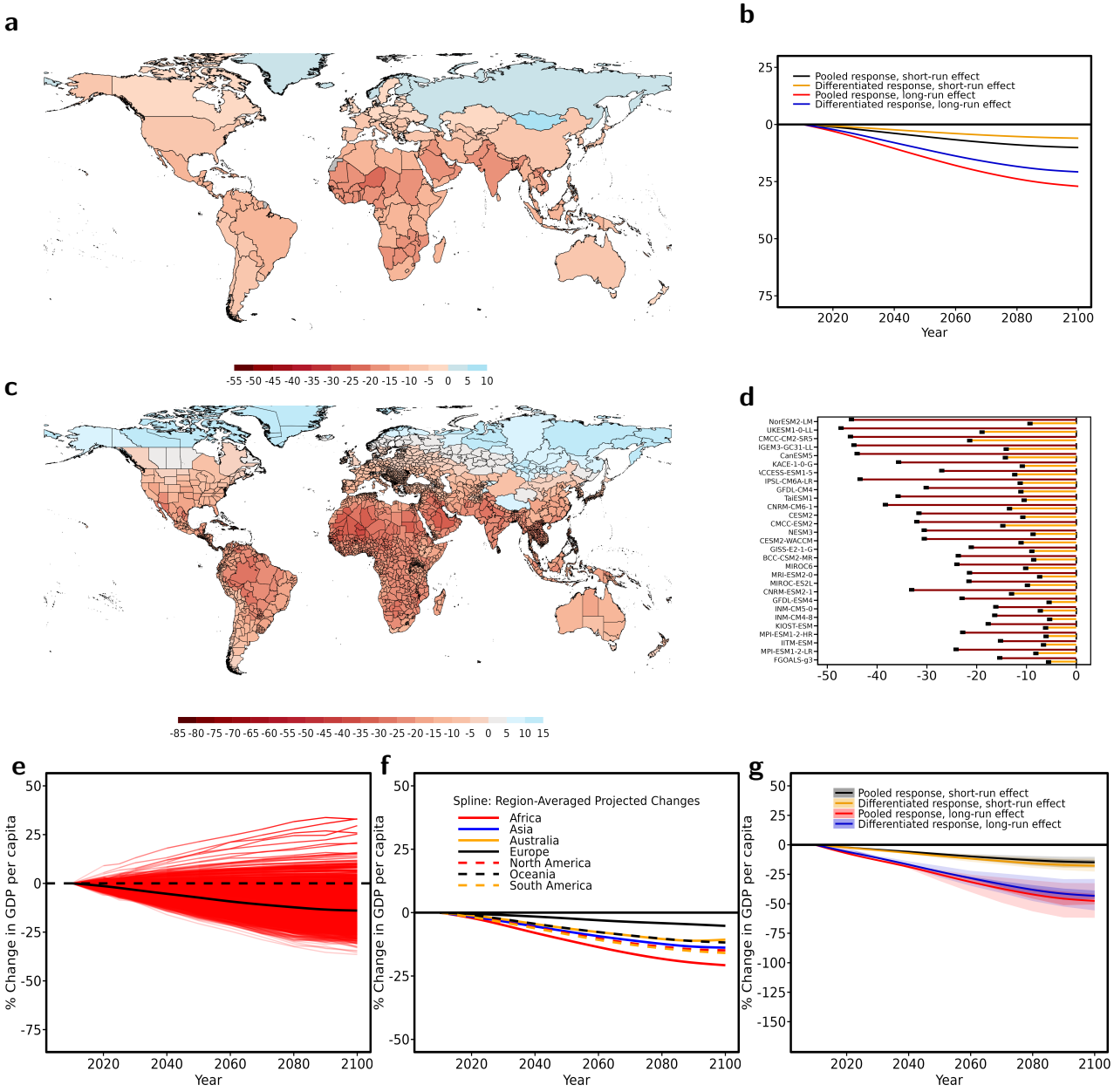

Figure 6: Projected climate-shift impacts (%) on per capita GDP, future epochs relative to constant historical 1980-2010 temperature means, SSP2-4.5 moderate warming scenario, 15 'likely' CMIP6 global climate models (GCMs).

a Spatially distributed country-level multi-model medians of 15 'likely' CMIP6 Global Climate Models (GCMs) simulated impacts, epoch 2099, econometrically structured from country-level climatic data matched with year-to-year per capita GDP realisations (*à la Burke et al (2015)*). Chosen equation specification to calibrate the projections is pooled FE-OLS accounting for short-run temperature effects only. **b** Comparing projected damages across FE-OLS model specifications using the same econometric approach as in **a**: pooled versus differentiated (each income group is then allowed its own temperature-GDP response function); short run versus long run (the equation additionally accounts for lagged temperature regressors up to 5 years). See *Methods*, §2. **c** Spatially distributed province-level multi-model medians of 15 'likely' CMIP6 GCMs simulated estimates, epoch 2099, econometrically structured from sub-national administrative region-level climatic data matched with year-to-year gross regional per capita product realisations (*à la Kotz et al (2024)*, idem for **d-g**). Chosen equation specification to calibrate the projections is pooled FE-OLS accounting for short-run temperature effects only (idem for **d-f**). **d** Cross-region globally averaged projected damages (%), point-level estimates from each of the full set of 29 CMIP6 GCMs (including those falling inside and outside the 'likely' and 'very likely' ranges) at epoch 2099, SSP5-8.5 vigorous (red) versus SSP2-4.5 moderate (orange) warming scenarios. **e** Province-level mean trajectories of projected damages (%), multi-model medians of 15 'likely' CMIP6 GCMs. Black lines denote the global average. Impacts, in red, are normalised to 0 at epoch 2010. **f** Regionally averaged projected damages, multi-model medians of 15 'likely' CMIP6 GCMs. **g** Comparing projected damages across FE-OLS model specifications: pooled versus differentiated (each income group is allowed its own temperature-GDP response function); short run versus long run (the equation additionally specifies for lagged temperature regressors up to 5 years); see *Methods*, §2. Shading represents our exercise of intra-GCM subset stratification, where the 34% and 10% confidence intervals reflect the 'likely' and 'very likely' ranges (respectively) across the 15 GCMs that formed of the basis of our projections following Hausfather et al (2022)'s recommended procedure (see §2.2.)

4 Discussion and conclusion

Does the macro-level relationship between temperature and output comprehensively reflect the patterns observed sub-nationally (and ultimately, at the micro-level)? If so, how do these spatially granular effects aggregate to the national and global scales? This monograph contributes to addressing these two questions. First, we show that country-averaged temperature deviations smooth out critical weather variability relevant for causal inference in climate econometrics. Next, we find that global mid- and end-century damages conceal substantially larger magnitudes when projecting climate change implications on regional economic production.

This monograph elucidates the heterogeneity of countries' and subnational provinces' economic product responses to plausibly exogenous year-to-year fluctuations in temperature and precipitation using an unbalanced panel covering the 1970–2018 period. We draw on both the Penn World Tables version 10.01 (166 countries) and the MCC-PIK Database of Subnational Economic Output (1,661 regions), and attribute output responses to both weather fluctuations (the major propagation channels of climate change) and adaptation (which manifests itself over time in response to climate shift). Our econometric approach is top-down. The identification strategy thus isolates most of time-series and cross-sectional variations in ambient climate measurements by exploiting the higher spatial resolution of the global administrative province-level economic dataset from Wenz et al (2023).

Both panel models approximate a global non-linear U-shaped temperature-per capita output response function, allowing us to extend Burke et al (2015)'s approach - limited to countries - to the level of sub-national administrative provinces - where Kotz et al (2024) is standing. Our results not only provide an empirical replication of the former (despite differences in data source, time span, and spatial/temporal resolution of the historical climate fields), but also establish a bridge with the latter. Moreover, we find that accounting for small-scale variations in localized climatic exposure and intra-country economic heterogeneity yields larger global econometric responses relative to those estimated using country-level data. These results are robust to alternative (i) econometric estimators (parametric, semi-parametric, non-parametric), (ii) temperature functional forms (2^{nd}-to-8^{th} polynomial orders), (iii) specifications of the

flexible trend function (i.e., increasing its Chebychev polynomial orders from quadratic to octic; and variation in its spatial clustering).

We then project climate change–driven permanent damages on the level of GDP per capita by compounding physical risk induced-productivity growth deviations over time. These transitory shocks are calculated through combining our non-linear responses estimated over the period 1970-2018 with an ensemble of NEX-GDDP CMIP6 simulations from 29 global climate models (GCMs), which we extrapolate to 3,672 provinces covering 95% of global economic production. We find substantial agreement among GCMs on average end-century per capita declines of up to $< 70\%$ attributable to climate change-driven shifts in average temperature (*the* central component of chronic physical climate risk), with the largest effects in regions bordering the equator and the tropics (i.e., West Africa, Central America, South Asia), under a vigorous SSP5-8.5 warming scenario. However, while in generally good agreement with Burke et al (2015)'s country-level projections, our province-level calibrated per capita GDP changes show systematically larger mean values.

Results draw two important conclusions. First, our study provides a basis for producing spatially disaggregated projections of climate change-induced economic damages that consistently encompass the majority of administrative regions responsible for 95% of global economic production. Second, the steeper response curves unveiled from regional data yield aggregated projection losses that fundamentally alter the conclusions of previous global GDP models.

We suggest that existing country-based estimates of climate change damages may have underestimated the true economic cost of future physical risks. Our findings also reveal substantial variability in projected macroeconomic damages depending on choices of econometric calibration. While pooled and differentiated approaches produce similar patterns, incorporating lagged temperature regressors (up to five years) yields significantly larger cumulative changes in per capita GDP. This emphasizes the importance of accounting for long-term dynamic effects when calibrating the temperature–output response function and connects our results with the most recent literature (Bilal and Känzig, 2024; Kotz et al, 2024).

Our study provides a basis for making more regionally localised projections of climate change-induced economic damages but is not without caveats. Recent method-

ological advances have improved the representation of discounting (Drupp et al, 2018; Newell et al, 2022) and climate dynamics (Millar et al, 2017) in Integrated Assessment Models (IAMs) used to estimate the Social Cost of Carbon (SCC) (Rennert et al, 2022). Traditional IAMs have long struggled to account for the heterogeneous impacts of climate change across sectors and regions. Often, these relied on sector-specific damage studies (Anthoff and Tol, 2013), meta-analyses (Nordhaus, 2017), or reduced-form approaches that approximated causal effects at the most aggregate level (Burke and Tanutama, 2019; Kalkuhl and Wenz, 2020; Callahan and Mankin, 2022). The integration of regionally-informed damage functions (i.e., based on more spatially-disaggregated climate–productivity data) could lead to upward revisions of SCC values (Ricke et al, 2018).

Caveats are primarily associated with the competitively higher spatial resolution of global data set of reported sub-national economic output (DOSE) (Wenz et al, 2023) that was derived by assembling values from numerous statistical agencies and yearbooks prior to apply harmonisation methods free of linear interpolations. First, the 'reported' nature of the DOSE project implies that its internal validity is inherently limited by the accuracy of national and regional administrations in displaying their economic output. Despite the increased spatial and temporal coverage of DOSE in comparison to most pre-existing datasets, data gaps in both dimensions remain, and so the use of satellite-derived data products could be a promising avenue for filling out these gaps. *Spatially*, sub-national output data for a large number of African and Middle-Eastern countries, suggesting a sampling skewed towards relatively wealthier western regions (over-represented), and leaving an incomplete geographic coverage globally. It is an obstacle faced by Kotz et al (2024); which we addressed in the projection stage following a two-stage method described in §2.2. *Temporally*, DOSE tends to be unbalanced with the majority of observations taking place over the last three decades of coverage (1990–2020) compared to the earlier decades (1960–1990). A final limitation is that converting sub-national nominal GRP values in local currencies to real GRP data in USD is not straight-forward, partly due to the lack of auxiliary data at the sub-national level (i.e., GDP deflators are generally unavailable at the global scale).

Moreover, historical fields from NASA's Global Land Data Assimilation System (GLDAS— Rodell et al, 2004) may suffer from limitations associated with the relatively

coarse spatial resolution (0.25 deg. grid) of this dataset which incompletely captures localized hydrological processes. For instance, used land surface models (Noah-LSM, VIC) rely on parametrization that oversimplify our representation of complex processes, soil properties (e.g., satellite-based soil moisture or snow cover data) and vegetation types. Although reanalyses represent the most robust historical climate data currently available, its atmospheric forcing data (e.g., precipitation, temperature, radiation) may propagate measurement errors throughout the system (Viviers et al, 2024). Similar arguments limit the accuracy of NEX-GDDP CMIP6's ensemble of 29 global climate models (GCMs) simulated under the Coupled Model Intercomparison, Phase VI (CMIP6— Eyring et al, 2016) exercise. Certain feedbacks, such as those involving ice-sheet dynamics or vegetation-atmosphere interactions, are either poorly represented or absent (Zelinka et al, 2020). This explains the *'hot model problem'* discussed earlier in §2.2 of the monograph. Other remaining sources of uncertainty propagation are attributable to downscaling and bias-correction which might potentially alter local climate projections in CMIP6 (Lafferty et al, 2023). A more exhaustive discussion on the limits of the methodologies used to construct the GLDAS, NEX-GDDP and DOSE datasets and their recommended usage is provided in Appendix, §A.1.

Ultimately, the economic framework formalized in Eq. 2, in which total production $Y_{i,\ell,t}$ depends on the function $f_i(T_{\ell,t})$ capturing how overall productivity in industry i responds to instantaneous temperature changes T, presents a critical limitation. This model presumes *additive separability* across sectors and geographic units, treating firms as *atomistic* entities operating independently. However, climate change is likely to generate productivity shocks (scaling up to output losses) that propagate throughout the global production system. The true economic cost of physical climate risk is expected to extend beyond individual firms that respond only to isolated changes in their immediate climatic conditions. Reasons include the existence of substantial inter-firm spillovers, trade dependencies, and the potential emergence of novel price dynamics when physical risk events display temporal or spatial correlation. Intuitively, disruptions in a firm's supply chain would magnify beyond the direct exposure of the firm itself. If such effects are non-negligible, the empirical methodology employed here—which quantifies region $\times$ country–specific impacts in isolation—may underestimate the net macroeconomic implications of physical climate risks. This would not be the case only if these signals

are already implicitly captured in observed GDP dynamics. Whether this condition holds remains an open empirical question.

References

[1] Allen, M. R., Fernandez, S. J., Fu, J. S., & Olama, M. M. (2016). Impacts of climate change on sub-regional electricity demand and distribution in the southern United States. Nature Energy, 1(8), 1-9.

[2] Angrist, J. D., & Pischke, J. S. (2009). Mostly harmless econometrics: An empiricist's companion. Princeton university press.

[3] Anthoff, D., & Tol, R. S. (2013). The uncertainty about the social cost of carbon: A decomposition analysis using fund. Climatic change, 117, 515-530.

[4] Arguez, A., Durre, I., Applequist, S., Squires, M., Vose, R., Yin, X., & Bilotta, R. (2010). NOAA's U.S. Climate Normals (1981–2010). NOAA National Centers for Environmental Information.

[5] Arguez, A., & Vose, R. S. (2011). The definition of the standard WMO climate normal: The key to deriving alternative climate normals. Bulletin of the American Meteorological Society, 92(6), 699-704.

[6] Auffhammer, M., & Aroonruengsawat, A. (2011). Simulating the impacts of climate change, prices and population on California's residential electricity consumption. Climatic change, 109, 191-210.

[7] Auffhammer, M., Hsiang, S. M., Schlenker, W., & Sobel, A. (2013). Using weather data and climate model output in economic analyses of climate change. Review of Environmental Economics and Policy.

[8] Auffhammer, M., Baylis, P., & Hausman, C. H. (2017). Climate change is projected to have severe impacts on the frequency and intensity of peak electricity demand across the United States. Proceedings of the National Academy of Sciences, 114(8), 1886-1891.

[9] Auffhammer, M. (2022). Climate Adaptive Response Estimation: Short and long run impacts of climate change on residential electricity and natural gas consumption. Journal of Environmental Economics and Management, 114, 102669.

[10] Barro, R. J. (2003). Determinants of economic growth in a panel of countries. Annals of economics and finance, 4, 231-274.

[11] Bearpark, T., Hogan, D., & Hsiang, S. (2025). Data anomalies and the economic commitment of climate change. Nature, 644(8075), E7-E11.

[12] Berg, K. A., Curtis, C. C., & Mark, N. C. (2024). Gdp and temperature: Evidence on cross-country response heterogeneity. European Economic Review, 169, 104833.

[13] Bilal, A., & Känzig, D. R. (2024). The macroeconomic impact of climate change: Global vs. local temperature (No. w32450). National Bureau of Economic Research.

[14] Blanc, E., Schlenker, W. (2017). The use of panel models in assessments of climate impacts on agriculture. Review of Environmental Economics and Policy.

[15] Bodirsky, B. L., Rolinski, S., Biewald, A., Weindl, I., Popp, A., & Lotze-Campen, H. (2015). Global food demand scenarios for the 21 st century. PloS one, 10(11), e0139201.

[16] Burke, M., Emerick, K., 2016. Adaptation to climate change: Evidence from US agriculture. American Economic Journal: Economic Policy, 8, 3, 106-40.

[17] Burke, M., & Tanutama, V. (2019). Climatic constraints on aggregate economic output (No. w25779). National Bureau of Economic Research.

[18] Burke, M., Hsiang, S. M., & Miguel, E. (2015). Global non-linear effect of temperature on economic production. Nature, 527(7577), 235-239.

[19] Callahan, C. W., & Mankin, J. S. (2022). Globally unequal effect of extreme heat on economic growth. Science Advances, 8(43), eadd3726.

[20] Cameron, A. C., Gelbach, J. B., & Miller, D. L. (2011). Robust inference with multiway clustering. Journal of Business & Economic Statistics, 29(2), 238-249.

[21] CIESIN, C. (2004). Gridded Population of the World (GPW), Version 3. Center for International Earth Science Information Network and Columbia University and Centro Internacional de Agricultura Tropical and Palisades. CIESIN, Columbia University, NY.

[22] Coffey, B., Stern, A., & Wing, I. S. (2015, January). Climate change impacts on us electricity demand: Insights from micro-consistent aggregation of a structural model. In International Energy Workshop (pp. 1-34). University of South Carolina.

[23] Dee, D. P., Uppala, S., Simmons, A. J., Berrisford, P., Poli, P., Kobayashi, S., ... & Vitart, F. (2011). The ERA-Interim reanalysis: Configuration and performance of the data assimilation system. Quarterly Journal of the royal meteorological society, 137(656), 553-597.

[24] Dell, M., Jones, B. F., & Olken, B. A. (2009). Temperature and income: reconciling new cross-sectional and panel estimates. American Economic Review, 99(2), 198-204.

[25] Dell, M., Jones, B. F., & Olken, B. A. (2012). Temperature shocks and economic growth: Evidence from the last half century. American Economic Journal: Macroeconomics, 4(3), 66-95.

[26] Dell, M., Jones, B. F., & Olken, B. A. (2014). What do we learn from the weather? The new climate-economy literature. Journal of Economic literature, 52(3), 740-798.

[27] Deryugina, T., & Hsiang, S. M. (2014). Does the environment still matter? Daily temperature and income in the United States (No. w20750). National Bureau of Economic Research.

[28] Deschênes, O., & Greenstone, M. (2011). Climate change, mortality, and adaptation: Evidence from annual fluctuations in weather in the US. American Economic Journal: Applied Economics, 3(4), 152-185.

[29] Drupp, M. A., Freeman, M. C., Groom, B., & Nesje, F. (2018). Discounting disentangled. American Economic Journal: Economic Policy, 10(4), 109-134.

[30] Eyring, V., Bony, S., Meehl, G. A., Senior, C. A., Stevens, B., Stouffer, R. J., & Taylor, K. E. (2016). Overview of the Coupled Model Intercomparison Project Phase 6 (CMIP6) experimental design and organization. Geoscientific Model Development, 9(5), 1937-1958. Bulletin of the American Meteorological society, 85(3), 381-394.

[31] Feenstra, R. C., Inklaar, R., & Timmer, M. P. (2015). The next generation of the Penn World Table. American economic review, 105(10), 3150-3182.

[32] Foley, J. A., DeFries, R., Asner, G. P., Barford, C., Bonan, G., Carpenter, S. R., ... & Snyder, P. K. (2005). Global consequences of land use. science, 309(5734), 570-574.

[33] Franco, G., & Sanstad, A. H. (2008). Climate change and electricity demand in California. Climatic Change, 87(Suppl 1), 139-151.

[34] Gennaioli, N., & La Porta, R. (2014). Florencio Lopez De Silanes & Andrei Shleifer. J Econ Growth, 19, 259-309.

[35] Graff Zivin, J., & Neidell, M. (2014). Temperature and the allocation of time: Implications for climate change. Journal of Labor Economics, 32(1), 1-26.

[36] Graff Zivin, J., Hsiang, S. M., & Neidell, M. (2018). Temperature and human capital in the short and long run. Journal of the Association of Environmental and Resource Economists, 5(1), 77-105.

[37] Granger, C. W., & Newbold, P. (1974). Spurious regressions in econometrics. Journal of econometrics, 2(2), 111-120.

[38] Haqiqi, I., Grogan, D. S., Hertel, T. W., Schlenker, W. (2021). Quantifying the impacts of compound extremes on agriculture. Hydrology and Earth System Sciences, 25(2), 551-564.

[39] Hausfather, Z., Marvel, K., Schmidt, G. A., Nielsen-Gammon, J. W., & Zelinka, M. (2022). Climate simulations: recognize the 'hot model' problem. Nature, 605(7908), 26-29.

[40] Heal, G., & Park, J. (2013). Feeling the heat: Temperature, physiology & the wealth of nations (No. w19725). National Bureau of Economic Research.

[41] Hsiang, S. M., & Jina, A. S. (2014). The causal effect of environmental catastrophe on long-run economic growth: Evidence from 6,700 cyclones (No. w20352). National Bureau of Economic Research.

[42] Hsiang, S. M., Burke, M., & Miguel, E. (2013). Quantifying the influence of climate on human conflict. Science, 341(6151), 1235367.

[43] Hsiang, S. M. (2010). Temperatures and cyclones strongly associated with economic production in the Caribbean and Central America. Proceedings of the National Academy of sciences, 107(35), 15367-15372.

[44] IPCC. (2021). Climate Change 2021: The Physical Science Basis. Contribution of Working Group I to the Sixth Assessment Report of the Intergovernmental Panel on Climate Change, Cambridge University Press, Cambridge, United Kingdom and New York, NY, USA.

[45] Kalkuhl, M., & Wenz, L. (2020). The impact of climate conditions on economic production. Evidence from a global panel of regions. Journal of Environmental Economics and Management, 103, 102360.

[46] Kotz, M., Wenz, L., Stechemesser, A., Kalkuhl, M., & Levermann, A. (2021). Day-to-day temperature variability reduces economic growth. Nature Climate Change, 11(4), 319-325.

[47] Kotz, M., Levermann, A., & Wenz, L. (2022). The effect of rainfall changes on economic production. Nature, 601(7892), 223-227.

[48] Kotz, M., Levermann, A., & Wenz, L. (2024). The economic commitment of climate change. Nature, 628(8008), 551-557.

[49] Lafferty, D. C., & Sriver, R. L. (2023). Downscaling and bias-correction contribute considerable uncertainty to local climate projections in CMIP6. npj Climate and Atmospheric Science, 6(1), 158.

[50] Linsenmeier, M. (2023). Temperature variability and long-run economic development. Journal of Environmental Economics and Management, 121, 102840.

[51] Mahlstein, I., Daniel, J. S., & Solomon, S. (2013). Pace of shifts in climate regions increases with global temperature. Nature Climate Change, 3(8), 739-743.

[52] Massetti, E., Mendelsohn, R. (2020). Temperature thresholds and the effect of warming on American farmland value. Climatic Change, 161(4), 601-615.

[53] McIntosh, C. T., & Schlenker, W. (2006). Identifying non-linearities in fixed effects models. UC-San Diego Working Paper.

[54] Meinshausen, M., Nicholls, Z. R., Lewis, J., Gidden, M. J., Vogel, E., Freund, M., ... & Wang, R. H. (2020). The shared socio-economic pathway (SSP) greenhouse gas concentrations and their extensions to 2500. Geoscientific Model Development, 13(8), 3571-3605.

[55] Mendelsohn R., Massetti E. (2017). The use of cross-sectional analysis to measure climate impacts on agriculture: theory and evidence. Review of Environmental Economics and Policy.

[56] Millar, R. J., Nicholls, Z. R., Friedlingstein, P., & Allen, M. R. (2017). A modified impulse-response representation of the global near-surface air temperature and atmospheric concentration response to carbon dioxide emissions. Atmospheric Chemistry and Physics, 17(11), 7213-7228.

[57] Miller, N. L., Hayhoe, K., Jin, J., & Auffhammer, M. (2008). Climate, extreme heat, and electricity demand in California. Journal of Applied Meteorology and Climatology, 47(6), 1834-1844.

[58] Moore, F. C., & Diaz, D. B. (2015). Temperature impacts on economic growth warrant stringent mitigation policy. Nature Climate Change, 5(2), 127-131.

[59] Newell, R. G., Pizer, W. A., & Prest, B. C. (2022). A discounting rule for the social cost of carbon. Journal of the Association of Environmental and Resource Economists, 9(5), 1017-1046.

[60] Nordhaus, W. D. (2006). Geography and macroeconomics: New data and new findings. Proceedings of the National Academy of Sciences, 103(10), 3510-3517.

[61] Nordhaus, W. D. (2017). Revisiting the social cost of carbon. Proceedings of the National Academy of Sciences, 114(7), 1518-1523.

[62] Orlowsky, B., & Seneviratne, S. I. (2012). Global changes in extreme events: regional and seasonal dimension. Climatic change, 110, 669-696.

[63] Ortiz-Bobea, A., Wang, H., Carrillo, C. M., Ault, T. R. (2019). Unpacking the climatic drivers of US agricultural yields. Environmental Research Letters, 14(6), 064003.

[64] Perron, P. (1989). The great crash, the oil price shock, and the unit root hypothesis. *Econometrica: Journal of the Econometric Society*, 1361–1401.

[65] Phillips, P. C., & Perron, P. (1988). Testing for a unit root in time series regression. *Biometrika*, 75(2), 335–346.

[66] Pindyck, R. S. (2013). Climate change policy: what do the models tell us?. Journal of Economic Literature, 51(3), 860-872.

[67] Rennert, K., Errickson, F., Prest, B. C., Rennels, L., Newell, R. G., Pizer, W., ... & Anthoff, D. (2022). Comprehensive evidence implies a higher social cost of CO2. Nature, 610(7933), 687-692.

[68] Ricke, K., Drouet, L., Caldeira, K., & Tavoni, M. (2018). Country-level social cost of carbon. Nature Climate Change, 8(10), 895-900.

[69] Rodell, M., Houser, P. R., Jambor, U. E. A., Gottschalck, J., Mitchell, K., Meng, C. J., ... & Toll, D. (2004). The global land data assimilation system. Bulletin of the American Meteorological society, 85(3), 381-394.

[70] Romitti, Y., & Sue Wing, I. (2022). Heterogeneous climate change impacts on electricity demand in world cities circa mid-century. Scientific reports,12, (1), 4280.

[71] Schlenker, W., Lobell, D. B. (2010). Robust negative impacts of climate change on African agriculture. Environmental Research Letters, 5(1), 014010.

[72] Schlenker, W., & Roberts, M. J. (2009). Nonlinear temperature effects indicate severe damages to US crop yields under climate change. Proceedings of the National Academy of sciences, 106(37), 15594-15598.

[73] Schlenker, W., & Walker, W. R. (2016). Airports, air pollution, and contemporaneous health. The Review of economic studies, 83(2), 768-809.

[74] Schötz, C. (2025). Spatial correlation in economic analysis of climate change. Nature, 644(8076), E27-E30.

[75] Seo, S. N., Mendelsohn, R., Dinar, A., Hassan, R., Kurukulasuriya, P. (2009). A Ricardian analysis of the distribution of climate change impacts on agriculture across agro-ecological zones in Africa. Environmental and Resource Economics, 43, 313-332.

[76] Sherwood, S. C., Webb, M. J., Annan, J. D., Armour, K. C., Forster, P. M., Hargreaves, J. C., ... & Zelinka, M. D. (2020). An assessment of Earth's climate sensitivity using multiple lines of evidence. Reviews of Geophysics, 58(4), e2019RG000678.

[77] Wing, I. S., De Cian, E., & Mistry, M. N. (2021). Global vulnerability of crop yields to climate change. Journal of Environmental Economics and Management, 109, 102462.

[78] Tokarska, K. B., Stolpe, M. B., Sippel, S., Fischer, E. M., Smith, C. J., Lehner, F., & Knutti, R. (2020). Past warming trend constrains future warming in CMIP6 models. Science advances, 6(12), eaaz9549.

[79] Viviers, C., van der Laan, M., Gaffoor, Z., & Dippenaar, M. (2024). Downscaling and validating GLDAS groundwater storage anomalies by integrating precipitation for recharge and actual evapotranspiration for discharge. Journal of Hydrology: Regional Studies, 54, 101879.

[80] Wenz, L., Carr, R. D., Kögel, N., Kotz, M., & Kalkuhl, M. (2023). DOSE–Global data set of reported sub-national economic output. Scientific Data, 10(1), 425.

[81] World Meteorological Organization (WMO). (2023). Global Annual to Decadal Climate Update 2023–2027. WMO-No. 1326, World Meteorological Organization, Geneva, Switzerland.

[82] Willmott, C. J., & Matsuura, K. (2012). Terrestrial air temperature and precipitation: Monthly and annual time series (1900–2010). Data Retrieved From: http://climate.geog.udel.edu/âĹijclimate/htmlpages/Global2011/README.GlobalTsT2011.html.

[83] Wood, S. N. (2004). Stable and efficient multiple smoothing parameter estimation for generalized additive models. Journal of the American Statistical Association, 99(467), 673-686.

[84] Zelinka, M. D., Myers, T. A., McCoy, D. T., Po Chedley, S., Caldwell, P. M., Ceppi, P., ... & Taylor, K. E. (2020). Causes of higher climate sensitivity in CMIP6 models. Geophysical Research Letters, 47(1), e2019GL085782.

A Appendix - For Online Publication

'The Global Geography of Long-Term Projected Macroeconomic Damages from Chronic Physical Risk and the Aggregation Problem'

Contents

A.1 Supplementary data discussion

This section discusses the limits of the methodologies used to construct the GLDAS, NEX-GDDP and DOSE datasets as well as their recommended usage.

A valid concern can arise from the statistical downscaling methodology employed in NASA's Earth Exchange Global Daily Downscaled Projections (NEX-GDDP CMIP6— Eyring et al, 2016) which does not adequately account for the effects of local land use changes (e.g., urban heat island effects or deforestation impacts), topography or highly localized climate dynamics (Zhang et al, 2024). This is particularly pronounced in regions with complex terrain or limited observational data such as high-altitude areas (Wu et al, 2023). Moreover, the literature has highlighted some models' tendency in underestimating precipitation in humid regions and overestimating temperature in arid zones, with for instance the multi-model ensemble (MME) simulations showing biased accuracy of resulting indices of drought and evapotranspiration in China (particularly in the Qinghai–Tibet Plateau and central Xinjiang, where observational data are sparse) (Liu et al, 2024). Climate extremes uncertainty (e.g, droughts or heavy rainfall) are incompletely solved due to limitations in the multi-model averaging process which over-homogenize (dampen) performance and sort out some of the frequency and intensity of extreme event variability crucial to impact assessments (like in the present study) (Dioha et al, 2024). Note that the downscaling itself introduces additional challenges in correctly capturing drought indices. While indices like SPI (Standardized Precipitation Index) perform better in specific regions, others like SPEI (Standardized Precipitation Evapotranspiration Index) may misrepresent conditions due to biases in the input climate variables (zhai et al, 2020). Temporal heterogeneity biases stem from a likely mismatch in seasonal and annual trends. While the models effectively reproduce long-term warming trends, they struggle to accurately represent inter-annual variability and seasonal cycles. This issue is particularly prominent in monsoon regions, where precipitation trends are seasonal specific-humidity is high (Sylvestre et al, 2024). Research directions to improve both spatial and temporal accuracy include dynamic downscaling methods that incorporate physical mechanisms (i.e., topography and land-atmosphere interactions) and advanced ensemble techniques (i.e., Bayesian model averaging).

Data from NASA's Global Land Data Assimilation System (GLDAS— Rodell et al, 2004), which relies on observation-based meteorological forcing precipitation and radiation data, suffer from similar limitations ranging from resolution constraints, forcing data quality, temporal coverage, model simplifications, validation of uncertainty and an inadequate representation of human activities (Mistry, 2019). GLDAS uses multiple land surface models (e.g., Noah, CLM, and Mosaic) which employ simplified representations of physical processes (e.g., assumptions in soil moisture dynamics or vegetation parameters might not reflect actual conditions). Also, processes like irrigation, urbanization, and land management are either oversimplified or excluded in some models; which may lead to inaccuracies in regions were the feedback effect of anthropogenic activities is significant (Gu et al, 2019). While validation of GLDAS outputs against independent regional/global datasets is ongoing, discrepancies often arise due to differences in spatial resolution, data sources, or model physics (Viviers et al, 2024). For instance, Ji et al (2015) compare the GLDAS daily surface air temperature at 0.25 deg. gridded resolution with two reference datasets: (a) Daymet data (2002 and 2010) for the conterminous U.S. at 1-km gridded resolution and (b) global meteorological observations (2000) from the Global Historical Climatology Network (GHCN). Other limitations such as larger uncertainty in the surface air temperature estimates over high mountainous areas are well documented in the literature, as well as missing data in the grid-cells close to water bodies (which can be filled using the appropriate interpolating technique: bilinear, near neighbour or inverse-distance mapping). Users of the GLDAS-derived data products in econometric analyses (De Cian et al, 2019; Sue Wing et al, 2021) have recommended to pay attention to these caveats.

The global data set of reported sub-national economic output (DOSE) (Wenz et al, 2023) exhibits several caveats, including temporal and spatial inconsistencies (i.e., only 83 countries are represented) mentioned earlier in the monograph. See Fig. A.1 for a look at the spatial coverage of administrative province-level per capita GDP time-series data (fraction of countries) in the raw DOSE product. Although the dataset harmonizes data for aggregate and sectoral outputs, variations in sectoral reporting standards across countries may introduce biases in sector-specific analyses. DOSE aggregates information and presents both the advantage and the

drawback of being strictly grounded in reported macroeconomic values from heterogeneous national statistical offices and yearbooks (i.e., Wenz et al (2023) voluntarily excluded interpolation methods to fill out missing data); which limits the continuous nature of time series in under-reported provinces. Finally, boundary consistency challenges remain due to historical change leading to mismatches when we integrate with geospatial climate information in §2.2. A relevant assessments of the social cost of carbon (SCC) implications of reduced-form steeper damage functions estimated from DOSE can be found in Wenz et al (2024).

A.2 Identifying non-linearities in a fixed effects model

McIntosh and Schlenker (2006) demonstrated that structuring a fixed-effects model with a higher-order polynomial temperature function allows a mix of within-country and cross-country sources of variation to play out. Contrary to the standard interpretation wherein fixed effects models are identified solely by deviations from the group mean, a quadratic explanatory variable causes group means to re-enter the identification which has implications for our global GDP econometric model. A summary of the formalization is presented below.

One can algebraically demonstrate that a quadratic term in the fixed effects estimator captures non-linearity between units.Let $x_{i,t}$ in group i in period t to be covariate drawn from a distribution with group mean μ_i. Assuming the true data-generating process can be written as:

$$y_{i,t} = \beta_1 x_{i,t} + \beta_2 x_{i,t}^2 + \beta_3 (x_{i,t} - \mu_i)^2 + c_i + \epsilon_{i,t} \tag{28}$$

This specification incorporates three distinct channels through which $y_{i,t}$ can display a non-linear association with $x_{i,t}$. The first mechanism involves the potential non-linear dependence of the fixed effects (c_i) on the covariate, or alternatively, the possibility that the conditional mean of the outcome across units exhibits convexity or concavity in the distribution of x. To evaluate this, one could perform a dummy-variable fixed effect regression and subsequently examine the relationship between the dummy coefficients and the group-specific averages of x. Nevertheless, since the primary objective of employing the within transformation is to eliminate c_i from the outcomes, we presume that such convexity lies outside the focus of researchers utilizing fixed-effects models and therefore omit it from further analysis.

The two critical types of non-linearities pertinent to fixed-effects models are the global non-linearity stemming from a quadratic relationship in $x_{i,t}$ and the within-unit non-linearity originating from a quadratic term in $(x_{i,t} - \mu_i)$. Specifically, if $\beta_3 = 0$ in Eq. 28, the model simplifies to a quadratic functional form with fixed effects, a structure extensively examined in prior studies and referred to here as the *global* model. Conversely, if $\beta_2 = 0$, the specification includes only deviations from the group mean, which we denote as the *within* model. Finally, the *hybrid* model

extends this framework by allowing both β_2 and β_3 to take non-zero values.
Consider the standard estimate of the *global* model:

$$y_{it} = \beta_1 x_{it} + \beta_2 x_{it}^2 + c_i + \varepsilon_{it} \tag{29}$$

The key insight into the difference between global and within non-linearity comes from the fact that equation Eq. (29) first squares the covariate and then demeans it. Recall that

$$\mu_i = \mathbb{E}[x_{it} \mid i], \quad \text{which can be estimated by } \bar{x}_i = \frac{1}{T}\sum_{t=1}^{T} x_{it}.$$

To fix notation, let $\tilde{x}_{it} = x_{it} - \bar{x}_i$ and $\tilde{x}_i^2 = \frac{1}{T}\sum_{t=1}^{T} x_{it}^2$. The quantity which we arrive at by squaring and then demeaning, which we denote by $\ddot{x}_{it}^2$, can be written as

$$\ddot{x}_{it}^2 = [x_{it} - \bar{x}_i + \bar{x}_i]^2 - \bar{x}_i^2 = \tilde{x}_{it}^2 + 2\tilde{x}_{it}\bar{x}_i + [\bar{x}_i]^2 - \bar{x}_i^2.$$

In other words, the canonical use of non-linear fixed effects given by Eq. (29) does not measure non-linearity within units, as the terminology used to describe the estimator might suggest, because $\ddot{x}_{it}^2$ is in general not equal to $\tilde{x}_{it}^2$. Further, we see that by squaring the covariate before demeaning it, we re-introduce a function of the mean of the covariate into the identification.
What does the standard non-linear fixed effects estimator measure? A simple way to see this is to use our DGP to write out the mean of the outcome for each fixed effect unit. Taking averages over group i one gets:

$$\bar{y}_i = \beta_1 \bar{x}_i + \beta_2 \bar{x}_i^2 + \beta_3 (x_{it} - \mu_i)^2 + c_i + \varepsilon_i \tag{30}$$

First noting that

$$(x_{it} - \mu_i)^2 - (x_{it} - \mu_i)^2 = \tilde{x}_{it}^2 - 2x_{it}\mu_i + \mu_i^2 = \frac{1}{T}\sum_{t=1}^{T}\left[x_{it}^2 - 2x_{it}\mu_i + \mu_i^2\right] =$$

$$x_{it}^2 - 2x_{it}\mu_i + \mu_i^2 - \bar{x}_i^2 + 2\bar{x}_i\mu_i - \mu_i^2 = \tilde{x}_{it}^2 - 2x_{it}\mu_i.$$

We can subtract Eq. (30) from Eq. (28) to give an explicit representation of both

the global and the within variation in the conditional mean as:

$$\mathbb{E}[y_{it} \mid x_{it}] = \beta_1 \bar{x}_i + \beta_2 \bar{x}_i^2 + \beta_3 \left[\tilde{x}_{it}^2 - \bar{x}_i^2\right] \tag{31}$$

$$= \left[\beta_1 - 2\beta_3 \mu_i\right] \tilde{x}_{it} + \left[\beta_2 + \beta_3\right] \tilde{x}_{it}^2 \tag{32}$$

$$= \left[\beta_1 + 2\beta_2 \mu_i\right] \tilde{x}_{it} + \left[\beta_2 + \beta_3\right] \tilde{x}_{it}^2 - \left[\bar{x}_i^2 - \mu_i^2\right]. \tag{33}$$

Several notable aspects emerge regarding the practical application of non-linear functional forms with fixed effects, as highlighted by these equations. Equation Eq. (31) specifies the appropriate model to simultaneously account for both global and within-unit non-linearities. When the two types of non-linearity are expressed in the additively separable form outlined in Eq. (28), it becomes necessary to incorporate two distinct squared terms: the squared demeaned variable, which captures *global* non-linearities, and the demeaned squared variable, which accounts for *within-group* non-linearities. This combined approach is referred to as the *hybrid estimator*.

Eq. (32) and Eq. (33) demonstrate the implications of using a model that is misspecified by including only one type of non-linearity as a regressor while the other is also present in the data-generating process (DGP). Eq. (32) reveals that estimating Eq. (29) in the presence of within-group non-linearities can induce bias not only in the estimation of the quadratic coefficient but also in the linear coefficient. To accurately recover global non-linearity, it is essential to square the covariate and subsequently demean it, provided that within-group non-linearity is absent from the data. In such cases, $\beta_3 = 0$, leading to the recovery of $b_1 = \beta_1$ and $b_2 = \beta_2$.

Eq. (33) addresses the opposite scenario, illustrating that a model which accounts only for within-group non-linearity will be misspecified unless $\beta_2 = 0$, indicating the absence of global non-linearity in the DGP. When $\beta_2 \neq 0$, the presence of global non-linearity introduces potential bias into both the linear and quadratic terms. For an extended review of this methodological issue, see the reference paper McIntosh and Schlenker (2006).

A.3 Tables and figures

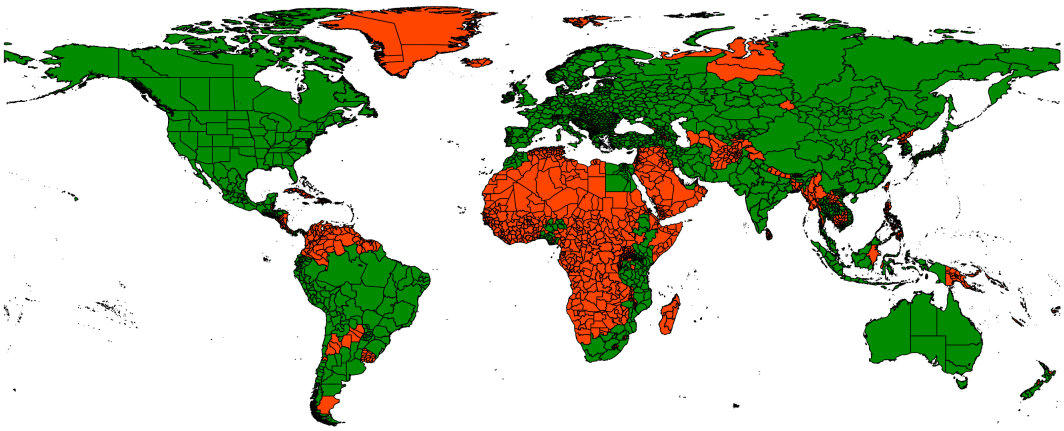

Figure A.1: Spatial coverage of the global data set of reported sub-national economic output (DOSE) (Wenz et al, 2023) across administrative provinces.
Notes: Colours green and red denote the sub-national administrative provinces (i) covered by the raw DOSE dataset (1,661 regions) over 1970-2018 years versus (ii) those where time-series per capita GDP data are insufficient for panel regressions (respectively). For (i), see §A.1 for a detailed discussion on the reporting and aggregation methods used in Wenz et al (2023). For (ii), we overcome missing administrative data in DOSE by extrapolating our gridded CMIP6 climate change simulations available globally for locations with no reported economic outputs and obtain a synthetic 'enhanced' vectorized matrix linking projected per capita GDP impacts to each administrative provinces, and offering a consistent coverage of all countries (166) and sub-national regions (3,672) globally (see §2.6).

Table A.1: Classification of GCMs to correct Hausfather et al (2022)'s hot model problem

GCM	ID	Model Classification
ACCESS-ESM1-5	1	likely
BCC-CSM2-MR	2	likely
CESM2	3	not-likely
CESM2-WACCM	4	not-likely
CMCC-CM2-SR5	5	likely
CMCC-ESM2	6	likely
CNRM-CM6-1	7	not-likely
CNRM-ESM2-1	8	not-likely
CanESM5	9	not-likely
EC-Earth3	10	none
EC-Earth3-Veg-LR	11	not-likely
FGOALS-g3	12	likely
GFDL-CM4	13	likely
GFDL-ESM4	14	likely
HadGEM3-GC31-LL	15	not-likely
IITM-ESM	15	not-likely
INM-CM4-8	16	likely
INM-CM5-0	17	none
IPSL-CM6A-LR	18	likely
KACE-1-0-G	19	none
KIOST-ESM	20	none
MIROC6	21	likely
MIROC-ES2L	22	likely
MPI-ESM1-2-HR	23	likely
MPI-ESM1-2-LR	24	likely
MRI-ESM2-0	25	likely
NorESM2-LM	26	likely
NorESM2-MM	27	none
TaiESM1	28	none
UKESM1-0-LL	29	not-likely

Note: This model classification is based on Hausfather et al's (2022) recommended procedure of excluding models with TCR and ECS outside "likely" ranges (1.4-2.2°C, 66% likelihood, and 2.5-4°C, 90% likelihood, respectively). That leaves us with 15 "likely" GCMs that form the basis of our modelling of projected economic impacts and which accounts for the 'hot models' identified in the last generation of climate model simulations in CMIP6. For a more exhaustive review of this probem, see Hausfather et al (2022).

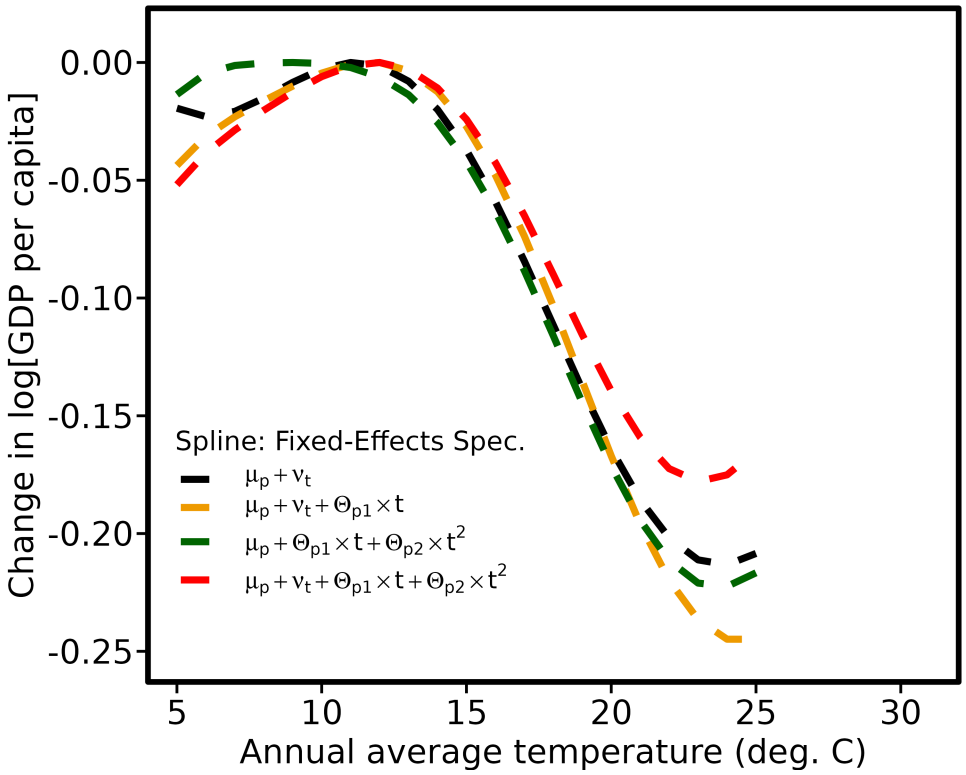

Figure A.2: Robustness test: Parametric FE-OLS global log[GDP per capita] responses to administrative province-annual average temperature exposure per year [deg.°C] against varying specifications of the Fixed-Effects (FEs).

Parametric FE-OLS splines are restricted with a 3^{rd} polynomial order function of average temperature exposure. Predicted responses are obtained by multiplying point-level estimated coefficients with the average temperature distribution reflected in the x-axis. Assuming index p denotes administrative provinces of the estimation dataset; red, green, orange, and black dashed lines indicate the following specifications of the constant terms (respectively): province-by-year fixed effects and province-specific quadratic time trends ($\mu_p + \nu_t + \Theta_{p,1}t + \Theta_{p,2}t^2$); province fixed effects and province-specific quadratic time trends ($\mu_p + \Theta_{p,1}t + \Theta_{p,2}t^2$); province-by-year fixed effects and province-specific linear time trends ($\mu_p + \nu_t + \Theta_{p,1}t$); province-by-year fixed effects excluding province-level time trends ($\mu_p + \nu_t$). For all GAM regressions, standard errors are clustered at the administrative province-level. Across all FEs specifications, parametric FE-OLS cubic functions of average temperature show highly similar non-linear shapes that empirically confirm our main parametric FE-OLS result displayed in panel **a** Fig. 3.

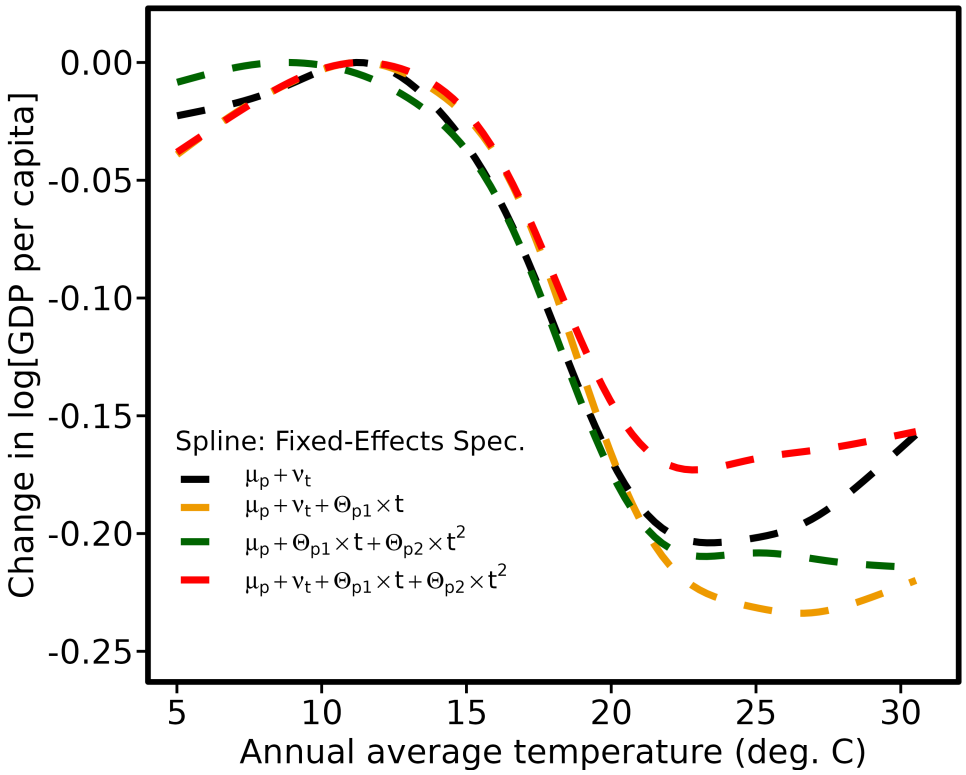

Figure A.3: Robustness test: Non-parametric Generalized Additive Model (GAM) global log[GDP per capita] responses to administrative province-annual average temperature exposure per year [deg.°C] against varying specifications of the Fixed-Effects (FEs).
Assuming index p denotes administrative provinces of the estimation dataset; red, green, orange, and black dashed lines indicate the following specifications of the constant terms (respectively): province-by-year fixed effects and province-specific quadratic time trends ($\mu_p + \nu_t + \Theta_{p,1}t + \Theta_{p,2}t^2$); province fixed effects and province-specific quadratic time trends ($\mu_p + \Theta_{p,1}t + \Theta_{p,2}t^2$); province-by-year fixed effects and province-specific linear time trends ($\mu_p + \nu_t + \Theta_{p,1}t$); province-by-year fixed effects excluding province-level time trends ($\mu_p + \nu_t$). For all GAM regressions, standard errors are clustered at the administrative province-level. Across all FEs specifications, non-parametric GAM responses yield highly similar non-linear shapes that empirically confirm our main non-parametric result displayed in panel **b** Fig. 3.

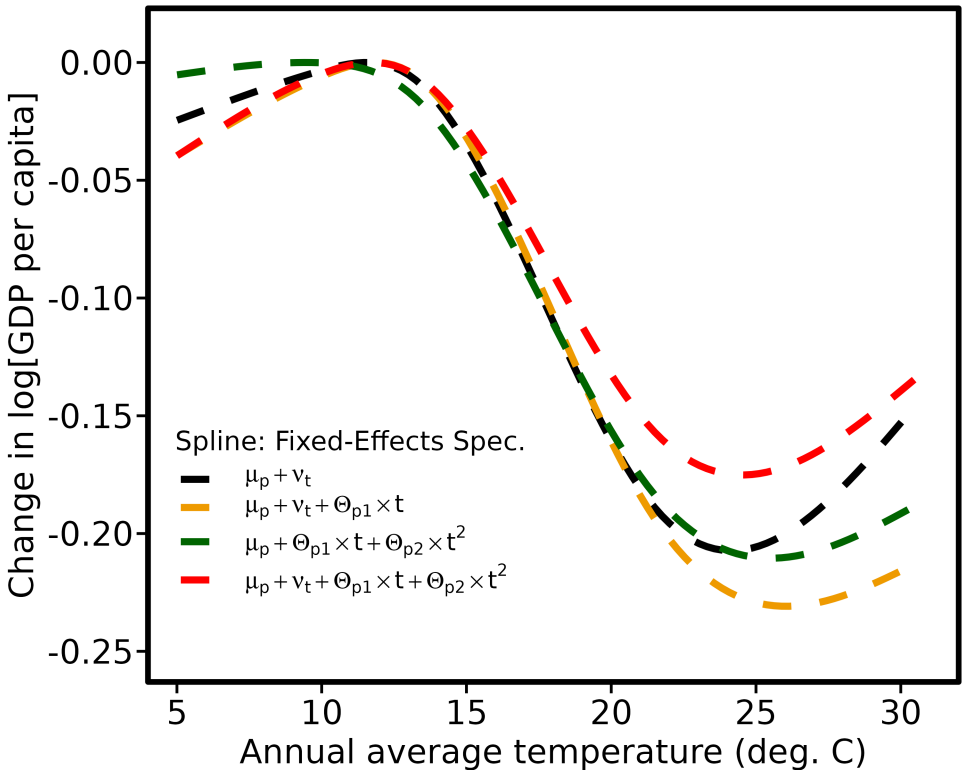

Figure A.4: Robustness test: Semi-parametric restricted cubic splines of global log[GDP per capita] responses to administrative province-annual average temperature exposure per year [deg.°C] against varying specifications of the Fixed-Effects (FEs).

Semi-parametric restricted cubic splines are calibrated with 6 Knots. Knots are locations along a predictor variable's range where pieces of the smooth function join; and thus where the shape of the smooth function can change. Splines fit the data in sections divided by these Knots, with each section's shape adjusted to minimize error. Assuming index p denotes administrative provinces of the estimation dataset; red, green, orange, and black dashed lines indicate the following specifications of the constant terms (respectively): province-by-year fixed effects and province-specific quadratic time trends ($\mu_p + \nu_t + \Theta_{p,1}t + \Theta_{p,2}t^2$); province fixed effects and province-specific quadratic time trends ($\mu_p + \Theta_{p,1}t + \Theta_{p,2}t^2$); province-by-year fixed effects and province-specific linear time trends ($\mu_p + \nu_t + \Theta_{p,1}t$); province-by-year fixed effects excluding province-level time trends ($\mu_p + \nu_t$). For all GAM regressions, standard errors are clustered at the administrative province-level. Across all FEs specifications, semi-parametric restricted cubic splines show highly similar non-linear shapes that empirically confirm our main semi-parametric result displayed in panel **c** Fig. 3.

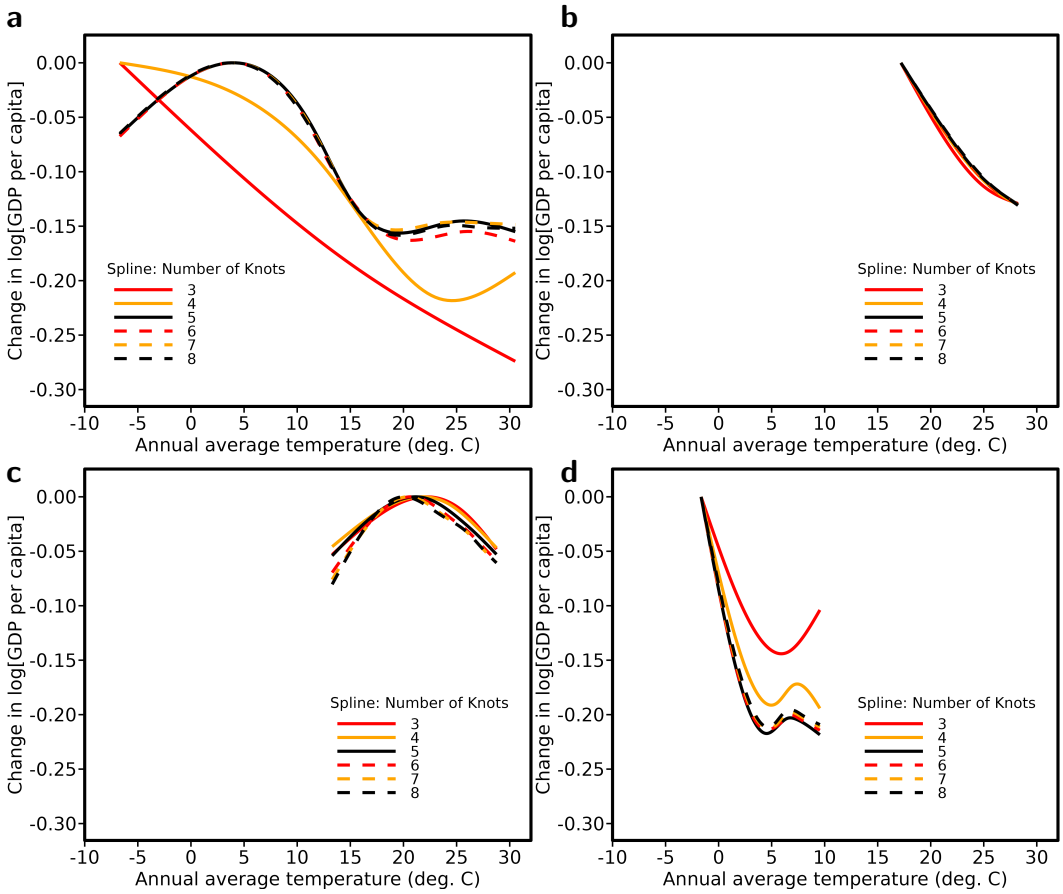

Figure A.5: Regionally-stratified non-linear log[GDP per capita] responses to administrative province-annual average temperature exposure per year [deg.°C] in typical climate zones.
Panels show semi-parametric restricted cubic splines with up to 3-8 Knots estimated regionally on typical climate zones (i.e., **a** Asia [temperate continental]; **b** Brazil [tropical savanna]; **c** India [tropical monsoon]; **d** Sweden [temperate to subarctic]). Knots are locations along a range of predictor variables where pieces of the smooth function join; and thus where the shape of the smooth function can change. Splines fit the data in sections divided by these Knots, with each section' shape adjusted to minimize error. All regionally stratified semi-parametric regressions in **a-b-c-d** include (sub-national) province-specific quadratic time trends in years of sample, province-by-year fixed effects and a quadric function of precipitation controls.

Table A.2: Global Δlog(GDP/Pop) responses to the quadratic FF - GDP per capita from WDI & weather from NASA's 0.25° GLDAS cells spatially collapsed to ISOs weighting by gridded population density from GPW dataset

Estimation period	1970-2018						1970-1994						1995-2018					
FEs specification	I	II	III	IV	V	VI	I	II	III	IV	V	VI	I	II	III	IV	V	VI
$Temp._{i,t}$	0.01230*	0.01230*	0.01250*	0.00954*	0.00739*	-0.00024	0.01271*	0.01271*	0.01008*	0.01160*	0.01321*	0.00004	0.00573*	0.00573*	0.00531*	0.00279	0.00250	-0.00058
	(0.002)	(0.002)	(0.001)	(0.015)	(0.044)	(0.486)	(0.012)	(0.012)	(0.023)	(0.041)	(0.032)	(0.968)	(0.031)	(0.031)	(0.036)	(0.301)	(0.279)	(0.262)
$(Temp._{i,t})^2$	-0.00042*	-0.00042*	-0.00042*	-0.00032*	-0.00027*	-0.00001	-0.00064*	-0.00064*	-0.00049*	-0.00059*	-0.00048*	-0.00001	-0.00026*	-0.00026*	-0.00027*	-0.00016+	-0.00015+	-0.00001+
	(0.000)	(0.000)	(0.000)	(0.002)	(0.003)	(0.144)	(0.000)	(0.000)	(0.001)	(0.000)	(0.004)	(0.71)	(0.004)	(0.004)	(0.001)	(0.088)	(0.06)	(0.091)
$Precip._{i,t}$	-0.000129	-0.000129	0.000157	-0.000158	-0.000115	0.000528	0.001726+	0.001726+	0.002208*	0.002228*	0.002781*	0.000796	-0.000377+	-0.000377+	-0.000274	-0.00041*	-0.000705*	0.000508
	(0.601)	(0.601)	(0.521)	(0.505)	(0.658)	(0.335)	(0.051)	(0.051)	(0.018)	(0.01)	(0.005)	(0.483)	(0.096)	(0.097)	(0.254)	(0.046)	(0.001)	(0.276)
$(Precip._{i,t})^2$	-0.000001	-0.000001	-0.000001	0.000000	0.000000	-0.000005	-0.000021*	-0.000021*	-0.000024*	-0.000025*	-0.000031*	-0.000010	0.000000	0.000000	0.000001	0.00000	0.000003*	-0.000004
	(0.591)	(0.591)	(0.357)	(0.831)	(0.848)	(0.381)	(0.014)	(0.014)	(0.009)	(0.003)	(0.001)	(0.495)	(0.92)	(0.92)	(0.65)	(0.71)	(0.001)	(0.363)
Adj-R^2	0.25	0.25	0.21	0.18	0.13	0.07	0.4	0.4	0.38	0.31	0.21	0.05	0.37	0.37	0.33	0.31	0.19	0.07
Obs.	6,697	6,697	6,697	6,697	6,697	6,697	2,849	2,849	2,849	2,849	2,849	2,849	3,848	3,848	3,848	3,848	3,848	3,848

Notes: *, and + denote statistical significance at 5% and 10% level, respectively. FF: Functional Form - herein, quadratic functions of weather components. Unless otherwise indicated, all panel fixed-effect OLS regressions include standard errors, in parentheses, clustered at the country level. Temperature is measured in °C and precipitation in metres. Constant terms are specified as follows: (I) country-by-year fixed effects and country-specific quadratic time trends; (II) continent-by-year fixed effects and country-specific quadratic time trends; (III) country fixed effects and country-specific quadratic time trends; (IV) country-by-year fixed effects and country-specific linear time trends; (V) country-by-year fixed effects excluding country-level time trends; (VI) continent-by-year fixed effects excluding country-level time trends.

Table A.3: Global Δlog(GDP/Pop) responses to the quadratic FF - GDP per capita from PWT & weather from NASA's 0.25° GLDAS cells spatially collapsed to ISOs weighting by gridded population density from GPW dataset

Estimation period	1970-2018						1970-1994						1995-2018					
FEs specification	I	II	III	IV	V	VI	I	II	III	IV	V	VI	I	II	III	IV	V	VI
$Temp._{i,t}$	0.01018*	0.01018*	0.00986*	0.01115*	0.00579	-0.00011	0.01300+	0.01300+	0.00556	0.01253+	0.00961	0.00157+	0.00716*	0.00716*	0.00634*	0.00269	0.00226	-0.00163
	(0.026)	(0.026)	(0.015)	(0.018)	(0.196)	(0.632)	(0.055)	(0.055)	(0.269)	(0.077)	(0.147)	(0.085)	(0.038)	(0.038)	(0.048)	(0.414)	(0.491)	(0.108)
$(Temp._{i,t})^2$	-0.00039*	-0.00039*	-0.00035*	-0.00039*	-0.00022+	-0.00001*	-0.00059*	-0.00059*	-0.00033*	-0.00060*	-0.00040*	-0.00005+	-0.00026*	-0.00026*	-0.00029*	-0.00013	-0.00015	0.00002
	(0.003)	(0.003)	(0.002)	(0.004)	(0.055)	(0.025)	(0.006)	(0.006)	(0.046)	(0.004)	(0.034)	(0.055)	(0.024)	(0.024)	(0.006)	(0.259)	(0.207)	(0.314)
$Precip._{i,t}$	0.00061	0.00061	0.000629	0.000632	0.001037+	0.000866	0.002546*	0.002546*	0.002809*	0.002271*	0.002752*	0.000918	-0.000504	-0.000504	-0.000679	-0.000401	-0.000471	0.000819
	(0.205)	(0.205)	(0.21)	(0.186)	(0.092)	(0.344)	(0.005)	(0.005)	(0.004)	(0.01)	(0.001)	(0.42)	(0.297)	(0.297)	(0.161)	(0.366)	(0.495)	(0.29)
$(Precip._{i,t})^2$	-0.00001*	-0.00001*	-0.000007	-0.000011*	-0.000015*	-0.000010	-0.000026*	-0.000026*	-0.000027*	-0.000023*	-0.000027*	-0.000011	0.000000	0.000000	0.000004	-0.000001	-0.000002	-0.000009
	(0.035)	(0.035)	(0.159)	(0.04)	(0.018)	(0.343)	(0.005)	(0.005)	(0.006)	(0.013)	(0.002)	(0.418)	(0.988)	(0.988)	(0.465)	(0.85)	(0.844)	(0.31)
Adj-R^2	0.25	0.25	0.21	0.19	0.12	0.07	0.38	0.38	0.37	0.31	0.23	0.05	0.39	0.39	0.35	0.31	0.2	0.07
Obs.	6,893	6,893	6,893	6,893	6,893	6,893	3,197	3,197	3,197	3,197	3,197	3,197	3,696	3,696	3,696	3,696	3,696	3,696

Notes: *, and + denote statistical significance at 5% and 10% level, respectively.FF: Functional Form - herein, quadratic functions of weather components. Unless otherwise indicated, all panel fixed-effect OLS regressions include standard errors, in parentheses, clustered at the country level. Temperature is measured in °C and precipitation in metres. Constant terms are specified as follows: (I) country-by-year fixed effects and country-specific quadratic time trends; (II) continent-by-year fixed effects and country-specific quadratic time trends; (III) country fixed effects and country-specific quadratic time trends; (IV) country-by-year fixed effects and country-specific linear time trends; (V) country-by-year fixed effects excluding country-level time trends; (VI) continent-by-year fixed effects excluding country-level time trends.

Table A.4: Global Δlog(GDP/Pop) responses to the interaction FF - GDP per capita from WDI & weather from NASA's 0.25° GLDAS cells spatially collapsed to ISOs weighting by gridded population density from GPW dataset

Estimation period	1970-2018						1970-1994						1995-2018					
FEs specification	I	II	III	IV	V	VI	I	II	III	IV	V	VI	I	II	III	IV	V	VI
Temp.$_{i,t}$	0.01245*	0.01245*	0.01254*	0.00974*	0.00728*	-0.00033	0.01309*	0.01309*	0.01046*	0.0121*	0.01372*	0.00007	0.00546*	0.00546*	0.00509*	0.00264	0.00245	-0.00073
	(0.002)	(0.002)	(0.001)	(0.012)	(0.042)	(0.399)	(0.011)	(0.011)	(0.018)	(0.033)	(0.027)	(0.928)	(0.036)	(0.036)	(0.04)	(0.321)	(0.286)	(0.33)
Temp.$_{i,t} \times \overline{T}_i$	-0.00086*	-0.00086*	-0.00085*	-0.00066*	-0.00054*	-0.00001	-0.00129*	-0.00129*	-0.00100*	-0.0012*	-0.00098*	-0.00001	-0.00052*	-0.00052*	-0.00053*	-0.00031+	-0.00031+	-0.00001
	(0.000)	(0.000)	(0.000)	(0.001)	(0.002)	(0.422)	(0.000)	(0.000)	(0.001)	(0.000)	(0.003)	(0.68)	(0.004)	(0.004)	(0.001)	(0.085)	(0.05)	(0.64)
Precip.$_{i,t}$	-0.000046	-0.000046	0.000091	-0.000078	0.000032	0.000602	0.001496+	0.001496+	0.002033*	0.001957*	0.002577*	0.000638	-0.000621	-0.000621	-0.000636	-0.000548+	-0.001078*	0.000579
	(0.907)	(0.907)	(0.828)	(0.826)	(0.937)	(0.456)	(0.096)	(0.096)	(0.031)	(0.03)	(0.012)	(0.535)	(0.116)	(0.117)	(0.129)	(0.081)	(0.001)	(0.428)
Precip.$_{i,t} \times \overline{P}_i$	-0.000004	-0.000004	-0.000002	-0.000003	-0.000004	-0.000007	-0.000036*	-0.000036*	-0.000043*	-0.000043*	-0.000056*	-0.000008	0.000005	0.000005	0.000010	0.000004	0.000017*	-0.000006
	(0.59)	(0.59)	(0.798)	(0.686)	(0.596)	(0.513)	(0.036)	(0.036)	(0.017)	(0.017)	(0.005)	(0.561)	(0.499)	(0.499)	(0.233)	(0.482)	(0.003)	(0.519)
Adj-R^2	0.25	0.25	0.21	0.18	0.13	0.07	0.4	0.4	0.38	0.31	0.21	0.05	0.37	0.37	0.33	0.31	0.2	0.07
Obs.	6,697	6,697	6,697	6,697	6,697	6,697	2,849	2,849	2,849	2,849	2,849	2,849	3,848	3,848	3,848	3,848	3,848	3,848

Notes: *, and + denote statistical significance at 5% and 10% level, respectively. FF: Functional Form - herein, interaction of weather components. Unless otherwise indicated, all panel fixed-effect OLS regressions include standard errors, in parentheses, clustered at the country level. Temperature is measured in °C and precipitation in metres. Constant terms are specified as follows: (I) country-by-year fixed effects and country-specific quadratic time trends; (II) continent-by-year fixed effects and country-specific quadratic time trends; (III) country fixed effects and country-specific quadratic time trends; (IV) country-by-year fixed effects and country-specific linear time trends; (V) country-by-year fixed effects excluding country-level time trends; (VI) continent-by-year fixed effects excluding country-level time trends.

Table A.5: Global Δlog(GDP/Pop) responses to the interaction FF - GDP per capita from PWT & weather from NASA's 0.25° GLDAS cells spatially collapsed to ISOs weighting by gridded population density from GPW dataset

Estimation period	1970-2018						1970-1994						1995-2018					
FEs specification	I	II	III	IV	V	VI	I	II	III	IV	V	VI	I	II	III	IV	V	VI
Temp.$_{i,t}$	0.01057*	0.01057*	0.00997*	0.01138*	0.00583	-0.00023	0.01373*	0.01373*	0.00597	0.01340+	0.01024	0.00154*	0.00665*	0.00665*	0.00593+	0.00245	0.00184	-0.00194
	(0.018)	(0.018)	(0.012)	(0.013)	(0.181)	(0.544)	(0.044)	(0.044)	(0.237)	(0.059)	(0.123)	(0.04)	(0.047)	(0.047)	(0.056)	(0.441)	(0.56)	(0.133)
Temp.$_{i,t} \times \overline{T}_i$	-0.00081*	-0.00081*	-0.00071*	-0.00081*	-0.00044*	-0.00001	-0.00122*	-0.00122*	-0.00067*	-0.00125*	-0.00084*	-0.00005*	-0.00050*	-0.00050*	-0.00055*	-0.00024	-0.00029	0.00003
	(0.001)	(0.001)	(0.001)	(0.002)	(0.045)	(0.303)	(0.005)	(0.005)	(0.042)	(0.002)	(0.026)	(0.019)	(0.027)	(0.028)	(0.006)	(0.259)	(0.205)	(0.288)
Precip.$_{i,t}$	0.000018	0.000018	-0.000076	0.000158	0.000397	0.000546	0.002411*	0.002411*	0.002725*	0.002089*	0.002563*	0.000872	-0.000813	-0.000813	-0.000876+	-0.000671	-0.001129+	0.000274
	(0.97)	(0.97)	(0.881)	(0.718)	(0.516)	(0.549)	(0.012)	(0.012)	(0.007)	(0.028)	(0.004)	(0.393)	(0.104)	(0.104)	(0.08)	(0.136)	(0.054)	(0.757)
Precip.$_{i,t} \times \overline{P}_i$	-0.000006	-0.000006	0.000004	-0.000010	-0.000015	-0.000005	-0.000049*	-0.000049*	-0.000052*	-0.000042*	-0.000049*	-0.000011	0.000008	0.000008	0.000013	0.000005	0.000014	-0.000001
	(0.561)	(0.561)	(0.724)	(0.27)	(0.216)	(0.65)	(0.015)	(0.015)	(0.013)	(0.042)	(0.007)	(0.382)	(0.513)	(0.513)	(0.257)	(0.602)	(0.291)	(0.943)
Adj-R^2	0.25	0.25	0.21	0.19	0.12	0.07	0.38	0.38	0.37	0.31	0.23	0.05	0.39	0.39	0.35	0.31	0.2	0.06
Obs.	6,893	6,893	6,893	6,893	6,893	6,893	3,197	3,197	3,197	3,197	3,197	3,197	3,696	3,696	3,696	3,696	3,696	3,696

Notes: *, and + denote statistical significance at 5% and 10% level, respectively. FF: Functional Form - herein, interaction of weather components. Unless otherwise indicated, all panel fixed-effect OLS regressions include standard errors, in parentheses, clustered at the country level. Temperature is measured in °C and precipitation in metres. Constant terms are specified as follows: (I) country-by-year fixed effects and country-specific quadratic time trends; (II) continent-by-year fixed effects and country-specific quadratic time trends; (III) country fixed effects and country-specific quadratic time trends; (IV) country-by-year fixed effects and country-specific linear time trends; (V) country-by-year fixed effects excluding country-level time trends; (VI) continent-by-year fixed effects excluding country-level time trends.

Table A.6: Global log(GDP/Pop) responses to the quadratic FF - GDP per capita from WDI & weather from NASA's 0.25° GLDAS cells spatially collapsed to ISOs weighting by gridded population density from GPW dataset

Estimation period	1970-2018						1970-1994						1995-2018					
FEs specification	I	II	III	IV	V	VI	I	II	III	IV	V	VI	I	II	III	IV	V	VI
Temp.$_{i,t}$	0.01360+	0.01360+	0.01149	0.02661*	0.11314*	-0.03596	0.01362+	0.01362+	0.01637*	0.02647*	0.09847*	-0.02565	0.01214+	0.01214+	0.01219+	0.01361+	0.05643*	-0.03771
	(0.083)	(0.083)	(0.131)	(0.032)	(0.003)	(0.147)	(0.054)	(0.054)	(0.018)	(0.015)	(0.002)	(0.24)	(0.059)	(0.059)	(0.061)	(0.075)	(0.022)	(0.23)
(Temp.$_{i,t}$)^2	-0.00048+	-0.00048+	-0.00068*	-0.00096*	-0.00409*	0.00073	-0.00057*	-0.00057*	-0.00059*	-0.00090*	-0.00297*	0.00017	-0.00043*	-0.00043*	-0.00059*	-0.00052+	-0.00252*	0.00094
	(0.057)	(0.057)	(0.003)	(0.02)	(0.000)	(0.454)	(0.015)	(0.015)	(0.01)	(0.004)	(0.002)	(0.594)	(0.039)	(0.039)	(0.004)	(0.052)	(0.000)	(0.478)
Precip.$_{i,t}$	-0.000843	-0.000843	-0.000812	0.000851	0.003147+	-0.030280	0.002348*	0.002348*	0.003327*	0.001906	-0.000497	-0.057065	-0.000656	-0.000656	-0.000561	-0.001838*	0.003338+	-0.024707
	(0.245)	(0.245)	(0.233)	(0.46)	(0.087)	(0.167)	(0.021)	(0.021)	(0.001)	(0.212)	(0.866)	(0.207)	(0.191)	(0.192)	(0.274)	(0.036)	(0.066)	(0.137)
(Precip.$_{i,t}$)^2	0.000007	0.000007	0.000003	-0.000002	-0.000019+	0.000223	-0.000030*	-0.000030*	-0.000039*	-0.000025	0.000012	0.000666	-0.000003	-0.000003	-0.000003	0.000015*	-0.000018+	0.000143
	(0.114)	(0.114)	(0.483)	(0.735)	(0.082)	(0.444)	(0.006)	(0.006)	(0.000)	(0.11)	(0.695)	(0.304)	(0.417)	(0.417)	(0.42)	(0.005)	(0.068)	(0.473)
Adj-R^2	1	1	0.99	0.99	0.97	0.51	1	1	1	1	0.99	0.56	1	1	1	1	0.99	0.47
Obs.	6,862	6,862	6,862	6,862	6,862	6,862	2,996	2,996	2,996	2,996	2,996	2,996	3,866	3,866	3,866	3,866	3,866	3,866

Notes: *, and + denote statistical significance at 5% and 10% level, respectively. FF: Functional Form - herein, quadratic functions of weather components. Unless otherwise indicated, all panel fixed-effect OLS regressions include standard errors, in parentheses, clustered at the country level. Temperature is measured in °C and precipitation in metres. Constant terms are specified as follows: (I) country-by-year fixed effects and country-specific quadratic time trends; (II) continent-by-year fixed effects and country-specific quadratic time trends; (III) country fixed effects and country-specific quadratic time trends; (IV) country-by-year fixed effects and country-specific linear time trends; (V) country-by-year fixed effects excluding country-level time trends; (VI) continent-by-year fixed effects excluding country-level time trends.

Table A.7: Global log(GDP/Pop) responses to the quadratic FF - GDP per capita from PWT & weather from NASA's 0.25° GLDAS cells spatially collapsed to ISOs weighting by gridded population density from GPW dataset

Estimation period	1970-2018						1970-1994						1995-2018					
FEs specification	I	II	III	IV	V	VI	I	II	III	IV	V	VI	I	II	III	IV	V	VI
Temp.$_{i,t}$	0.01914+	0.01914+	0.01900+	0.03704*	0.14466*	0.01386	0.00672	0.00672	0.00787	0.00610	0.12382*	0.02145	0.01892*	0.01892*	0.01759*	0.01776+	0.07074*	0.00573
	(0.068)	(0.068)	(0.057)	(0.025)	(0.000)	(0.8)	(0.476)	(0.476)	(0.307)	(0.581)	(0.000)	(0.728)	(0.018)	(0.018)	(0.017)	(0.071)	(0.000)	(0.913)
(Temp.$_{i,t}$)^2	-0.00052	-0.00052	-0.00084*	-0.00119+	-0.00510*	-0.00073	-0.00032	-0.00032	-0.00032	-0.00035	-0.00389*	-0.00095	-0.00056*	-0.00056*	-0.00073*	-0.00060+	-0.00280*	-0.00049
	(0.131)	(0.131)	(0.007)	(0.053)	(0.000)	(0.593)	(0.336)	(0.336)	(0.296)	(0.353)	(0.000)	(0.489)	(0.035)	(0.036)	(0.003)	(0.083)	(0.000)	(0.743)
Precip.$_{i,t}$	0.000944	0.000944	0.000920	0.002608	-0.001860	-0.072634+	0.002696*	0.002696*	0.003893*	0.000848	-0.000007	-0.086163	-0.002005*	-0.002005*	-0.002207*	-0.001700	0.001245	-0.059647*
	(0.568)	(0.568)	(0.584)	(0.322)	(0.597)	(0.068)	(0.007)	(0.007)	(0.000)	(0.562)	(0.998)	(0.125)	(0.029)	(0.029)	(0.02)	(0.541)	(0.78)	(0.032)
(Precip.$_{i,t}$)^2	-0.000020	-0.000020	-0.000024	-0.000029	0.000043	0.000956+	-0.000032*	-0.000032*	-0.000043*	-0.000014	-0.000002	0.001131	0.000013	0.000013	0.000015	0.000006	0.000000	0.000791*
	(0.413)	(0.413)	(0.33)	(0.294)	(0.269)	(0.076)	(0.003)	(0.003)	(0.000)	(0.455)	(0.959)	(0.132)	(0.21)	(0.21)	(0.147)	(0.86)	(0.994)	(0.042)
Adj-R^2	0.99	0.99	0.99	0.99	0.96	0.54	1	1	1	0.99	0.98	0.52	1	1	1	1	0.98	0.54
Obs.	7,047	7,047	7,047	7,047	7,047	7,047	3,351	3,351	3,351	3,351	3,351	3,351	3,696	3,696	3,696	3,696	3,696	3,696

Notes: *, and + denote statistical significance at 5% and 10% level, respectively.FF: Functional Form - herein, quadratic functions of weather components. Unless otherwise indicated, all panel fixed-effect OLS regressions include standard errors, in parentheses, clustered at the country level. Temperature is measured in °C and precipitation in metres. Constant terms are specified as follows: (I) country-by-year fixed effects and country-specific quadratic time trends; (II) continent-by-year fixed effects and country-specific quadratic time trends; (III) country fixed effects and country-specific quadratic time trends; (IV) country-by-year fixed effects and country-specific linear time trends; (V) country-by-year fixed effects excluding country-level time trends; (VI) continent-by-year fixed effects excluding country-level time trends.

Table A.8: Global log(GDP/Pop) responses to the interaction FF - GDP per capita from WDI & weather from NASA's 0.25° GLDAS cells spatially collapsed to ISOs weighting by gridded population density from GPW dataset

Estimation period	1970-2018						1970-1994						1995-2018					
FEs specification	I	II	III	IV	V	VI	I	II	III	IV	V	VI	I	II	III	IV	V	VI
Temp.$_{i,t}$	0.01352+	0.01352+	0.01113	0.02570*	0.11220*	-0.03255	0.01435*	0.01435*	0.01700*	0.02732*	0.10214*	-0.03097	0.01274*	0.01274*	0.01278*	0.01309+	0.05246*	-0.03318
	(0.087)	(0.088)	(0.146)	(0.036)	(0.003)	(0.213)	(0.046)	(0.046)	(0.015)	(0.012)	(0.002)	(0.178)	(0.047)	(0.047)	(0.049)	(0.084)	(0.026)	(0.3)
Temp.$_{i,t} \times \overline{T}_i$	-0.00096+	-0.00096+	-0.00134*	-0.00186*	-0.00822*	0.00053	-0.00116*	-0.00116*	-0.00121*	-0.00182*	-0.00608*	0.00027	-0.00091*	-0.00091*	-0.00123*	-0.00102+	-0.00491*	0.00071
	(0.058)	(0.058)	(0.004)	(0.021)	(0.000)	(0.539)	(0.013)	(0.013)	(0.009)	(0.004)	(0.002)	(0.465)	(0.029)	(0.029)	(0.002)	(0.052)	(0.000)	(0.57)
Precip.$_{i,t}$	-0.000911	-0.000911	-0.001016	0.001549	0.002081	-0.043418	0.002352*	0.002352*	0.003408*	0.001934	-0.001062	-0.050951	-0.001472+	-0.001472+	-0.001650+	-0.003115*	0.003448	-0.037594
	(0.403)	(0.403)	(0.361)	(0.414)	(0.507)	(0.264)	(0.03)	(0.03)	(0.002)	(0.222)	(0.743)	(0.311)	(0.083)	(0.083)	(0.068)	(0.039)	(0.261)	(0.273)
Precip.$_{i,t} \times \overline{P}_i$	0.000018	0.000018	0.000012	-0.000021	-0.000026	0.000491	-0.000060*	-0.000060*	-0.000079*	-0.000050	0.000037	0.000600	0.000011	0.000011	0.000016	0.000067*	-0.000053	0.000409
	(0.422)	(0.422)	(0.589)	(0.544)	(0.708)	(0.432)	(0.008)	(0.008)	(0.000)	(0.122)	(0.596)	(0.442)	(0.589)	(0.589)	(0.462)	(0.027)	(0.361)	(0.471)
Adj-R^2	1	1	0.99	0.99	0.97	0.51	1	1	1	1	0.99	0.55	1	1	1	1	0.99	0.47
Obs.	6,862	6,862	6,862	6,862	6,862	6,862	2,996	2,996	2,996	2,996	2,996	2,996	3,866	3,866	3,866	3,866	3,866	3,866

Notes: *, and + denote statistical significance at 5% and 10% level, respectively. FF: Functional Form - herein, interaction of weather components. Unless otherwise indicated, all panel fixed-effect OLS regressions include standard errors, in parentheses, clustered at the country level. Temperature is measured in °C and precipitation in metres. Constant terms are specified as follows: (I) country-by-year fixed effects and country-specific quadratic time trends; (II) continent-by-year fixed effects and country-specific quadratic time trends; (III) country fixed effects and country-specific quadratic time trends; (IV) country-by-year fixed effects and country-specific linear time trends; (V) country-by-year fixed effects excluding country-level time trends; (VI) continent-by-year fixed effects excluding country-level time trends.

Table A.9: Global log(GDP/Pop) responses to the interaction FF - GDP per capita from PWT & weather from NASA's 0.25° GLDAS cells spatially collapsed to ISOs weighting by gridded population density from GPW dataset

Estimation period	1970-2018						1970-1994						1995-2018					
FEs specification	I	II	III	IV	V	VI	I	II	III	IV	V	VI	I	II	III	IV	V	VI
Temp.$_{i,t}$	0.01830+	0.01830+	0.01770+	0.03605*	0.14563*	0.00534	0.00695	0.00695	0.00798	0.00655	0.13042*	0.01188	0.01928*	0.01928*	0.01801*	0.01622+	0.06619*	0.00414
	(0.077)	(0.077)	(0.072)	(0.029)	(0.000)	(0.915)	(0.471)	(0.472)	(0.314)	(0.561)	(0.000)	(0.849)	(0.014)	(0.014)	(0.013)	(0.089)	(0.001)	(0.928)
Temp.$_{i,t} \times \overline{T}_i$	-0.00101	-0.00101	-0.00162*	-0.00235+	-0.01040*	-0.00061	-0.00065	-0.00065	-0.00063	-0.00071	-0.00807*	-0.00077	-0.00116*	-0.00116*	-0.00151*	-0.00115+	-0.00548*	-0.00058
	(0.131)	(0.131)	(0.007)	(0.055)	(0.000)	(0.627)	(0.34)	(0.34)	(0.305)	(0.346)	(0.000)	(0.576)	(0.028)	(0.028)	(0.002)	(0.086)	(0.000)	(0.669)
Precip.$_{i,t}$	0.000093	0.000093	-0.000570	0.001861	-0.004058	-0.071791+	0.002644*	0.002644*	0.003891*	0.000770	-0.000522	-0.090347	-0.002576*	-0.002576*	-0.00293*	-0.003081	-0.000926	-0.057077*
	(0.938)	(0.938)	(0.656)	(0.508)	(0.271)	(0.087)	(0.016)	(0.016)	(0.001)	(0.631)	(0.876)	(0.141)	(0.009)	(0.009)	(0.004)	(0.23)	(0.848)	(0.047)
Precip.$_{i,t} \times \overline{P}_i$	-0.000019	-0.000019	-0.000013	-0.000041	0.000143+	0.001022+	-0.000063*	-0.000063*	-0.000086*	-0.000025	0.000008	0.001255	0.000041+	0.000041+	0.00005*	0.000048	0.000057	0.000841+
	(0.555)	(0.555)	(0.712)	(0.487)	(0.086)	(0.095)	(0.008)	(0.008)	(0.000)	(0.531)	(0.919)	(0.149)	(0.057)	(0.057)	(0.025)	(0.4)	(0.586)	(0.056)
Adj-R^2	0.99	0.99	0.99	0.99	0.96	0.54	1	1	1	0.99	0.98	0.52	1	1	1	1	0.98	0.54
Obs.	7,047	7,047	7,047	7,047	7,047	7,047	3,351	3,351	3,351	3,351	3,351	3,351	3,696	3,696	3,696	3,696	3,696	3,696

Notes: *, and + denote statistical significance at 5% and 10% level, respectively. FF: Functional Form - herein, interaction of weather components. Unless otherwise indicated, all panel fixed-effect OLS regressions include standard errors, in parentheses, clustered at the country level. Temperature is measured in °C and precipitation in metres. Constant terms are specified as follows: (I) country-by-year fixed effects and country-specific quadratic time trends; (II) continent-by-year fixed effects and country-specific quadratic time trends; (III) country fixed effects and country-specific quadratic time trends; (IV) country-by-year fixed effects and country-specific linear time trends; (V) country-by-year fixed effects excluding country-level time trends; (VI) continent-by-year fixed effects excluding country-level time trends.

Table A.10: Global log(GDP/Pop) responses to the quadratic FF - regional GDP per capita from DOSE & weather from NASA's 0.25° GLDAS cells spatially collapsed to GID(1)s weighting by gridded population density from the GPW dataset

Estimation period	1970-2018						1970-1994						1995-2018					
FEs specification	I	II	III	IV	V	VI	I	II	III	IV	V	VI	I	II	III	IV	V	VI
$Temp._{i,t}$	0.01859*	0.01859*	0.02061*	0.02729*	0.03252*	0.03650	-0.02355*	-0.02355*	-0.02118*	-0.02891*	0.01361	0.07254	0.02306*	0.02306*	0.02401*	0.01637*	0.02722*	0.03192
	(0.000)	(0.000)	(0.000)	(0.000)	(0.000)	(0.325)	(0.000)	(0.000)	(0.002)	(0.000)	(0.226)	(0.238)	(0.000)	(0.000)	(0.000)	(0.000)	(0.000)	(0.367)
$(Temp._{i,t})^2$	-0.00079*	-0.00079*	-0.00091*	-0.00115*	-0.00144*	-0.00358*	0.00062+	0.00062+	0.00055	0.00131*	0.00074	-0.00542+	-0.00089*	-0.00089*	-0.00096*	-0.00045*	-0.00159*	-0.00338*
	(0.000)	(0.000)	(0.000)	(0.000)	(0.000)	(0.031)	(0.058)	(0.058)	(0.106)	(0.000)	(0.181)	(0.084)	(0.000)	(0.000)	(0.000)	(0.001)	(0.000)	(0.023)
$Precip._{i,t}$	-0.001118*	-0.001118*	-0.001264*	-0.001403*	-0.001376	0.031499	0.000145	0.000145	0.000462	0.001098	0.002868*	0.045559+	-0.000423	-0.000423	-0.000559	-0.001014+	-0.001372	0.031513
	(0.034)	(0.034)	(0.013)	(0.022)	(0.148)	(0.186)	(0.869)	(0.869)	(0.601)	(0.195)	(0.008)	(0.094)	(0.44)	(0.44)	(0.304)	(0.054)	(0.155)	(0.194)
$(Precip._{i,t})^2$	0.000008	0.000008	0.000008	0.000018*	0.000027*	-0.000246	-0.000001	-0.000001	-0.000003	-0.000008	-0.000029*	-0.000380+	-0.000004	-0.000004	-0.000004	0.000015*	0.000030*	-0.000249
	(0.11)	(0.11)	(0.106)	(0.001)	(0.002)	(0.208)	(0.886)	(0.886)	(0.709)	(0.314)	(0.007)	(0.088)	(0.418)	(0.418)	(0.449)	(0.001)	(0.001)	(0.211)
Adj-R^2	0.99	0.99	0.99	0.99	0.96	0.5	1	1	1	0.99	0.99	0.7	0.99	0.99	0.99	0.99	0.97	0.43
Obs.	37,988	37,988	37,988	37,988	37,988	37,988	9,757	9,757	9,757	9,757	9,757	9,757	28,231	28,231	28,231	28,231	28,231	28,231

Notes: *, and + denote statistical significance at 5% and 10% level, respectively.FF: Functional Form - herein, quadratic functions of weather components. Unless otherwise indicated, all panel fixed-effect OLS regressions include standard errors, in parentheses, clustered at the country level. Temperature is measured in °C and precipitation in metres. Constant terms are specified as follows: (I) province-by-year fixed effects and province-specific quadratic time trends; (II) continent-by-year fixed effects and province-specific quadratic time trends; (III) province fixed effects and province-specific quadratic time trends; (IV) province-by-year fixed effects and province-specific linear time trends; (V) province-by-year fixed effects excluding province-level time trends; (VI) continent-by-year fixed effects excluding province-level time trends.

Table A.11: Global log(GDP/Pop) responses to the interaction FF - regional GDP per capita from DOSE & weather from NASA's 0.25° GLDAS cells spatially collapsed to GID(1)s weighting by gridded population density from the GPW dataset

Estimation period	1970-2018						1970-1994						1995-2018					
FEs specification	I	II	III	IV	V	VI	I	II	III	IV	V	VI	I	II	III	IV	V	VI
$Temp._{i,t}$	0.01827*	0.01827*	0.02032*	0.02726*	0.03379*	0.05373	-0.02437*	-0.02437*	-0.02168*	-0.02893*	0.01405	0.11227	0.02292*	0.02292*	0.02400*	0.01654*	0.02816*	0.04765
	(0.000)	(0.000)	(0.000)	(0.000)	(0.000)	(0.242)	(0.000)	(0.000)	(0.003)	(0.000)	(0.23)	(0.246)	(0.000)	(0.000)	(0.000)	(0.000)	(0.000)	(0.249)
$Temp._{i,t} \times \overline{T}_i$	-0.00153*	-0.00153*	-0.00178*	-0.00230*	-0.00305*	-0.00350*	0.00128+	0.00128+	0.00111	0.00257*	0.00139	-0.00591	-0.00176*	-0.00176*	-0.00192*	-0.00091*	-0.00334*	-0.00324*
	(0.000)	(0.000)	(0.000)	(0.000)	(0.000)	(0.024)	(0.052)	(0.053)	(0.107)	(0.000)	(0.221)	(0.101)	(0.000)	(0.000)	(0.000)	(0.001)	(0.000)	(0.015)
Adj-R^2	0.99	0.99	0.99	0.99	0.96	0.48	1	1	1	0.99	0.99	0.68	0.99	0.99	0.99	0.99	0.97	0.41
Obs.	37,988	37,988	37,988	37,988	37,988	37,988	9,757	9,757	9,757	9,757	9,757	9,757	28,231	28,231	28,231	28,231	28,231	28,231

Notes: *, and + denote statistical significance at 5% and 10% level, respectively. FF: Functional Form - herein, interaction of contemporaneous temperature with its baseline average. Unless otherwise indicated, all panel fixed-effect OLS regressions include standard errors, in parentheses, clustered at the province level. Temperature is measured in °C. Constant terms are specified as follows: (I) province-by-year fixed effects and province-specific quadratic time trends; (II) continent-by-year fixed effects and province-specific quadratic time trends; (III) province fixed effects and province-specific quadratic time trends; (IV) province-by-year fixed effects and province-specific linear time trends; (V) province-by-year fixed effects excluding province-level time trends; (VI) continent-by-year fixed effects excluding province-level time trends.

Table A.12: Global Δlog(GDP/Pop) responses to the quadratic FF - regional GDP per capita from DOSE & weather from NASA's 0.25° GLDAS cells spatially collapsed to GID(1)s weighting by gridded population density from the GPW dataset

Estimation period	1970-2018						1970-1994						1995-2018					
FEs specification	I	II	III	IV	V	VI	I	II	III	IV	V	VI	I	II	III	IV	V	VI
$Temp._{i,t}$	0.01295*	0.01295*	0.00904*	0.00925*	0.00552*	-0.00023	-0.03659*	-0.03659*	-0.03614*	-0.03595*	-0.00072	-0.00206	0.01404*	0.01404*	0.00909*	0.00961*	0.00670*	-0.00022
	(0.000)	(0.000)	(0.000)	(0.000)	(0.005)	(0.321)	(0.000)	(0.000)	(0.000)	(0.000)	(0.916)	(0.548)	(0.000)	(0.000)	(0.000)	(0.000)	(0.001)	(0.488)
$(Temp._{i,t})^2$	-0.00055*	-0.00055*	-0.00058*	-0.00040*	-0.00029*	0.00000	0.00190*	0.00190*	0.00183*	0.00193*	0.00046	0.00005	-0.00058*	-0.00058*	-0.00061*	-0.00052*	-0.00036*	0.00000
	(0.000)	(0.000)	(0.000)	(0.000)	(0.005)	(0.936)	(0.000)	(0.000)	(0.000)	(0.000)	(0.148)	(0.671)	(0.000)	(0.000)	(0.000)	(0.000)	(0.000)	(0.916)
$Precip._{i,t}$	-0.001316*	-0.001316*	-0.001457*	-0.001304*	-0.000824*	-0.000100	-0.001203	-0.001203	-0.000900	-0.000606	-0.000007	0.001120	-0.000205	-0.000205	-0.000574	-0.001424*	-0.001022*	-0.000167
	(0.006)	(0.006)	(0.002)	(0.001)	(0.012)	(0.273)	(0.302)	(0.302)	(0.416)	(0.528)	(0.993)	(0.249)	(0.623)	(0.623)	(0.178)	(0.004)	(0.008)	(0.347)
$(Precip._{i,t})^2$	0.000009*	0.000009*	0.000009*	0.000008*	0.000007*	0.000002+	0.000006	0.000006	0.000004	0.000001	-0.000002	-0.000011	0.000001	0.000001	0.000004	0.000007*	0.000009*	0.000003
	(0.016)	(0.016)	(0.017)	(0.008)	(0.002)	(0.069)	(0.585)	(0.585)	(0.668)	(0.951)	(0.841)	(0.378)	(0.726)	(0.726)	(0.322)	(0.042)	(0.001)	(0.166)
Adj-R^2	0.15	0.15	0.13	0.11	0.05	0.03	0.26	0.26	0.25	0.21	0.12	0.06	0.22	0.22	0.2	0.13	0.07	0.03
Obs.	36,583	36,583	36,583	36,583	36,583	36,583	9,080	9,080	9,080	9,080	9,080	9,080	27,503	27,503	27,503	27,503	27,503	27,503

Notes: *, and + denote statistical significance at 5% and 10% level, respectively.FF: Functional Form - herein, quadratic functions of weather components. Unless otherwise indicated, all panel fixed-effect OLS regressions include standard errors, in parentheses, clustered at the province level. Temperature is measured in °C and precipitation in metres. Constant terms are specified as follows: (I) province-by-year fixed effects and province-specific quadratic time trends; (II) continent-by-year fixed effects and province-specific quadratic time trends; (III) province fixed effects and province-specific quadratic time trends; (IV) province-by-year fixed effects and province-specific linear time trends; (V) province-by-year fixed effects excluding province-level time trends; (VI) continent-by-year fixed effects excluding province-level time trends.

Table A.13: Global Δlog(GDP/Pop) responses to the interaction FF - regional GDP per capita from DOSE & weather from NASA's 0.25° GLDAS cells spatially collapsed to GID(1)s weighting by gridded population density from the GPW dataset

Estimation period	1970-2018						1970-1994						1995-2018					
FEs specification	I	II	III	IV	V	VI	I	II	III	IV	V	VI	I	II	III	IV	V	VI
$Temp._{i,t}$	0.01248*	0.01248*	0.00845*	0.00895*	0.00550*	-0.00036+	-0.03876*	-0.03876*	-0.03850*	-0.03772*	0.00047	-0.00057	0.01367*	0.01367*	0.00861*	0.00915*	0.00639*	-0.00043
	(0.000)	(0.000)	(0.001)	(0.000)	(0.006)	(0.096)	(0.000)	(0.000)	(0.000)	(0.000)	(0.948)	(0.855)	(0.000)	(0.000)	(0.001)	(0.000)	(0.002)	(0.305)
$Temp._{i,t} \times \overline{T}_i$	-0.00104*	-0.00104*	-0.00110*	-0.00075*	-0.00059*	0.00001	0.00394*	0.00394*	0.00382*	0.00396*	0.00079	0.00001	-0.00113*	-0.00113*	-0.00117*	-0.00098*	-0.00071*	0.00001
	(0.000)	(0.000)	(0.000)	(0.000)	(0.005)	(0.615)	(0.000)	(0.000)	(0.000)	(0.000)	(0.227)	(0.881)	(0.000)	(0.000)	(0.000)	(0.000)	(0.000)	(0.614)
Adj-R^2	0.15	0.15	0.13	0.11	0.05	0.03	0.26	0.26	0.24	0.21	0.12	0.05	0.22	0.22	0.2	0.13	0.07	0.03
Obs.	36,583	36,583	36,583	36,583	36,583	36,583	9,080	9,080	9,080	9,080	9,080	9,080	27,503	27,503	27,503	27,503	27,503	27,503

Notes: *, and + denote statistical significance at 5% and 10% level, respectively. FF: Functional Form - herein, interaction of contemporaneous temperature with its baseline average. Unless otherwise indicated, all panel fixed-effect OLS regressions include standard errors, in parentheses, clustered at the province level. Temperature is measured in °C. Constant terms are specified as follows: (I) province-by-year fixed effects and province-specific quadratic time trends; (II) continent-by-year fixed effects and province-specific quadratic time trends; (III) province fixed effects and province-specific quadratic time trends; (IV) province-by-year fixed effects and province-specific linear time trends; (V) province-by-year fixed effects excluding province-level time trends; (VI) continent-by-year fixed effects excluding province-level time trends.

A.4 Nomenclature

CMIP6	Coupled Model Intercomparison, Phase VI
DOSE	MCC-PIK Database of Subnational Economic Output
ECMWF ...	European Centre for Medium-Range Weather Forecasts
ECS	Equilibrium Climate Sensitivity
ERA5	ECMWF Reanalysis V.5
GAM	Generalized Additive Model
GCMs	Global Climate Models
GLDAS	Global Land Data Assimilation System
GSFC	Goddard Space Flight Center
IAMs	Integrated Assessment Models
MPC	Microsoft Planetary Computer
NEX-GDDP	NASA Earth Exchange Global Daily Downscaled Projections
NOAH-LSM	NOAH-Land Surface Model
PWT	Penn World Table
RCPs	Representative Concentration Pathways
SCC	Social Cost of Carbon
SSPs	Shared Socioeconomic Pathways
TCR	Transient Climate Response
VIC	Variable Infiltration Capacity

References

[S1.] De Cian, E., Pavanello, F., Randazzo, T., Mistry, M. N., & Davide, M. (2019). Households' adaptation in a warming climate. Air conditioning and thermal insulation choices. Environmental Science & Policy, 100, 136-157.

[S2.] Dioha, E. C., Chung, E. S., Ayugi, B. O., Babaousmail, H., & Sian, K. T. C. L. K. (2024). Quantifying the Added Value in the NEX-GDDP-CMIP6 Models as Compared to Native CMIP6 in Simulating Africa's Diverse Precipitation Climatology. Earth Systems and Environment, 8(2), 417-436.

[S3.] Gu, X., Li, J., Chen, Y. D., Kong, D., & Liu, J. (2019). Consistency and discrepancy of global surface soil moisture changes from multiple model-based data sets against satellite observations. Journal of Geophysical Research: Atmospheres, 124(3), 1474-1495.

[S4.] Ji, L., Senay, G. B., & Verdin, J. P. (2015). Evaluation of the Global Land Data Assimilation System (GLDAS) air temperature data products. Journal of Hydrometeorology, 16(6), 2463-2480.

[S5.] Liu, T., Zhu, X., Tang, M., Guo, C., & Lu, D. (2024). Multi-model ensemble bias-corrected precipitation dataset and its application in identification of drought-flood abrupt alternation in China. Atmospheric Research, 307, 107481.

[S6.] Mistry, M. N. (2019). Historical global gridded degree-days: A high-spatial resolution database of CDD and HDD. Geoscience Data Journal, 6(2), 214-221.

[S7.] Sylvestre, F., Mahamat-Nour, A., Naradoum, T., Alcoba, M., Gal, L., Paris, A., ... & Gaya, D. (2024). Strengthening of the hydrological cycle in the Lake Chad Basin under current climate change. Scientific Reports, 14(1), 24639.

[S8.] Wenz, L., Kotz, M., Callahan, C., & Stechemesser, A. (2024). Persistent macroeconomic damages raise social cost of carbon.

[S9.] Wu, F., Jiao, D., Yang, X., Cui, Z., Zhang, H., & Wang, Y. (2023). Evaluation of NEX-GDDP-

CMIP6 in simulation performance and drought capture utility over China–based on DISO. Hydrology Research, 54(5), 703-721.

[S10.] Zhai, J., Mondal, S. K., Fischer, T., Wang, Y., Su, B., Huang, J., ... & Uddin, M. J. (2020). Future drought characteristics through a multi-model ensemble from CMIP6 over South Asia. Atmospheric Research, 246, 105111.

[S11.] Zhang, J., Li, C., Zhang, X., & Zhao, T. (2024). Improving simulations of extreme precipitation events in China by the CMIP6 global climate models through statistical downscaling. Atmospheric Research, 303, 107344.

About EDHEC Climate Institute

EDHEC Business School has been recognised for over 20 years for its expertise in finance. Its approach to climate finance is founded on a commitment to equipping finance professionals and decision-makers with the insights, tools, and solutions necessary to navigate the challenges and opportunities presented by climate change. EDHEC has developed a significant research capacity on the financial measurement of climate risk, which relies on the best researchers in climate finance, and brings together experts in climate risks as well as in quantitative analysis.

The EDHEC Climate Institute (ECI) focuses on helping private and public decision-makers manage climate-related financial risks and make the most of financial tools to support the transition to a low-emission economy that is more resilient to climate change. It has a long track record as an independent and critical reference centre in helping long-term investors to understand and manage the financial implications of climate change on asset prices and the management of investments and climate action policies. The institute has also developed an expertise in physical risks, developing proprietary research frameworks and innovative approaches. ECI is also conducting advanced research on climate transition risks, with a focus on supply chain emissions (Scope 3), consumer choices, and emerging technologies.

As part of its mission, ECI collaborates with academic partners, businesses, and financial players to establish targeted research partnerships. This includes making research outputs, publications, and data available in open source to maximise impact and accessibility.

EDHEC | Climate Institute

For more information, please contact:
maud.gauchon@climateimpactedhec.com

climateinstitute.edhec.edu

LONDON
10 Fleet Place, Ludgate
London EC4M 7RB - United Kingdom
Tel: +44 (0)207 332 56 00

NICE
400, Promenade
des Anglais - BP3116
06202 Nice
Cedex 3 – France
Tel: +33 (0)4 93 18 78 87

PARIS
16-18, rue du 4 Septembre
75002 Paris – France
Tel: +33 (0)1 53 32 76 30

SINGAPORE
1 George Street
#15-02 Singapore 049145
Tel: +65 (0)6438 0030